Coral Colony-Scale Rugosity Metrics and Applications for Assessing Temporal Trends in the Structural Complexity of Coral Reefs.

Coral colonies measured on the Great Barrier Reef, left to right, *Turbinaria*, *Favia*, *Acropora*, *Fungia* and *Leptoria.*

Submitted by Emily Husband to the University of Exeter as a thesis for the degree of Masters by Research, In March 2019.

I certify that all material in this thesis which is not my own work has been identified and that any material that has previously been submitted and approved for the award of a degree by this or any other University has been acknowledged.

Signature ……

Abstract

Globally, coral reefs are experiencing reductions in structural complexity, primarily due to a loss of key reef building taxa. Monitoring these changes is difficult due to the time-consuming nature of *in-situ* measurements and lack of data concerning coral genus-specific contributions to reef structure. This research aimed to develop a new technique that uses coral colony level data to quantify reef rugosity (a 3-dimensional measure of reef structure) from three sources of coral survey data: 2D video imagery, line intercept data and UAV imagery. A database of coral colony rugosity data, comparing coral colony planar and contour length for 40 coral genera, 14 morphotypes and 9 abiotic reef substrates, was created using measurements from the Great Barrier Reef and Natural History Museum. Mean genus rugosity was identified as a key trait related to coral life history strategy. Linear regression analyses ($y = mx$) revealed statistically significant ($p < 0.05$) relationships between coral colony size and rugosity for every coral genus, morphotype and substrate. The gradient governing these relationships was unique for each coral taxa, ranging from mean = 1.23, for (encrusting) A*canthastrea*, to m = 3.84, for (vase-shape) *Merulina.* These gradients were used as conversion factors to calculate reef rugosity from linear distances measured in video transects of both artificial reefs, used as a control test, and *in-situ* natural coral reefs, using Kinovea software. This calculated, 'virtual' rugosity had a strong, positive relationship with *in-situ* microscale rugosity ($r^2 = 0.96$) measured from the control transects, but not with that measured at the meso-scale in natural, highly heterogeneous reef environments ($r^2 < 0.2$). This showed that the technique can provide accurate rugosity information when considered at the coral colony level. The conversion factors were also applied to historic line intercept data from the Seychelles, where temporal changes in calculated rugosity were consistent with changes in coral cover between 2008 and 2017. Finally, on application to 2,283 corals digitised from UAV imagery of the Maldives, the conversion factors enabled calculation of rugosity for three 100 m^2 reef areas and prediction of how this rugosity will decrease during two future scenarios of coral reef degradation and community change. The study highlights that the application of genera-specific coral rugosity data to both new and existing coral reef survey datasets could be a valuable tool for monitoring reef structural complexity over large spatial scales.

Acknowledgements

First of all, I have to thank my supervisor, Professor Chris Perry, for presenting and trusting me with this opportunity and for his unwavering guidance, support and endless answering of questions during the last 18 months. I hope I have done this project justice.

Thank you also to Dr. Mike Salter for helping me get to grips with coral reef fieldwork and to Liv and Tess for additional fieldwork assistance.

A huge thank you to the Natural History Museum for letting me use their dry-invertebrate collection for creation of the rugosity database; to Dr. Ines Lange and Prof. Chris Perry for collecting video transect data for this project, and to Professor Nick Graham for the use of his line intercept data. Thanks also to Alex Whittle and Dr. Nick Cox for their invaluable statistical knowledge and guidance with R-studio and Stata.

Additional and significant thanks must go to Dr. Rob Yarlett, for patiently listening to and answering *all* of my questions about coral reef research, and to Ines, Jen and our Coral Reef Coffee Group for always encouraging me.

To the Amory Office and Geography PGSs – thank you for making me feel welcome in Exeter.

Thank you to Katie for proof reading my thesis, putting the commas in the right places and informing me of which word in this thesis is most interesting for Scrabble.

Finally, thank you to all my family and friends who have ‘listened’ to incessant coral chat and not given up on me despite all of the protests that this ‘would be completed next month…’

Table of Contents

List of figures

List of tables

List of appendices

List of equations

Abbreviations

LiDAR	Light Detection and Ranging
DEM	Digital Elevation Model
S.D.	Standard Deviation
SfM	Structure from Motion
DTM	Digital Terrain Model
UAV	Unmanned Aerial Vehicle
AIMS	Australian Institute of Marine Science
GBRMPA	Great Barrier Reef Marine Park Authority
OBIA	Object Based Image Analysis

Chapter 1. Introduction

1.1 Introduction and Literature Review

Coral reefs and structural complexity

Coral reefs are highly dynamic and ecologically diverse ecosystems dominated by the presence of scleractinian corals (Hoegh-Guldberg, 1999 and Bellwood *et al.,* 2004). Despite occupying just 0.2 % of the Earth's oceans, they harbour one third of all marine species, significantly contribute to global biological, chemical and physical processes and provide many invaluable services for human societies (Spalding and Grenfell, 1997, Reaka-Kudla, 1997, Moberg and Folke, 1999, Spalding *et al.,* 2001, Bertels *et al.,* 2008 and Lentz, 2012). In recent decades, large scale coral mortality and reductions in coral cover have increased worldwide concern for the health and stability of coral reefs (Bellwood *et al.,* 2004, Bruno and Selig, 2007 and De'ath *et al.,* 2012). These changes largely result from multiple anthropogenic and natural forces acting synergistically at both global and local scales (Alvarez-Filip, 2010 and Perry *et al.,* 2013). Globally, ocean warming, ocean acidification and, to a lesser extent, rising sea level threaten the narrow envelope of environmental conditions corals require to survive (Downs *et al.,* 2005, Eakin *et al.,* 2009 and Purkis, 2017). However, increasing nutrient input to the oceans from sewage and fertilizer runoff, overfishing, coastline modification, and associated increases in sediment stress and turbidity, destructive tourism and exploitation of coral substrate for building material form a more local group of stressors which can be as equally destructive to coral communities (see figure 1.1, Alvarez-Filip, 2010, and Purkis *et al.,* 2017).

One of the most devastating consequences of these stressors is the collapse of the intricate carbonate (coral) frameworks which form the foundation of reefs and contribute to their structural complexity (figure 1.1, Norse, 1993, Garpe *et al.,* 2006, Hoegh-Guldberg *et al.,* 2007, Perry *et al.,* 2013 and Graham and Nash, 2013). The structural complexity of coral reefs is integral to the functionality and resilience of reef ecosystems (Peterson *et al.,* 1998 and Nash *et al.,* 2013). More structurally complex reefs provide more ecological niches, shelter and hiding places for fish and algae and surfaces for coral larvae

attachment. They are also more efficient at dissipating wave energy, providing greater shoreline protection for tropical coastlines (Rogers *et al.,* 1982, Sheppard *et al.,* 2005, Mumby, 2006 and Harris *et al.,* 2018). Consequently, structural complexity is strongly correlated with fish diversity, abundance and biomass and is responsible for many of the ecosystems services provided by coral reefs and the socioeconomic value they create (Cranfield *et al.,* 2004, Perry *et al.,* 2013, Harborne *et al.,* 2012, Hattori and Shibuno, 2015 and Richardson *et al.,* 2017). Coral colony structural complexity (relating to coral growth form) is also an integral trait for determining the life history strategy of coral genera and thus predicting how coral reefs may respond to ongoing stressors and disturbance (Darling *et al.,* 2012).

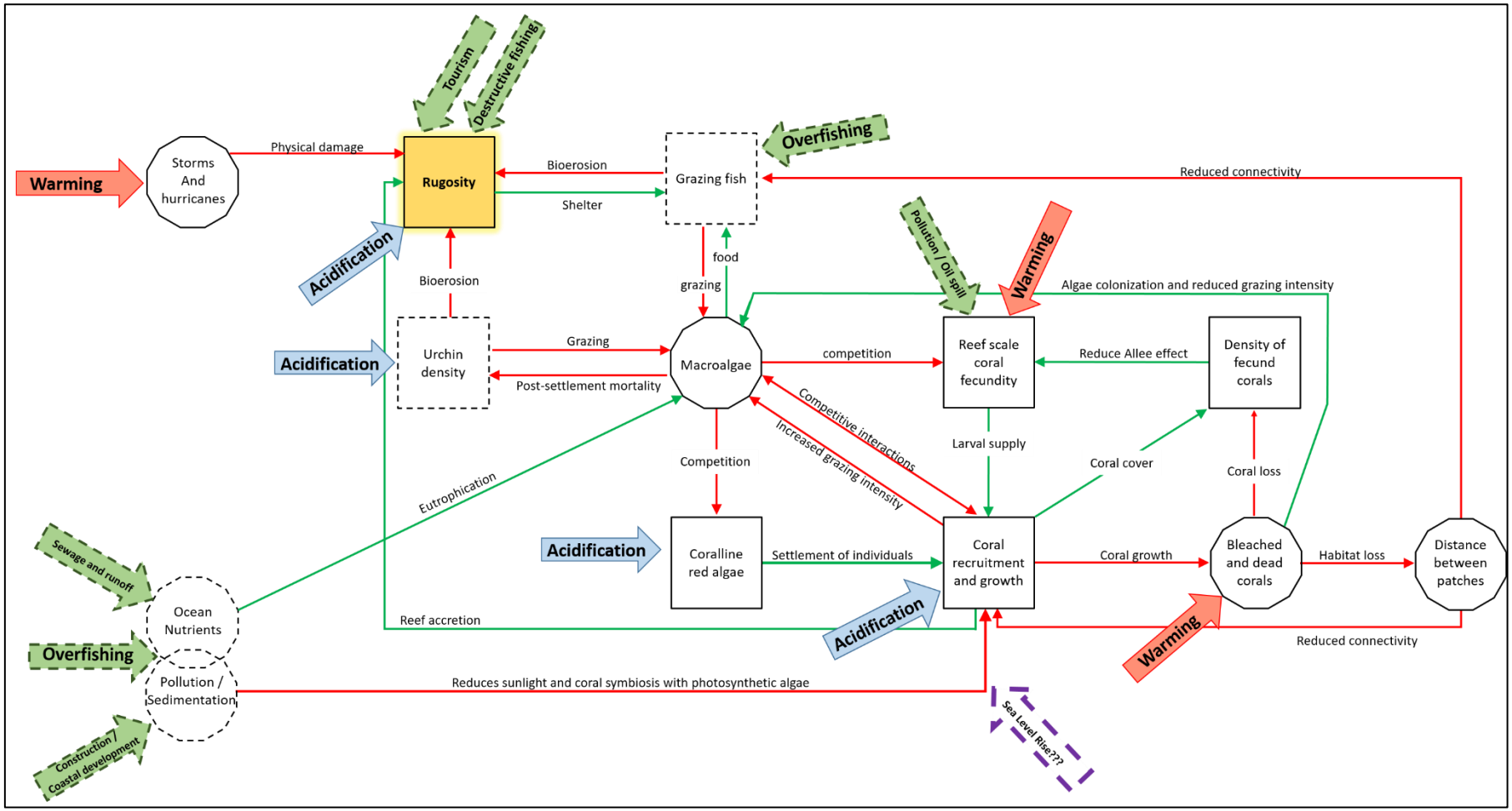

Figure 1.1. Pathways of disturbance to ecological feedback processes on a coral reef caused by anthropogenic and environmental factors. Damage associated with ocean acidification are indicated by blue arrows, global warming by red arrows and with specified human activity by green arrows. Potential damage from sea level rise is indicated by a purple arrow. Boxes joined by red arrows represent a negative (decreasing) influence of the first factor on the box indicated and by green arrows, a positive (increasing) influence of the first factor on the box indicated. Through time, the magnitude of factors in hexagonal boxes will increase and factors in rectangular boxes will decrease. Boxes or arrows with dashed lines are (in part) amenable to local management intervention or reduction through human action. Adapted from Hoegh-Guldberg *et al.,* (2007).

Corals are structurally diverse taxa, exhibiting a large range of morphologies that disproportionately contribute to the reefs structural complexity. As such, the overall structural complexity of any coral reef is heavily dependent on the species composition of coral communities (Alvarez-Filip *et al.,* 2013 and Richardson *et al.,* 2017). Recently, local and global stressors have caused mass modification of coral communities (Garpe *et al.,* 2006, Maynard *et al.,* 2008, and Alvarez-Filip *et al.,* 2013). On many reefs, major reef building taxa, with competitive life history strategies, are being replaced with less structurally important, weedy, generalist and stress tolerant corals (Darling *et al.,* 2012 and Alvarez-Filip *et al.,* 2013). In the Pacific, the abundance of reef-building corals has decreased by as much as 72 % since 1968 and on many Caribbean reefs by 50 % since 1970 (Gardner *et al.,* 2003, Bruno and Selig, 2007 and Yates *et al.,* 2017). In worst case scenarios, the ecosystems are shifting to macro-algae dominated states as fleshy algae overgrows dead coral skeletons (Done*,* 1992, Bellwood *et al.,* 2004, Alvarez-Filip *et al.,* 2013 and Bozec *et al.,* 2015). These shifts reduce reef carbonate production, such as recognised on the Great Barrier Reef where calcification decreased by 14.2 % between 1990 and 2005 (Hoegh-Guldberg *et al.,* 2007 and De'ath *et al.,* 2009). If carbonate production continues to decease, carbonate erosion may eventually exceed reef accretion. This not only decreases the ability of coral reef growth to keep pace with projected sea level rise, but also decreases reef structural complexity, reef functionality and, ultimately, causes a loss of the essential ecosystem services reefs provide (McManus and Polsenberg, 2004, Hoegh-Guldberg *et al.,* 2007, Perry *et al.,* 2013, Alvarez-Filip 2013 and Kennedy *et al.,* 2013).

Although it is common for coral reefs to undergo numerous natural state changes throughout time, due to physical damage caused by storms, bio erosion and/or disease, recently, there have been increasing reports of structural complexity declines and reefs persistently shifting to algae dominated states. This is generally accepted as resulting from an increase in the stressors and disturbance events which often precede these state changes and reduce the resilience of reefs to macroalgae dominance (McManus and Polsenberg, 2004). The relative importance of these stressors varies among location and even across single reefs, but either directly or indirectly, they result in reduced carbonate production (Hoegh-Guldberg *et al.,* 2007 and De'ath *et al.,* 2009).

Short lived shifts to states of net erosion have already been identified at numerous reefs post-local disturbance (Perry *et al.,* 2008). Globally, the presence of flatter and structurally homogenous reefs has increased from 20 % to 75 % since 1970 (Alvarez-Filip *et al.,* 2009) and it is observed that 19 % of coral reefs have been completely degraded (Burke *et al.,* 2011).

Since the development of SCUBA (~60 years ago) there has been an exponential increase in research examining the role of structural complexity in coral reef ecosystems (Graham and Nash, 2013). Yet, despite general agreement over the importance of this characteristic, there is no standard technique for quantifying structural complexity and no consensus regarding the best spatial scale to measure it at (Commito and Rusignuolo, 2000, Frost *et al.,* 2005 and Knudby and LeDrew, 2007). At present, inconsistencies in local surveys and a lack of historical baseline data is limiting efforts to comprehensively assess the full extent of global structural complexity declines (Sweatman *et al.,* 2011, Beijbom *et al.,* 2012 and Hedley *et al.,* 2016). Consequently, there is an increasing need for a globally applicable and standardized technique that can quantify and map the spatial variability of structural complexity at ecologically relevant spatial scales (Zawada *et al.,* 2010, Graham and Nash, 2012 and Hedley *et al.,* 2016). This research will aim to develop such a technique, taking into consideration current limitations of existing methods used to measure coral reef structural complexity. It will also demonstrate how this developed technique could be advantageous for quantifying coral reef rugosity and monitoring this under future climate change and increasing anthropogenic stressor scenarios.

Measuring rugosity *in-situ*

The structural complexity of coral reefs is commonly monitored using records of coral reef rugosity, a measure of the roughness or irregularity of the coral reefs surface and a proxy of structural complexity (Magno and Villanoy, 2006, Knudby and LeDrew, 2007 and Knudby *et al.,* 2007). Traditionally, rugosity is measured and quantified in the field using the rugosity index: the ratio between the known horizontal projection area of a linked chain and the length of this after being draped across a coral habitat transect, strictly following its topographic contours, as demonstrated in figure 1.2 (Risk, 1972). Recently, turning wheels

have also been used to measure contour length (Richardson *et al.,* 2017). Higher ratios between the planar and contour length represent greater spatial heterogeneity and substratum complexity. They also correlate strongly with greater coral reef biodiversity - in particular, metrics relating to fish abundance which validates the method as a representative measure of reef structural complexity (Risk, 1972, Luckhurst and Luckhurst, 1978, Knudby and LeDrew, 2007 and Alvarez-Filip, 2011). The rugosity index, also referred to as the chain-tape method, has been used extensively in coral reef research due to its ability to capture the essence of coral reef rugosity as a simple ratio, with little requirement for extensive field skills. Consequently, historical research using the technique has provided vital comparable records of reef rugosity which have helped recognise global declines in structural complexity, such as those throughout the Caribbean during the last 40 years (Alvarez-Filip *et al.,* 2009 and Sweatman *et al.,* 2011).

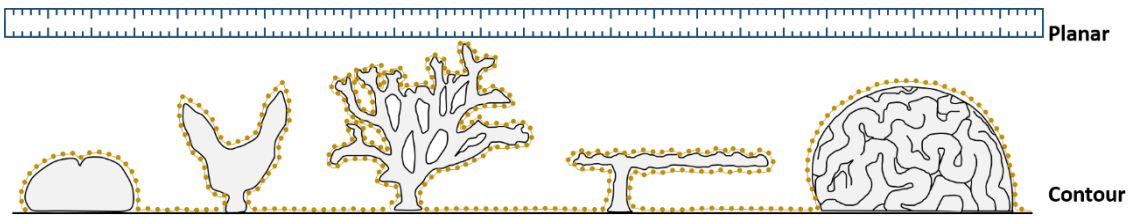

Figure 1.2. A representation of the chain-tape method used to calculate the rugosity index. The gold studded line represents the chain used to measure the contour length and the ruler, the planar transect length. From left to right, the coral morphologies represented are free-living, vase, branching, tabular and massive. Rugosity = contour length / planar length (Risk, 1972). Adapted from Friedman *et al.,* (2012).

The chain-tape is also advantageous in its capability to measure rugosity at a coral colony scale, relevant for determining the contribution of different coral taxa to overall reef rugosity. This is achieved by examining the dominant coral substrates, or species present along transects with overall transect rugosity data (Knudby and LeDrew, 2007 and Alvarez-Filip *et al.,* 2011). Recently, this species level approach has been refined with scientists measuring the rugosity of individual coral colonies to derive mean rugosity values for various coral species (Alvarez-Filip *et al.,* 2013, Richardson *et al.,* 2017 and González-Barrios and Alvarez-Filip, 2018). This has been valuable in revealing that areas

of high structural complexity are often taxa rich, but, dominated by one or a few species of structurally important coral, such as those with competitive life history strategies and branching or plate morphologies (Darling *et al.,* 2012). It also highlights the initial advantages of rugosity monitoring techniques that can measure rugosity at a coral colony measurement scale (Alvarez-Filip *et al.,* 2010, Burns *et al.,* 2015 and Alvarez-Filip *et al.,* 2011).

Despite widespread acceptance of the chain-tape technique, issues have arisen with rugosity index values due to their dependency on the size of linkages comprising the measurement chain, or diameter of turning wheels used to measure the reef contour (Luckhurst and Luckhurst, 1978, Knudby and LeDrew, 2007, and Richardson *et al.,* 2017). For example, at Lizard Island, the rugosity of variable coral habitats, and magnitude of structural complexity difference between them, has been found to inconsistently vary with turning wheel diameter (Nash *et al.,* 2013 and Richardson *et al.,* 2017). The same is true for colony level rugosity measurement and attempts to determine the mean rugosity of individual coral taxa (Knudby and LeDrew, 2007 and Richardson *et al.,* 2017). This scale dependency influences the strength of the relationship between rugosity and coral reef biodiversity metrics and often results in inconsistent knowledge as to which coral species are the most structurally important for coral reef ecosystems (Luckhurst and Luckhurst, 1978, Knudby and LeDrew, 2007 and Richardson *et al.,* 2017). Although such scale dependency allows rugosity to be measured at researcher defined spatial scales, the choice of chain length or wheel diameter introduces an element of subjectivity to the technique. This decreases the validity of comparisons between rugosity values for similar locations, but that have been measured at different scales. Further (albeit unintentional) subjectivity results from the difficulty of draping the chain in a perfectly straight line, parallel to the defined transect in the field. Any side to side variation in chain placement will lead to overestimations of rugosity values, decreasing the validity of the transect rugosity measurement (Friedman *et al.,* 2012 and Leon *et al.,* 2015).

The rugosity index has also been criticised for only being able to capture gross scale rugosity, especially if the chain or wheel is not accurately or sufficiently draped into every crevasse, however small, along transects. This is exemplified

by the stronger relationships identified between chain-tape rugosity and large fish biodiversity data than those seen for smaller fish – a result of the ability of fish to hide in tiny crevasses that cannot be captured by the draped chain (McCormick, 1994, Luckhurst and Luckhurst, 1978 and Gratwicke and Speight, 2005). Consequently there is much scepticism as to whether the technique is sufficient for measuring coral colony scale rugosity, especially with past research highlighting an inability of rugosity index values to differentiate between variable coral morphotypes (McCormick, 1994).

Alternative *in-situ* metrics developed to better capture the true variability of rugosity over small scales have had limited success. The variance of and mean coral height, number of tall, complex, and all corals, and sum of coral and complex coral heights have been used as proxies for structural complexity. However, on the Meso-American Barrier Reef, they were able to explain only ~ 50 % of fish assemblage data, known to strongly correlate with the rugosity index, and were poor predictors of intra-habitat variation (Harborne, 2006 and Harborne *et al.,* 2012). Reef slope angle, sponge presence and octocoral height have also been examined as proxies for structural complexity, but, each characteristic presented unique, relative, non-linear and complex relationships with fish biodiversity data (Newman *et al.,* 2015). All of these alternative metrics displayed weaker correlations with biodiversity than the rugosity index (Newman *et al.,* 2015, Harborne and Mumby, 2012). Furthermore, these metrics are often measured throughout quadrats or along entire transects, failing to consider the contribution of individual coral colonies or species, to overall rugosity. This limits their suitability for examining rugosity at coral colony scales. (Risk, 1972, Luckhurst and Luckhurst, 1978 and McCormick, 1994).

Regardless of their success, any metric requiring *in-situ* measurement and physical contact with coral reefs carries the disadvantage of being labour and time intensive. They are consequently inefficient, especially considering physiological limitations on dive time (He *et al.,* 2012). These factors limit the applicability of the above methods for monitoring rugosity at global reef scales and, to date, has led to a spatial bias in monitoring efforts towards shallow reefs that are easily accessible, have local research stations, or are most at risk from tourist activity (Hedley *et al.,* 2016 and Gutierrez-Heredia *et al.,* 2016). The

methods also have environmental implications as chains or measuring devices easily tangle with the coral and disturb reef organisms and coral substrate (Dustan *et al.,* 2013).

Non-contact *in-situ* methods can minimise this environmental impact, and provide a more time efficient method to monitor reef complexity, unrestricted by spatial scales (Polunin and Roberts, 1993 and Graham *et al.,* 2003). Diver visual assessment, using rating scales to represent increasing coral reef complexity for defined areas, has been partly successful, with visual assessment scores strongly correlating with rugosity index values for survey areas (Sheppard, *et al.,* 2002, Long, *et al.,* 2004 and Wilson, 2007). However, visual assessment is highly subjective and prone to inter-observe bias, exemplified by the low (1/3) agreement of visual topographic estimates between paired divers in the Seychelles (Wilson, 2007). Additionally, the method is not accurate enough to account for small scale spatial variability in rugosity, required to examine individual coral colonies as opposed to large (multiple metres) areas of reef (Wilson, 2007).

Development of optical remote sensing

In recent decades, remote sensing technologies have been established as effective, non-invasive alternatives for measuring coral reef health both *in-situ* and from the air. Having been used to map coral reefs since the beginning of the Landsat program (Smith *et al.,* 1975), they are considered the only approach capable of monitoring modern shallow coral reefs over large spatial scales (Fuad, 2010, Anderson and Gaston, 2013, Figueira *et al.,* 2015 and Purkis, 2017). *In-situ* or low altitude aerial photography is a low-cost, high resolution resource that can provide a synoptic view of large areas of reef for monitoring (Goodman *et al.,* 2013). When applied to photographs, optical intensity analysis, somewhat analogous to visual assessment, enables scale independent measurement of habitat differences, using the intensity of image pixels as a proxy for structural complexity. The technique is based on the observation that variable habitat substrates present variable optical intensities (Shumway *et al.,* 2007). The technique has been successful at distinguishing broad scale habitat differences between predominantly sand and rock marine environments in Lake Tanganika, but, is less successful at identifying

intermediate, mixed habitats. Furthermore, although optical rugosity correlates with fish biodiversity data, it is much less accurate at substrate identification than the rugosity index (Shumway, 2007). Consequently, despite demonstrating the potential of remote sensing technologies for providing rapid, broad scale marine habitat comparisons, optical intensity analysis is not suitable for monitoring small scale rugosity, especially at a colony scale, in highly heterogeneous coral reef environments.

More recently developed technologies have increased the capacity of remote sensing techniques to efficiently monitor coral reef rugosity at smaller scales. Light Detection and Ranging (LiDAR), for example, has revolutionised the way coral reefs are studied over much larger areas than can be captured in photographs used in optical intensity analysis (Goodman *et al.,* 2013). LiDAR uses repeat pulses of laser light beams to provide highly precise representations of complex topographic structures, including seafloor characteristics, at a rapid measurement rate of > 64 km^2/hr (Lefsky *et al.,* 2002, Knudby *et al.,* 2007, Costa *et al.,* 2009 and Goodman *et al.,* 2013). By accurately measuring the surface contour and direct geometric distance between consecutive elevation points along designated transects, LiDAR derived bathymetric data can represent the two variables of the rugosity index. Data from the Experimental Advanced Airborne Research Lidar (EAARL) device have resulted in accurate (< 1 m positional accuracy), large scale maps of reef rugosity for vast (> 3000 m 2) areas of the Biscayne National Park in the Florida Keys. These have successfully differentiated, rougher lagoonal patch reefs from outer bank reefs and allowed identification of eroded areas of Acropora Palmata corals (Wright and Brock, 2002 and Brock *et al.,* 2004).

Structural complexity and rugosity data can also be extracted from virtual transects created on LiDAR data derived demographic elevation models (DEM) and surface models (Goodman *et al.,* 2013). This is achieved by obtaining the ratio of seascape surface area to the 2D planimetric area, based on Dahl's (1973) surface index (Brock *et al.,* 2006, Kuffner *et al.,* 2007, Knudby *et al.,* 2007 and Wedding *et al.,* 2008). Such data has successfully allowed variable coral substrates to be distinguished on reefs. For example, rugosity index values obtained from a 1 m cell DEM have enabled differentiation between live,

massive and stony corals, as the main structural element of reefs in the Biscayne National Park, and dead coral and hard bottom constituents (Brock *et al.,* 2006). Similar data has been used to identify a relationship between rugosity and distance from reef slope edge, demonstrating that airborne LiDAR can detect broad scale reef rugosity, of the seafloor, as well as reef structure at a substrate scale (Kuffner *et al.,* 2007).

Despite these advantages, LiDAR derived rugosity has presented mixed results when correlated with fish biodiversity data and *in-situ* chain-tape rugosity. For coral habitats in the Biscayne National Park, in Southeast Florida, LiDAR rugosity only demonstrates weak ($r^2 < 0.2$) relationships with *in-situ* rugosity and fish biodiversity metrics (Brock *et al.,* 2004). This predominately results from the typical 0.8 – 2 m point sounding spacing permitted by current LiDAR airborne devices, providing topographic data at an insufficient resolution to capture fine scale rugosity relevant to fish behaviour (Brock *et al.,* 2004, Kuffner *et al.,* 2007, Knudby *et al.,* 2007 and Walker *et al.,* 2009). Conversely, in Hawaii, LiDAR rugosity calculated at a 4 m grid size had a strong ($r = 0.61$) relationship with *in-situ* rugosity and was a statistically significant predictor of fish abundance, species richness and biomass when calculated at multiple scales up to 25 m, in some cases explaining > 60 % fish presence at variable reef sites (Wedding *et al.,* 2008). These low rugosity resolutions would, however, be insufficient to differentiate individual coral colonies or assemblages strictly on the basis of their topographic variation.

LiDAR derived rugosity also suffers from scale dependency issues analogous to those of the rugosity index. The relationships identified between fish biodiversity and LiDAR derived rugosity weaken as DEM grid cell size increases, showing LiDAR rugosity accuracy to be affected by subjective choice of scale of measurement. It is also affected by the neighbourhood of cells considered in the rugosity calculation, as determined by kernel size (Kuffner *et al.,* 2007). Furthermore, LiDAR rugosity accuracy is dependent on the coral environment under investigation and LiDAR sensor performance in waters with variable depth and turbidity. Two key limitations of LiDAR also result from the low availability of commercial LiDAR systems, which prevent its widespread use, and inability to penetrate water ~ > 40 m. This decreases its applicability as a

globally standardised monitoring technique (Wedding *et al.,* 2008 and Costa *et al.,* 2009). Consequently, only in the future, with the development of higher spatial resolution devices, will LiDAR be sufficient to boost the predictive power of remotely sensed coral reef rugosity (Goodman *et al.,* 2013).

Non-optical remote sensing techniques

Traditionally, optical sensors such as LiDAR and photography have been the primary data sources for remote study of coral reefs, but the use of these sensors is limited to shallow and non-turbid waters. Non-optical techniques can overcome this by using alternative sensors to measure surface profiles and rugosity (Mumby *et al.,* 2004). Digital pressure gauges are non-optical, non-invasive, diver operated sensors that record (deep) seafloor bathymetry through the conversion of pressure measurements to consecutive depth differences along transects (Dustan *et al.,* 2013). Digital reef rugosity, quantified as the standard deviation of the sensor output, has been found to exhibit strong relationships with fish species richness around Menjangan Island, highlighting the methods potential for providing a quantitative measure of coral reef niche dimensionality. This could be improved if better performing statistics than S.D. are used (Dustan *et al.,* 2013). Despite the high precision and decimetre resolution of pressure gauge measurements, thus far, digital reef rugosity has showed no significant relationship with coral community structure or coral cover. Furthermore, the overall accuracy of pressure measurements are greatly affected by wave swell and human error in how closely the diver carrying the pressure gauge follows the transect line and reef contours (Dustan *et al.,* 2013).

In contrast, acoustic remote sensors use pulsing sound and / or multiple echo returns to record complex seabed and reef habitat topography, and geomorphological structures, as well as depth, roughness and hardness characteristics of the seafloor (Chivers *et al.,* 1990, Schiagintweit, 1993 and Costa *et al.,* 2009). They are unaffected by optical water properties and, similarly to digital pressure gauges, can be used in deeper waters (> 70 m) than optical remote sensing devices (White *et al.,* 2003, Mumby *et al.,* 2004 and Costa *et al.,* 2009). Ship based sonar has been widely used for seafloor bathymetric mapping of multiple marine ecosystems, including coral reefs

(Lundblad *et al.,* 2006, Costa *et al.,* 2009 and Bejarano *et al.,* 2010). In particular, seabed backscatter information collected using the RoxAnn acoustic system has been considered a useful, easy to employ and cost-effective proxy for coral reef rugosity where more complex surfaces generate higher backscatter (White *et al.,* 2003, and Bejarano *et al.,* 2010).

Acoustic roughness signatures have successfully distinguished variable coral benthic habitats from one another, including sand, mud and coral dominated environments (White *et al.,* 2003). Additionally, for Glovers Atoll reefs in Belize, RoxAnn roughness data was a significant predictor ($r^2 = 0.66$) of the rugosity index and of common species fish abundance. Both examples show acoustic rugosity to be a more comparable proxy for *in-situ* topographic complexity than LiDAR (Kuffner *et al.,* 2007 and Bejarano *et al.,* 2010). Despite this, acoustic roughness often remains a weaker predictor of fish abundance than *in-situ* chain-tape rugosity. In part, like LiDAR, this results from the large footprint (> 30 cm diameter, though typically 2-20 m) of the RoxAnn sensor which limits the resolution of the roughness data and its ability to detect subtle differences in refuge sites throughout complex reefs (Benjarano *et al.,* 2010). It also frequently requires data interpolation between points, adding a factor of error to the measurement and increasing uncertainty for measuring fine scale rugosity, especially at a coral colony scale (White *et al.,* 2003).

The capacity of acoustic roughness to differentiate between medium and high areas of structural complexity is also significantly limited compared with its ability to distinguish areas of low complexity from medium and high areas. At finer resolutions RoxAnn benthic classification has only achieved accuracies of 28 % compared with ground truth data, with acoustic signatures of variable benthic habitats having large standard deviations and considerable overlap with other classes (White *et al.,* 2003). This is potentially an effect of the variable performance of acoustic sensors resulting from the slope of reef (von Szalay and McConnaughey, 2002), depth of the ensonified area (Collins and Voulgaris, 1993), sediment type within heterogeneous habitats (Bejarano *et al.,* 2010) and distance from reef edge (Kuffner *et al.,* 2007). The sensors also have limited applicability in shallow waters due to their typical attachment to boats for

deployment and consequently are unable to monitor the reefs most at risk from disturbance (Mumby *et al.,* 2004, Bak *et al.,* 2005 and Costa *et al.,* 2009).

Data integration

The integration of multiple remote sensing techniques providing distinct but complementary data, may be a more promising option for reef monitoring, especially if *in-situ* data is used in combination with satellite imagery which provides high temporal (weekly) and spatial (< 0.5 m) resolution data (Hedley *et al.,* 2016). For example, a combination of IKONOS satellite imagery with acoustic bathymetric data has enabled the production of DEMs from which digital rugosity can be calculated as a digital rugosity index or as the bathymetric variance between DEM kernels, an additional proxy of structural complexity (Purkis *et al.,* 2007). The addition of IKONOS imagery permits areas of variable rugosity and substrate type to be visually characterised from the DEM, a technique that has previously enabled successful identification of patch reefs, *Porites* bommie fields, reef slopes, reef flats and areas of low rugosity in the Diego Garcia reef system (Riegl and Purkis, 2005 and Purkis *et al.,* 2007). At present, both acoustic data and the use of DEM derived rugosity present a number of previously discussed challenges, and current satellite data cannot capture imagery at a high enough resolution to discern the structure of finer scale habitats (Scopélitis *et al.,* 2010). However, this multimodal example highlights the potential advantages of combining data from multiple instruments for providing a more comprehensive and reasonable approximation of coral reef topography than one method can achieve alone (Purkis *et al.,* 2007).

Measuring rugosity in 3D

A longstanding critique of remote sensing and *in-situ* techniques for measuring rugosity is their reduction of the full dimensionality of coral reefs and ignorance of the coral ‘canopy’ effect whereby upper coral layers or tabular, planar growth forms obscure additional structures and microhabitats below (Goatley and Bellwood, 2011). Chain-tape (or wheel) and digital gauge methods aim to capture the spaces under coral overhangs and in non-vertical recesses, but in reality, only capture a maximum 2D profile of reef rugosity (Bejarano, 2010). Conversely, although LiDAR aims to represent 3D seafloor topography, the

DEMs produced capture only the surface contour elevation of reefs representative of 2.5D topography (Zawada *et al.,* 2010). This prevents the true measurement of corals as multidimensional 3D structures with variable crevices, holes and tunnels throughout each coral matrix (Richardson *et al.,* 2017). These reductions in dimensionality simplify data collection at a cost to the quality and accuracy of the resulting structural complexity measurements.

Recently, structure from motion (SfM) photogrammetry has provided a non-invasive solution for high resolution, fine scale and precise computerised 3D reconstruction of objects and environments (Westoby *et al.,* 2012, McCarthy and Benjamin, 2014 and Burns *et al.,* 2016). The technique uses advanced algorithms and overlapping (underwater) image sequences to produce 3D point cloud and mesh models which can be exported as Digital Terrain Models (DTM) and orthomosaics. From these, 'virtual' rugosity can be calculated at cm and mm scales as the ratio between the contoured 3D surface mesh and its orthogonal projection onto a defined plane or transect (Leon *et al.,* 2015, Friedman *et al.,* 2010 and 2012, McKinnon *et al.,* 2011, Fonstad *et al.,* 2013, Burns *et al.,* 2015, and Storlazzi *et al.,* 2016). Measuring the rugosity of coral reefs virtually allows researchers to control the spatial resolution and scale of the measurement, and efficiently measure rugosity across multiple-permutations of the entire model, as opposed to being restricted to one or two transects *in-situ* (Burns *et al.,* 2015 and Bryson *et al.,* 2017). This provides a more robust representation of rugosity for survey sites and decreases the effects of subjective 'chain' placement in heterogeneous environments (Burns *et al.,* 2015 and Storlazzi *et al.,* 2016).

SfM DTM derived rugosity is strongly correlated ($r^2 > 0.80$) with and shows high accuracy (> 90 %) when compared with *in-situ* rugosity (Friedman *et al.,* 2012, Ferrari *et al.,* 2016 and Young *et al.,* 2017). Ferrari *et al.,* (2016) identified a mean accuracy of 85.3 ± 6 % when the virtual rugosity of 17 transects laid across a 2 km DTM section of Glovers Atoll were compared with *in-situ* chain-tape measurement. The high resolution of SfM products allows a unique examination of coral colony level rugosity, either from creating accurate models of individual colonies or from using multiple SfM products in combination to isolate individual colonies reefscape models (Lavy *et al.,* 2015, Ferrari *et al.,*

2016). Burns *et al.,* (2015), for example, utilised a SfM generated orthophoto to identify, digitise and calculate the rugosity of individual coral colonies from a 0.5 cm DEM of 150m^2 of the French Frigate Shoals. Colony scale SfM rugosity has also been able to successfully distinguish between a variety of coral species, morphotypes and abiotic substrate (Burns *et al.,* 2015 and Ferrari *et al.,* 2016). These improvements, in rugosity measurement, are possible due to the high precision of SfM products that can capture complex over and/or under hangs in coral habitats that are often missed by aforementioned non-3D techniques (Friedman *et al.,* 2012). They also demonstrate the potential of SfM techniques for monitoring present *and* historical coral reef rugosity with consideration of precise structural changes related to individual coral species (Burns *et al.,* 2015), especially as recent SfM techniques can incorporate historic monocular imagery (Ferrari *et al.,* 2016).

Despite these advantages, a number of limitations are preventing the widespread use of SfM photogrammetry for rugosity monitoring. Many of these result from the multiple decisions researchers face during the data collection and complex SfM computer processing stages, which also limit valid cross-study comparisons of rugosity gained from SfM models (Burns *et al.,* 2015 and Bryson *et al.,* 2017). As exemplified in figure 1.3, each processing decision has implications for the accuracy of SfM products and any rugosity data extracted from them (Bryson *et al.,* 2013, Carbonneau and Dietrich, 2017 and Young *et al.,* 2017). Additional limitations include the natural increase of virtual rugosity with increasing model resolution and strong coral morphotype effect on model accuracy (Friedman *et al.,* 2012 and Storlazzi *et al.,* 2016). This includes a significant relationship between virtual rugosity error, the surface heterogeneity of a reef and dominant coral types present on it (Bryson *et al.,* 2013). Data processing for complex and coarse branching corals also requires more photographs for reconstruction and SfM processing time than for less complex corals (Courtney *et al.,* 2007, Lavy *et al.,* 2015, House *et al.,* 2016 and Raoult *et al.,* 2017). Although beneficial to use only the highest resolution and most accurate SfM products, these are more susceptible to noise and uncertainty (Friedman *et al.,* 2012). They also require a greater image input, higher performance computers and, again, more processing time (Leon *et al.,* 2015 and Raoult *et al.,* 2017). Consequently, the technique suffers from a trade-off

between model accuracy and resolution with available processing time which limits its use for rapid monitoring of large reef areas post-disturbance (Gonzalez-Rivero *et al.,* 2014 and Raoult *et al.,* 2017).

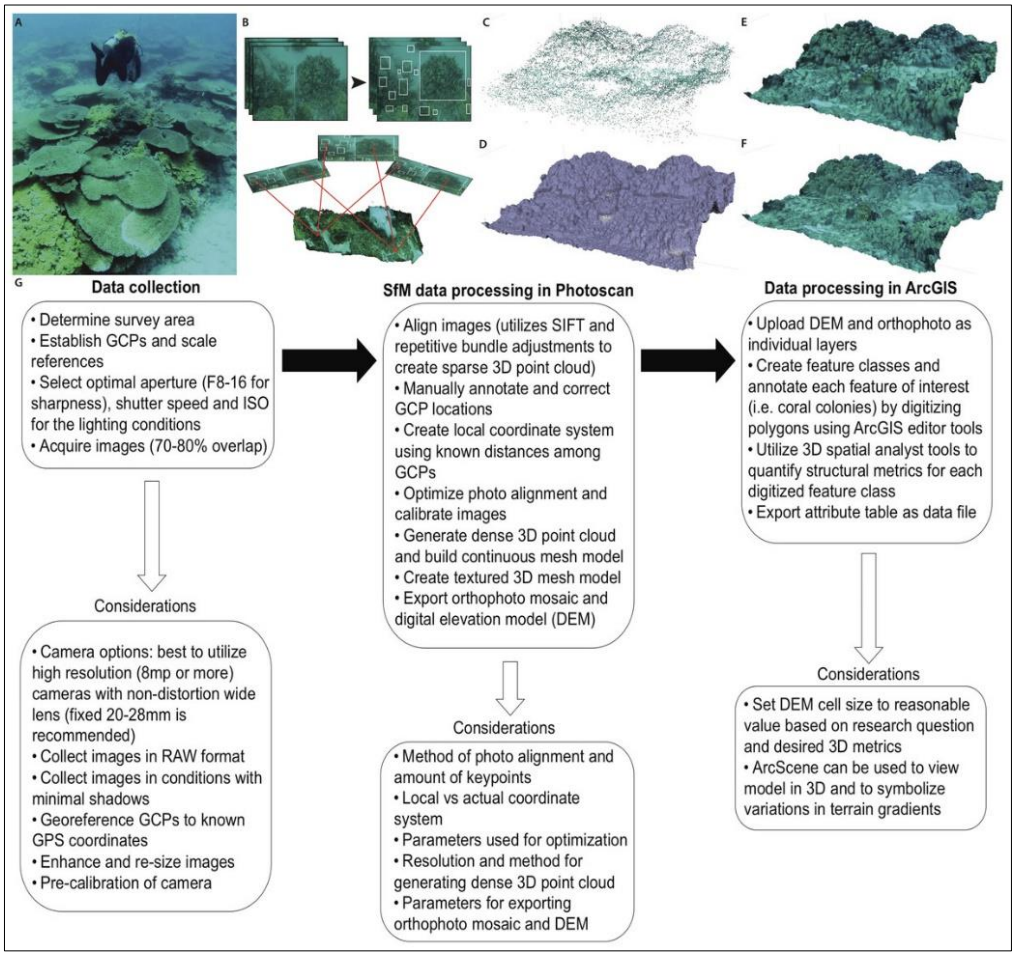

Figure 1.3. Primary steps and computer processing stages, requiring subjective choices from researchers, involved in a typical SfM workflow and their implications for subsequent processing stages (from Burns *et al.,* 2015, figure 1).

Any technique using SfM also has a high requirement for mathematical and programming knowledge and a high cost associated with the purchase and operation of stereo photogrammetry equipment required for photograph acquisition (Ferrari *et al.,* 2016). This is often mounted to expensive remotely operated or autonomous underwater robotic vehicles which demand extensive training experience are often restricted from monitoring the most critical shallow water coral reefs. (Brandou *et al.,* 2007, He *et al.,* 2012, Friedman *et al.,* 2012, and Burns *et al.,* 2015). This somewhat negates the advantages this technology

offers by being able to record images in deeper environments than permitted by aerial photography. Future advancements in SfM data acquisition and processing technology may improve processing times, usability by non-experts and reduce costs. However, at present the potential of SfM as a standardised and globally applicable transect and colony scale rugosity monitoring technique is limited by the SfM technology, limiting its usage to experts working over small reef areas (Figueira *et al.,* 2012, Gutierrez-Heredia *et al.,* 2016, Storlazzi *et al.,* 2016 and Young *et al.,* 2017).

Large scale rugosity monitoring

The growing use of Unmanned Aerial Vehicles (UAV) in ecological surveys could be a key development for increasing the spatial coverage of SfM, and other remote sensing techniques, due to their provision of large scale, high resolution aerial imagery (Anderson and Gaston, 2013 and Raoult *et al.,* 2017). Although a relatively new technique, fine scale, accurate SfM products have been produced from drone derived imagery for aquatic and coral reef ecosystems extending over areas in excess of 15 km^2. These include bathymetric maps and sub-centimetre resolution orthophotographs. When used in combination these allow broad scale analysis of habitat complexity and virtual rugosity (from bathymetric models) but, more importantly, identification of individual coral colony growth forms and, in some cases, their genera (Chirayath and Earle, 2016, Dietrich, 2017 and Casella *et al.,* 2017). These products, and therefore rugosity habitat surveys, have an incredibly high temporal resolution due to the ability for UAV surveys to be repeated at researcher selected time intervals as high as 20 minutes for areas < 1 km^2. This gives the technique an exceptionally high potential for use in rapid coral reef monitoring change detection work (Anderson and Gaston, 2013 and Casella *et al.,* 2017). With the continuing development of consumer grade small UAVs, which require little operational skill, drone derived rugosity could provide a cost-effective method for monitoring temporal change in reef structural complexity. If coupled with modelling approaches, this could help monitor the current coral reef crisis and predict future trajectories of the ecosystems (Purkis, 2017 and Casella *et al.,* 2017).

At present, however, the full potential of drone derived rugosity is not without significant drawbacks. The increase in spatial coverage permitted by UAV imagery increases data density and consequently processing time. SfM procedures using this data will present huge computational challenges requiring facilities unattainable at consumer, non-expert levels (Chirayath and Earle, 2016). More critically, UAV imagery is subject to multiple geo-referencing and distortion errors, in part resulting from ambient surface wave motion, which reduce image resolution (Dietrich, 2017 and Chirayath, 2014). Recently developed fluid lensing algorithms help correct these errors, but further increase data density and processing time. The algorithms are also limited in application by surface wave conditions, ambient irradiance and additional optical properties of the water column which distort UAV imagery. (Chirayath and Earle, 2016).

As a photographic method, UAV derived rugosity is a “top-down” technique and as such has a reduced ability to represent the internal habitat spaces within coral colonies, overhangs and recesses compared with *in-situ* measurement or SfM models derived from underwater imagery (Commito and Rusignuolo, 2000 and Friedman *et al.,* 2012). The principle disadvantages of drone derived rugosity are, however, those associated with SfM photogrammetry and the multitude of aforementioned propagative errors resulting from SfM data processing, its associated cost, time intensity and requirement of expert knowledge (Friedman *et al.,* 2012, Bryson *et al.,* 2013, Burns *et al.,* 2015, Lavy *et al.,* 2015, Storlazzi *et al.,* 2016, House *et al.,* 2016, Raoult *et al.,* 2017 and Young *et al.,* 2017). Consequently, at present there are compromises within and between imaging approaches used to gain rugosity information. Underwater camera and vehicle approaches can monitor deeper environments, but have many issues associated with SfM processing. UAV imagery, however, can provide high spatial coverage of shallow water coral reefs, but is limited to use in optimal surface conditions in clear, natural waters and does not capture the true 3D nature of coral colonies (Anderson and Gaston, 2013 and Chirayath and Earle, 2016).

The capabilities of remote sensing, especially using UAVs, for surveying coral reefs (and reef rugosity) are expected to increase with continued improvements in technology and computer algorithms (Hedley *et al.,* 2016). Yet, at present, it

appears that no single remote sensing instrument is able to provide optimally accurate rugosity data for all coral reef environments, spatial scales and purposes (Knudby *et al.,* 2007). Furthermore, due to their relative infancy compared with *in-situ* data collection, all remote sensing techniques still require the collection of ground truth data in some capacity to constrain or validate the rugosity measurements (Hedley *et al.,* 2016). This is often complex, unattainable at the large scales required and increases data collection time and cost – factors that remote sensing methods are intended to reduce (Harris *et al.,* 2015 and Hedley *et al.,* 2016). Such ground truth rugosity data is typically acquired using the chain-tape method (Wilson *et al.,* 2007), suggesting that at present this traditional technique is the preferred and optimal way of accurately measuring rugosity. This is validated by a meta-analysis revealing that 59 % of research examining habitat complexity used the rugosity index, compared to just 10.2 % of research using remote sensing methods, despite the numerous advantages they offer (Alvarez-Filip, 2009). Uncertainty therefore still persists with regard to the best technique for measuring rugosity. The rugosity index is accurate, but time consuming and limited to small areas, whereas SfM and UAV techniques can survey large areas, and individual coral colonies, but with reduced accuracy and additional requirements for expert knowledge and complex technology.

Combining multiple data sources

With consideration of the briefly aforementioned advantages of data combination (e.g. Purkis *et al.,* 2007 and Hedley *et al.,* 2016), a rugosity monitoring technique with real scope for overcoming this stalemate could be one that uses both remotely sensed and *in-situ* collected data. The combination of these sources mutually enhances the respective strengths of both and has been hypothesised as the ‘only realistic way’ to conduct broad scale, accurate habitat surveys (Davies *et al.,* 1997, Scopélitis *et al.,* 2010 and Hedley *et al.,* 2016). Previously, these data have been used in-tandem for advanced ecological characterisation and management of marine protected areas (Hedley *et al.,* 2016, Davies *et al.,* 1997). As an early example, Fuad *et al.,* (2010), used benthic habitat maps, created from visual interpretation of aerial imagery, and *in-situ* benthic coverage estimation to aid his survey site selection for rugosity and coral biodiversity measurement. This allowed a representative comparison

of rugosity across two reef sites in the Bunaken National Park. More recently, Hattori and Shibuno (2015) combined *in-situ* measurements of coral height with coral basal area and coverage measurements taken from high resolution aerial photography to calculate the volume of small patch reefs, used as a gross scale measure of rugosity, surrounding Shiraho Reef, Japan. The combination of photographs with *in-situ* field data also greatly enhances the potential of photography for reef monitoring (Goodman *et al.,* 2013).

Research using multiple data sources in combination could be advantageous for future rugosity measurement, however, the time intensive and human presence based nature of *in-situ* data collection will continue to present challenges for monitoring rugosity at entire coral ecosystem scales. There is still a large need for a rugosity monitoring technique that does completely replace the need for *in-situ* data collection whilst maintaining *in-situ* measurement levels of accuracy (Fuad, 2010 and Hedley *et al.,* 2016). One approach, that could eliminate the need for *in-situ* data, would be to establish a well constrained database of *in-situ* colony level rugosity data that could be readily applied to various benthic characteristics, substrates and coral colonies identified in imagery over large spatial scales. Such an approach may be even more advantageous if a relationship could be found between coral characteristics measureable from imagery and respective *in-situ* rugosity. Recent work by Richardson *et al.,* (2017) identified significant linear relationships between the maximum colony diameter and contour distance of three common coral taxa specific morphologies, for example. These coral size – rugosity relationships could be used to derive rugosity data from analysis of UAV or video camera imagery if the relationships are constrained and developed for more coral taxa.

The potential advantages of such taxa-specific database approaches have been demonstrated by work using mean coral species and genera rugosity data, to model coral community changes in the Caribbean and their subsequent effects on calcification (Alvarez-Filip et al,. 2013). Recently, González-Barrios and Alvarez-Filip (2018) combined mean coral species rugosity data, calculated from chain-tape rugosity measurements of > 500 colonies, with coral cover information and species calcification rates, for which a Caribbean database already exists (Perry *et al.,* 2013). From this, González-Barrios and Alvarez-Filip

(2018) were able to evaluate the functional status of selected Caribbean reefs. These examples highlight the potential of establishing and expanding the availability of standardised, species level rugosity data for coral reefs across the world. They also highlight the potential of combining multiples sources of *in-situ,* remotely sensed and model data for making substantial advances in coral reef rugosity monitoring (Goodman *et al.,* 2013). This research will consider the advantages offered by both approaches, of using genus level rugosity data and multiple data sources in combination, in the development of a new coral reef rugosity measurement technique. In doing this, the research will aim to overcome the current challenge of understanding how best to quantify and monitor coral reef structural complexity over large scales, at an ecologically relevant scale.

1.2 Rationale: The development of a new rugosity measurement technique.

The future trajectory of coral reefs is dependent on coral species specific rates of mortality in response to disturbance, erosion of structurally variable carbonate frameworks and the rate at which structurally important taxa are replaced by opportunistic species and macroalgae (Darling *et al.,* 2012, Alvarez-Filip *et al.,* 2013 and Bozec *et al.,* 2015). Given the accelerating rate of global coral reef degradation there is an urgent need to quantify and map the spatial variability of rugosity, as a proxy for structural complexity, at ecologically relevant scales (Zawada *et al.,* 2010 and Graham and Nash, 2013). So far, there has been a lack of quantitative species trait based methods within coral reef monitoring frameworks. These are important for determining life history strategies and coral response to future change (Westoby, 1998 and Darling *et al.,* 2012). The procurement of this information would significantly increase current knowledge regarding the impacts of disturbance, recovery capacity and trajectories of coral reef ecosystems in the future as framework building corals continue to die, rates of erosion overtake accretion and reefs eventually flatten (Hedley *et al.,* 2016 and Dustan *et al.,* 2013).

In a time of dwindling management resources the development of a simple technique to measure and monitor present rugosity, determine historical changes in structural complexity, and even predict future tipping points of coral reef environmental degradation is vital. If sufficient, it could also prove invaluable for providing the rapid response surveys often required after rapid onset disturbance events (Phinn *et al.,* 2012) and helping triage individual reefs for the most appropriate course of conservation and management (Dustan, 2013). Any new measurement technique should also take into consideration the contribution of individual coral colonies, their genus and morphology to the overall structural complexity of a coral reef (Hooper *et al.,* 2005 and Bozec *et al.,* 2015). This would greatly enhance the abilities and accuracy of reef management practices that have an emphasis on maintaining healthy populations of key reef structure building corals (Alvarez-Filip *et al.,* 2011).

This research aims to develop and explore the benefits of a new rugosity measuring and monitoring technique that uses coral colony scale rugosity data to accurately quantify rugosity for large areas of coral ecosystems at an ecologically relevant spatial scale. To achieve this, the research will create a database of coral colony rugosity data and apply this to various types of coral survey data as a prototype endeavour for future application to large scale UAV derived imagery.

To ensure its effectiveness, the new technique will be developed with consideration of criteria outlined by Hobson (1972) and Ferrari *et al.,* (2016) for, respectively, measuring surface complexity and accurate reef framework monitoring. These are outlined in table 1.1. As such, the technique will not only contribute to a much needed database of coral colony data, but also provide an urgently needed standardised means of monitoring rugosity across the world.

Table 1.1. Criteria set by Hobson (1972) and Ferrari *et al.,* (2016) to ensure that surface complexity and coral framework measuring and monitoring techniques are useful.

Hobson's (1972) criteria for ensuring the usefulness of a measure of surface complexity.	**Ferrari *et al.,* (2016) criteria for an accurate reef framework monitoring technique.**
The measure:	The technique:
1. Must be conceptually descriptive. 2. Must be easily measured in the field. 3. Must be capable of being measured and compared at a number of scales.	1. Must be efficient and cost-effective. 2. Must be applicable by non-experts. 3. Should ideally be applicable to historical data.

1.3 Overall aim

This research aims to develop a novel, accurate, time and cost-effective, Indo-Pacific applicable method for assessing and monitoring the rugosity of shallow coral reef ecosystems using coral colony level rugosity data.

1.4 Objectives

1. To develop a coral genus trait database containing coral colony level data from which taxa specific rugosity information can be extracted.
2. To identify whether coral colony rugosity is related to the life history strategies of respective coral genera.
3. To establish coral genera and morphotype specific relationships between coral colony size and rugosity for a range of common coral reef taxa.
4. To investigate a number of applications of the rugosity database for measuring rugosity.
   This will be achieved by applying any established coral colony size – rugosity relationship equations firstly to control video transect data from artificial coral reefs, and, subsequently to three mediums of *in-situ,* real world, coral reef survey data: (i) video transects, (ii) line intercept data and (iii) UAV imagery.

To achieve these objectives, this research thesis will be divided into three subsequent chapters. The next chapter (chapter 2) will explore the first three objectives concerned with establishing a coral rugosity trait database, whilst chapter 3 will explore the usefulness of the rugosity trait database with regard to gaining rugosity information from variable sources of coral reef survey data. Finally, chapter 4 will evaluate the developed rugosity measurement technique with reference to the criteria outlined by Hobson (1972) and Ferrari *et al.,* (2016).

Chapter 2. Establishment of a coral rugosity trait database

2.1 Study site

To establish a coral taxa specific rugosity database, the rugosity of coral colonies was measured on reefs surrounding Lizard and Heron Islands on the Great Barrier Reef, eastern Australia (figure 2.1). This data was supplemented with measurements of corals from the Natural History Museum's Indo-Pacific dry Invertebrate collection.

Lizard Island (14º40'S, 145 º27,E, elevation = ~395 m > MSL), with neighbouring Palfrey and South Islands, forms the Lizard Island group, a set of three late Permian granite continental Islands ~27 km from the Queensland coast (Rees *et al.,* 2006). The island is surrounded by fringing and platform reefs which enclose a lagoon with a maximum depth of 14 m (Pichon and Morrissey, 1981). The reef flat is largely degraded and dominated by soft and dead coral rubble, the reef edge and slope by hard corals, including *Porites cyclindrica*, and the shallow water fringing reefs along the north and south eastern shorelines, by *Acropora* spp. (Komyakova *et al.,* 2013 and Kleemann, 1996). The Island group has a tropical climate, austral summer wet season and a wave climate produced by prevailing south-easterly winds for 8 months of the year (Saunders *et al.,* 2015). The tidal range is ~3 m (Madin *et al.,* 2006 and Pichon and Morrissey, 1981).

Heron Island (23º25'S, 151 º55,E, maximum height = 7 m > MSL) is a vegetated, sand cay on the western side of a 28 km^2 platform reef, forming part of the Capricorn Bunker Group, ~80 km from Gladstone (Ahmad and Neil, 1994 and Jupp *et al.,* 1985). The Holocene platform of the modern reef top overlies submerged Pleistocene substrate, has a large central lagoon dominated by *Acropora* spp. and is isolated from the ocean at low tide (Santos *et al.,* 2011 and Ahmad and Neil, 1994). The platform emerges from 25 m water depth with a steep reef slope surrounded by a narrow intertidal crest. This encloses a shallow reef flat and sheltered back reef environment (Leon *et al.,* 2015). Prevailing winds are dominated by the south-easterly trade winds during the

austral winter and vary during the austral summer. The tidal range is 3.3m (Gourley and Jell, 1993).

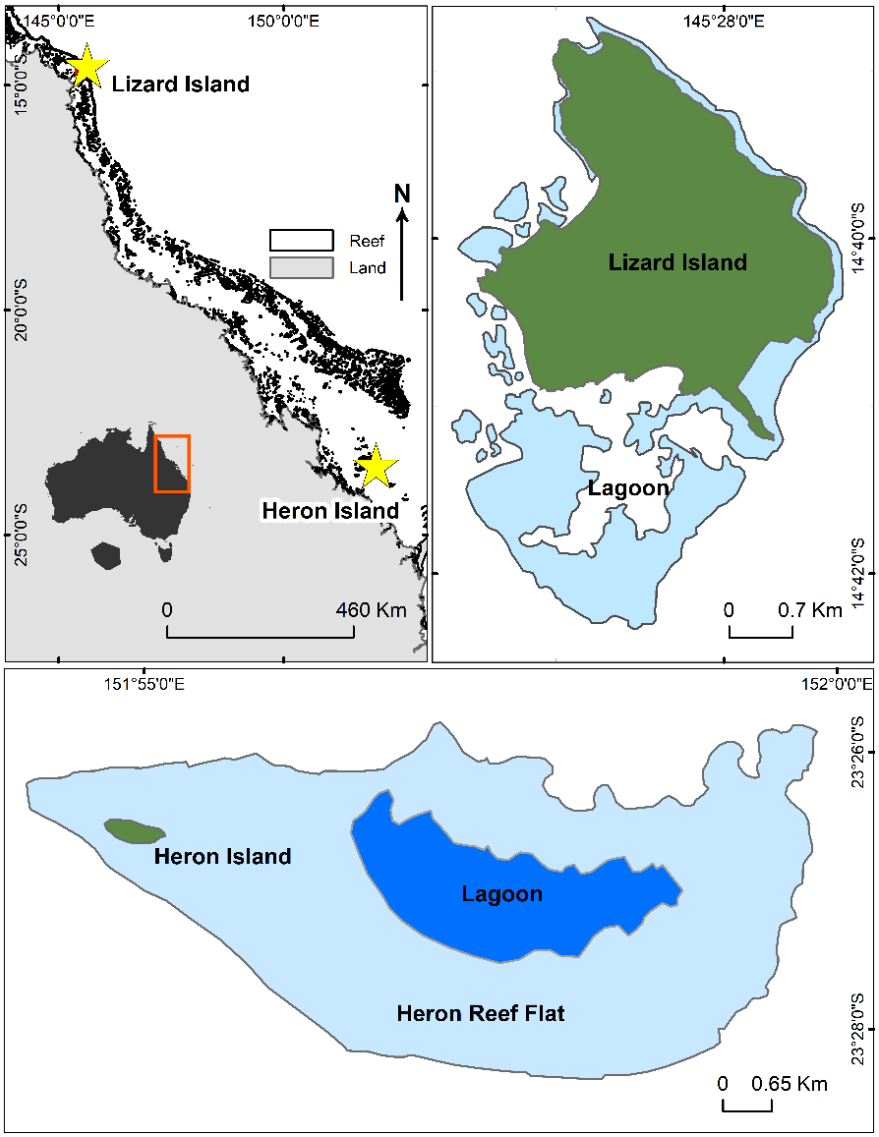

Figure 2.1. Study site map of Lizard Island and Heron Island on the Great Barrier Reef, eastern Australia - the locations of reefs on which coral colony rugosity data was collected.

2.2 Methods

Measuring coral colony rugosity

Structural complexity was represented by the rugosity index (Risk, 1972). The rugosity of > 800 individual coral colonies *in-situ* and from the NHM collections was measured using the traditional chain-tape technique (figure 2.2, Risk, 1972 and Knudby and LeDrew, 2007). In contrast to previous research, four rugosity measurements were taken from each colony across the length, width, and two diagonal diameter profiles to best represent the structural profile of each coral. The contour distance of each profile was measured by draping a fine, 0.5 cm link length chain over the coral colony in a straight line. Absolute care was taken to ensure the chain followed the exact topographic profile, poking it into every crack, crevice and groove forming the complex surface structure. The respective planar lengths of each profile were measured with a tape measure and the rugosity index calculated as the ratio between each contour and respective planar distance (Risk, 1972). The rugosity of a range of abiotic substrates (sand and coral rubble), also present on coral reefs, was measured using the rugosity index, as the ratio between the contour chain distance and a 1 m pipe (planar length) for multiple samples. All corals were photographed, identified to a genus level and their morphology noted.

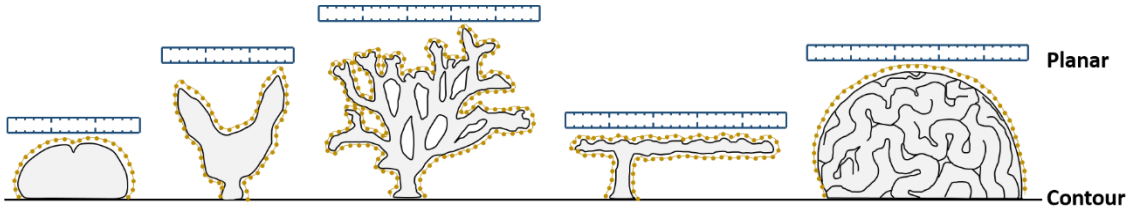

Figure 2.2. Representation of the rugosity index, measured using the chain-tape method, for individual coral colonies. From left to right, coral morphologies represented are free-living, vase, branching, tabular and massive. The gold studded line represents the chain and, the rulers the planar lengths. Coral colony rugosity = contour length / planar length.

Creation of a coral rugosity trait database

Coral colony rugosity data was used in the creation of a coral rugosity trait database that groups corals by genus and morphotype. Each genus was assigned a morphotype with the aid of English and Wilkinson (1994) coral lifeform categorisation and the Coral Trait Database (Madin *et al.,* 2016). Corals of the same genus that exhibited variable morphologies were further sub-divided into different categories to ensure the rugosity of each group was completely representative of the corals within it. For example, *Coscinaraea* was categorised into massive, encrusting and submassive corals. Coral colonies identified as *Acropora* or *Porites* genera were excluded from the overall morphotype groupings due to the broad range of genus specific, and readily recognisable morphologies these corals exhibit. This was partly in accordance with UNEP/AIMS (1993) coral lifeform categories. A summary of the coral morphotype groupings and abiotic substrates included in the database is provided in table 2.1. The mean rugosity of each coral genus and morphotype was calculated as the total sum of rugosity for each taxa divided by the number of colonies sampled in each group.

Table 2.1. Coral morphotype and abiotic substrate categories, with description, represented in the rugosity trait database.

Hard Coral	**Description**
Acropora	
Acropora Branching	Staghorn corals, long thin branches.
Acropora Corymbrose	Stout branches or flat topped clumps with a low bushy shape forming small tables or plates.
Acropora Digitate	Digitate, thick, stubby branches, usually regular and upright with dome shape corallites.
Acropora Hispidose	Colonies composed of prostrate, intertwined bottlebrush open branches.
Acropora plates and tables	Flat tables or plates with thin, short, fine and upwards (occasionally outwards) projecting branches stemming from a central or side attached leg. Mainly *A. efflorescens* or *A. cytherea.*
Porites	
Porites compressa	Cylindrical branches, commonly fused with rounded tips.
Porites cyclindrica	Spire like open branches.
Porites lobata	Hemispherical or helmet shaped massive corals.
Porites unknown	Short and stubby clustering branches with rounded tips.
Porites rus	Contorted or anastomosing branches, often clustered.
Other coral	
Branching	Open and closed branching coral often tapered, arborescent or clustered with rounded or spire like tips.
Large branching	Upright, flattened and widely separated, open branches. Mainly *Pocillopora eydouxi*.

Columnar	Forming separate columns, sometimes club shaped.
Massive	Hemispherical, solid, dome corals that have a similar shape in all directions.
Foliose	Colonies are irregular clusters of fluted, flat laminae, with thin, contorted, bifacial, upright fronds. Leafy or lettuce like appearance.
Mixed contorted	Mixed branch and plate morphologies form (often contorted) individual colonies. Mainly *Merulina ampliata.*
Submassive	Multi-lobate or "lumpy" corals. Tend to form small columns, knobs or wedges or can be mixed massive columnar.
Encrusting	Colonies overlie or attached to the substratum and often have low relief.
Flabello-meandroid	Massive / hemispherical colonies with phaceloid to meandroid, to flabello-meandroid morphologies and valleys with separate walls from adjacent valleys.
Single plates	Single plates, stemming horizontally outwards from a central or side branch sometimes covered with verrucae.
Contorted laminar	Thin sheets, laminae or elongate, upright bifacial fronds often forming vase- shaped colonies and whorls.
Free-living	Solitary circular to oval and dome shaped free-living corals with rounded ends.
Micro-atoll	Circular flat topped coral, dead on top and living around the perimeter.
Algae covered coral	
Branching coral	Recently dead coral with structure still intact and some colonisation by algae.
Other colonies	Dead coral covered in algae with little or no structure remaining.
Soft coral	
Soft coral	Soft bodied, non-calcareous corals.
Abiotic features	
Reef pavement	Limestone pavement.
Coral rubble	Continuous rubble, unconsolidated, dead branching and other coral fragments.
Rubble : Sand = 3:1	Coral rubble dominates space in-between sand and shell fragments.
Rubble : Sand = 1:1	Space is a mix of half sand and half coral rubble.
Sand 1 – low ripple	Sand, mainly flat, no contours.
Sand 2 – bioturbated (small)	Sand with small (< 10 cm high) ripples and grooves
Sand 3 – bioturbated (large)	Bioturbated sand with large (> 10 cm) peaks and troughs
Other taxa	
Clam	Giant clams

Coral life history strategies

To examine any relationship between coral rugosity and coral functional group, each coral genus was assigned a life history strategy (competitive, weedy, generalist or stress tolerant) in accordance with those identified for a range of corals by Darling *et al.,* (2012). For genera not included in Darling *et al* (2012) analysis or, where genera had been subdivided by morphotype, the life history strategy was newly assigned based on its morphotype whereby competitive corals tend to have branching and platy morphologies, and stress-tolerant corals have massive or encrusting morphologies (Darling *et al.,* 2012). The

coral rugosity database was further grouped by life history strategy and more broadly as fast (competitive) and slow growing (weedy, generalist and stress tolerant) corals. The mean rugosity for each of these groups was calculated and a one-way ANOVA used to determine any significant difference in rugosity between the life history strategy groups.

Coral size - rugosity relationships

For each genus and morphotype, the planar and contour lengths of each coral were plotted against one another to investigate any relationship between measurable coral characteristics and coral rugosity. Linear regression analysis was conducted, using *Stata,* to explore the nature, strength and significance of any relationship between coral colony size, represented by planar length, and rugosity, represented by contour length, for each genus and morphotype. The regression analysis ($y = mx$) was run with a suppressed intercept due to the impossibility for coral colonies to have a negative size or rugosity. Statistical tests were not performed for every coral genus to test whether the data met the assumptions required for linear analysis. However, based on the practical assumption that the coral contour distance would increase with coral size, as initially demonstrated by Richardson *et al.,* (2017), and visual analysis of the line of best fits applied in Excel, linear regression was deemed as suitable for this exploratory analysis (McCarroll, 2016).

2.3 Results

Creation of a coral rugosity trait database

The rugosity of 3028 coral profiles representing 40 coral genera, 14 coral morphotypes, 9 abiotic reef substrates, and giant clams were measured and recorded in a new coral rugosity trait database. Mean rugosity varied between coral genera (m = 1.27, S.D. = 0.17 for encrusting *Acanastrea* to m = 3.84, S.D. = 0.29 for vase shaped *Merulina*) and coral morphotype (m = 1.37, S.D. = 0.3 for free-living corals, to m = 3.44, S.D. = 0.68 for laminar contorted corals). The mean rugosity of the corals and abiotic substrates included in the rugosity database are summarised in table 2.2.

Table 2.2. Summary of the coral genera, morphotypes and abiotic substrate represented in the rugosity trait database with key summary information. *n* represents the number of each coral or substrate sampled, r^2 represents the correlation coefficients from the coral size-rugosity relationships and m, represents the respective gradients from these relationships.

Reef taxa or substrate **Acropora**	**Morphotype**	***n* =**	**Mean Rugosity**	**S.D.**	**r^2**	**m =**
Acropora branching	Branching	141	3.36	0.80	0.91	3.24
Acropora (stubby branches)	Plates and tables	21	2.12	0.29	0.85	2.07
Acropora (flat plate)	Plates and tables	40	2.20	0.61	0.47	2.08
Acropora (outwards branching)	Plates and tables	28	1.64	0.32	0.78	1.58
Acropora corymbrose	Corymbrose	130	2.27	0.73	0.44	2.18
Acropora digitate	Digitate	79	2.54	0.87	0.56	2.75
Acropora hispidose	Hispidose	11	2.27	0.54	- 0.66	2.06
Porites						
Porites compressa	Branching	6	2.38	0.43	0.49	2.25
Porites cyclindrica	Branching	76	2.60	0.58	0.94	3.08
Porites lobata	Massive	105	2.03	0.57	0.78	1.93
Porites unknown	Stubby branching	37	1.83	0.32	0.84	1.83
Porites rus	Contorted branching	18	2.84	0.90	0.33	2.40
Coral Genera						
Acanthastrea	Encrusting	36	1.27	0.17	0.64	1.23
Acanthastrea	Massive	32	1.56	0.24	0.72	1.57
Alveopora	Columnar	28	3.02	0.84	0.03	2.81
Astreopora	Encrusting	20	1.39	0.33	0.75	1.46
Astreopora	Massive	41	1.50	0.33	0.76	1.33
Coscinaraea	Encrusting	12	1.76	0.61	0.24	1.76
Coscinaraea	Massive	32	1.83	0.34	0.77	1.90
Coscinaraea	Submassive	10	1.53	0.29	0.94	1.57
Diploastrea	Massive	29	2.06	0.62	0.80	1.95
Diploria	Massive	80	1.85	0.31	0.83	1.84
Echinopora	Branching	23	2.69	0.42	0.75	2.63
Favia	Massive	80	1.83	0.30	0.93	1.83

Favites	Massive	92	1.74	0.39	0.79	1.81
Fungia	Free-living	52	1.28	0.20	0.73	1.28
Galaxea	Encrusting	16	1.33	0.16	0.89	1.33
Galaxea	Massive	80	1.71	0.26	0.82	1.76
Goniastrea	Massive	51	1.83	0.28	0.88	1.85
Goniopora	Massive	48	2.07	0.42	0.86	2.08
Heliopora	Fossil branching	8	2.06	0.79	-2.86	1.75
Herpolitha	Free-living	53	1.43	0.34	0.79	1.39
Isopora	Branching	30	2.50	0.67	0.62	2.06
Leptastrea	Encrusting	60	1.97	0.47	0.67	1.92
Leptastrea	Massive	72	2.03	0.39	0.71	2.00
Leptastrea	Submassive	20	1.99	0.38	0.48	1.94
Leptoria	Massive	52	1.75	0.44	0.02	1.51
Leptoria	Submassive	36	1.90	0.44	0.87	1.85
Lobophyllia	Flabello-meandroid	55	2.10	0.78	-0.13	1.77
Merulina	Mixed	64	2.05	0.51	0.80	2.16
Merulina	Contorted laminar	8	3.84	0.29	0.81	3.84
Montipora	Branching	66	2.81	0.93	0.49	2.57
Montipora	Plates and tables	37	2.00	0.48	0.74	2.11
Montipora	Contorted laminar	5	3.79	0.30	0.86	3.82
Mussa	Flabello-meandroid	8	2.10	0.28	0.46	2.11
Oulophyllia	Massive	28	1.96	0.40	0.74	1.97
Pachyseris	Plates and tables	43	2.00	0.85	0.56	1.79
Pavona	Encrusting	24	1.49	0.30	0.73	1.37
Pavona cactus	Foliose	100	2.88	0.73	0.60	2.92
Pavona clavus	Columnar	30	2.67	0.78	0.52	2.61
Pectina	Foliose	110	2.43	0.51	0.10	2.33
Platygyra	Massive	108	1.87	0.48	0.73	1.63
Pocillopora	Stubby branches	50	2.42	0.42	0.75	2.38
Pocillopora	Large open branches	44	3.54	0.85	0.69	3.72
Psammocora	Foliose	40	2.49	0.43	0.69	2.49
Sandolithia	Free-living	43	1.40	0.32	0.74	1.45
Seriatopora	Branching	60	2.46	0.60	0.58	2.49
Stylophora	Branching	69	2.80	0.68	0.59	2.67
Symphyllia	Flabello-meandroid	94	2.12	0.38	0.95	2.23
Trachyphyllia	Flabello-meandroid	80	2.57	0.40	0.55	2.55
Turbinaria (vase)	Contorted laminar	6	2.31	0.16	0.93	2.35
Turbinaria	Contorted laminar	55	3.56	0.66	0.89	3.63
Turbinaria	Plates and tables	15	2.40	0.31	0.67	2.34
Soft Coral						
Sinularia	Columnar	15	1.62	0.57	0.32	1.47
Lobophytum - Sacrophyton	Lettuce like	44	1.55	0.39	0.81	1.50
Lobophytum	Columnar	23	2.05	0.53	0.66	2.14
Coral Morphotypes						
Branching		302	2.61	0.71	0.66	2.48
Acropora Plates and tables		89	2.01	0.53	0.73	1.94
Columnar		58	2.84	0.82	0.46	2.68
Contorted laminar		86	3.44	0.68	0.87	3.50
Encrusting		191	1.64	0.52	0.71	1.62

Flabello-meandroid	237	2.27	0.55	0.76	2.02
Free-living	148	1.37	0.30	0.81	1.39
Foliose	250	2.62	0.63	0.50	2.61
Massive	829	1.83	0.41	0.85	1.78
Mixed contorted	68	1.99	0.55	0.79	2.18
Micro-atoll	9	2.23	0.51	0.62	2.09
Plates and tables	95	2.06	0.67	0.61	2.00
Submassive	74	1.85	0.46	0.88	1.84
Soft coral	82	1.70	0.51	0.61	1.61
Acropora Digitate and Corymbrose	209	2.36	0.89	0.46	2.32
Algae covered coral					
Branching coral	11	2.79	0.34	0.93	2.77
Other colonies	27	2.13	0.44	0.54	2.04
Giant clam					
Clam	15	2.03	0.44	-0.18	1.89
Abiotic substrate					
Coral rubble	20	1.16	0.11		
Rubble 1:1 Sand	9	1.29	0.13		
Rubble 3:1 Sand	20	1.31	0.07		
Limestone Pavement	7	1.39	0.05		
Sand 1 – low ripple	16	1.02	0.02		
Sand 2 – bioturbated (small)	20	1.07	0.05		
Sand 3 – bioturbated (large)	16	1.12	0.03		

Establishing coral size – rugosity relationships

Colony level analysis at both a genus and morphotype level, presented in figure 2.3, revealed positive correlations between the planar and respective contour lengths of coral colonies – correlations representative of a relationship between coral colony size and the coral colony's rugosity (summarised in table 2.2). When examined at a genus level, 77 % of these relationships were moderate to strong with r^2 values > 0.5. The strongest relationships, where $r^2 > 0.9$, were shown by branching *Acropora* (figure 2.3.1e), submassive *Coscinarea* (figure 2.3.13b), *Favia* (figure 2.3.10g)*, Porites Cylindrica* (figure 2.3.2b), *Symphyllia* (figure 2.3.7d) and vase shape *Turbinaria* (figure 2.3.5e). *Heliopora* (figure 2.3.15a)*, Acropora Hispidose* (figure 2.3.1h) and *Lobophyllia* (figure 2.3.7b) demonstrated the weakest correlations ($r^2 < 0$) between the two variables. At a morphotype level, columnar coral (figure 2.3.4a) was the only morphotype category where the correlation between colony planar and contour length was less than 0.5 ($r^2 = 0.46$). All other relationships were moderate to strong with the strongest presented by submassive corals ($r^2 = 0.88$, figure 2.3.13a). Linear

regression revealed all coral size - rugosity relationships for both coral genera and morphotypes as significant at a $p < .05$ confidence level. The individual results of this regression analysis, for all taxa, can be found in Appendix A.

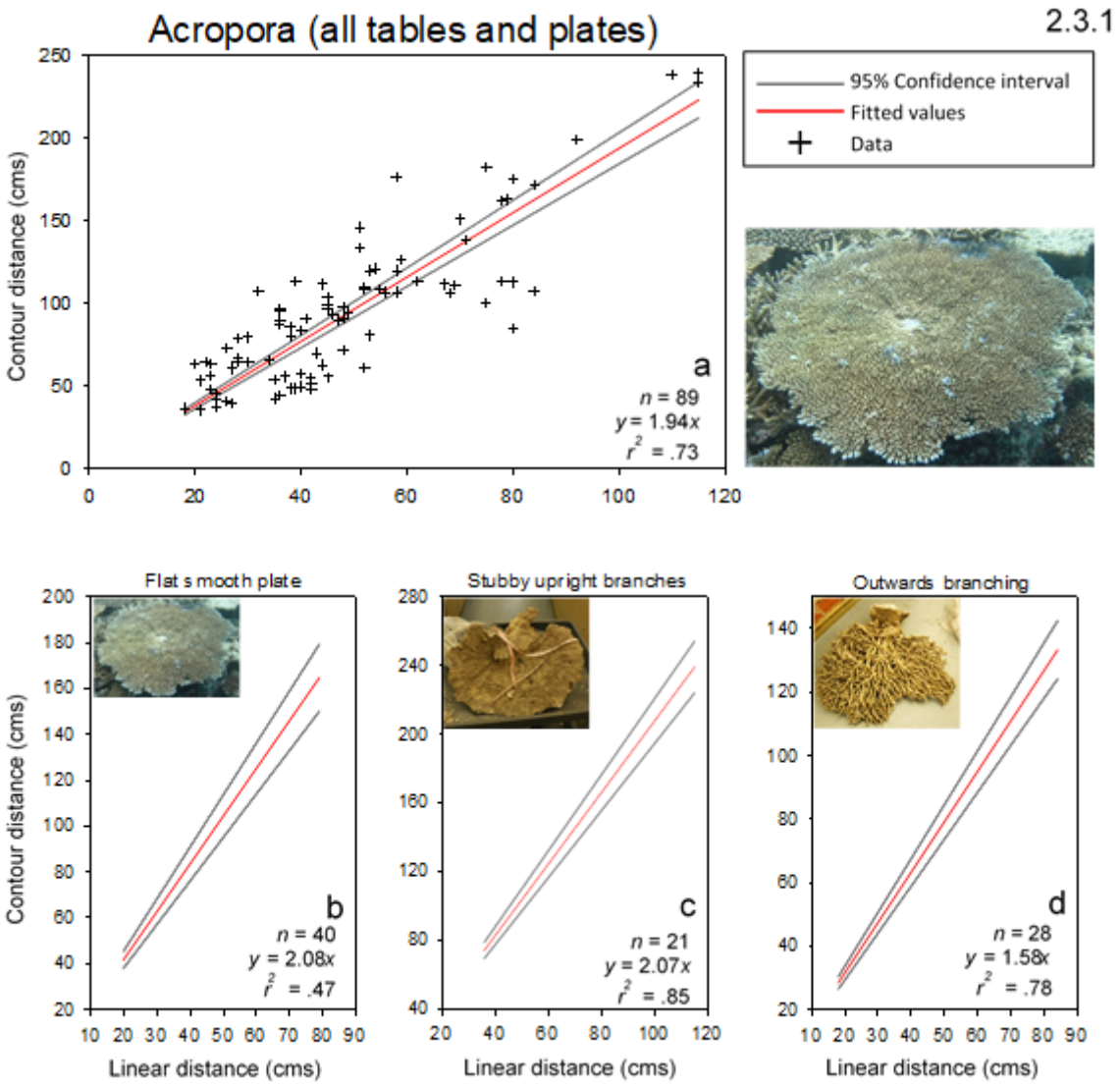

Figure 2.3. (following on pages 49-66) Size vs rugosity relationships for the coral genera, morphotypes and substrate represented in the rugosity database, plotted as confidence intervals (95 %). Size is represented by linear distance and rugosity by contour distance. The sample size (n), linear equation and r^2 value for each graph are shown with a representative image of each taxa. The figure is divided into 2.3.1-17 based on coral morphotype or substrate: 1. *Acropora* plates and tables and other *Acropora* morphotypes, 2. *Porites* morphotypes, 3. branching corals, 4. columnar corals, 5. contorted laminar corals, 6. encrusting corals, 7. flabello-meandroid corals, 8. foliose corals, 9. free-living corals, 10. massive corals, 11. mixed contorted corals, 12. plates and tables (non-Acropora), 13. submassive corals, 14. soft corals, 15. corals not included in other morphological groups, 16. algae covered coral and 17. molluscs. Specific coral genus, morphotype or substrate are indicated above each graph and are referred to in subsequent text using the letter on the graphs.

Genus: Acropora, additional morphotypes

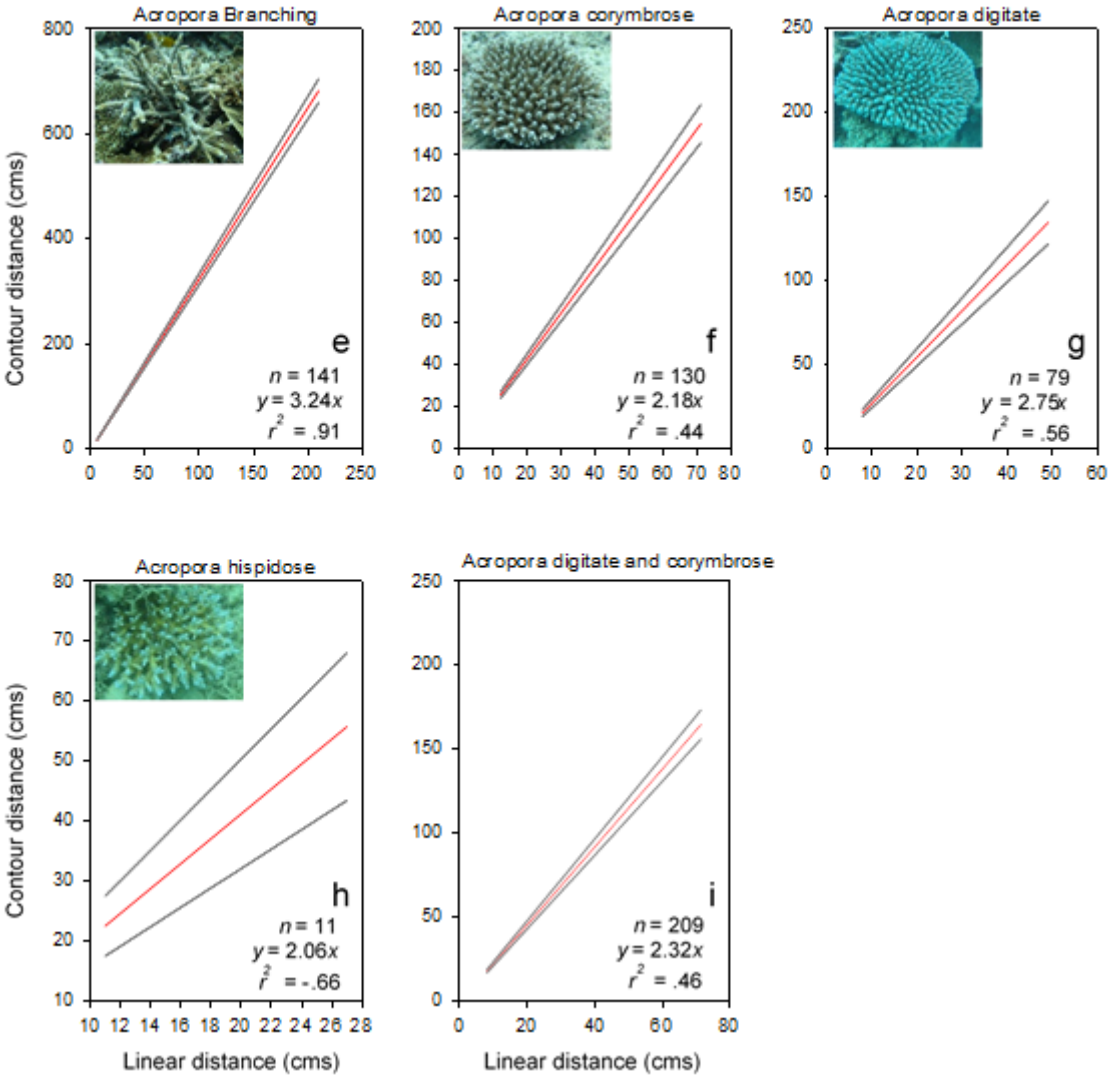

Genus: Porites

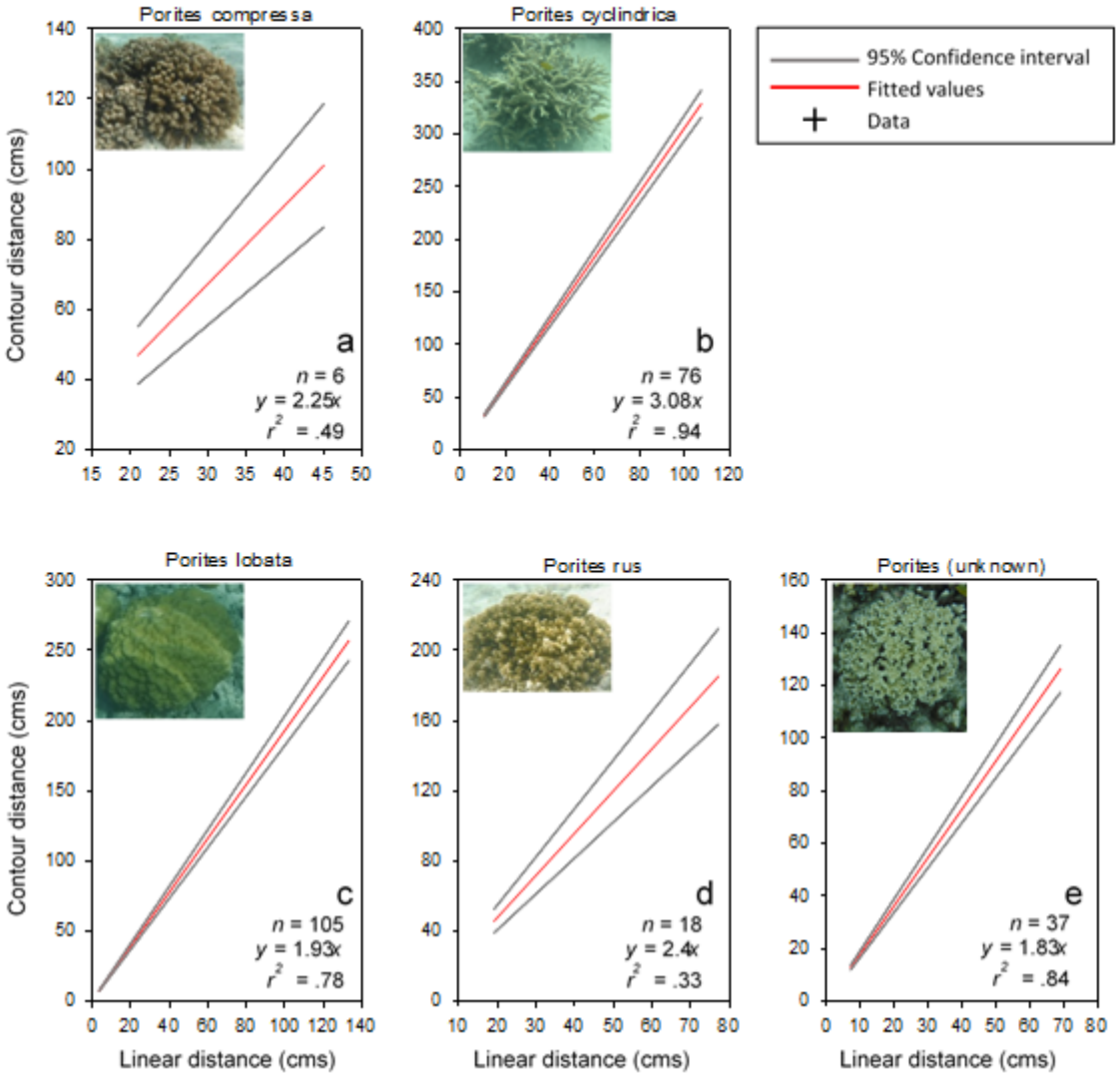

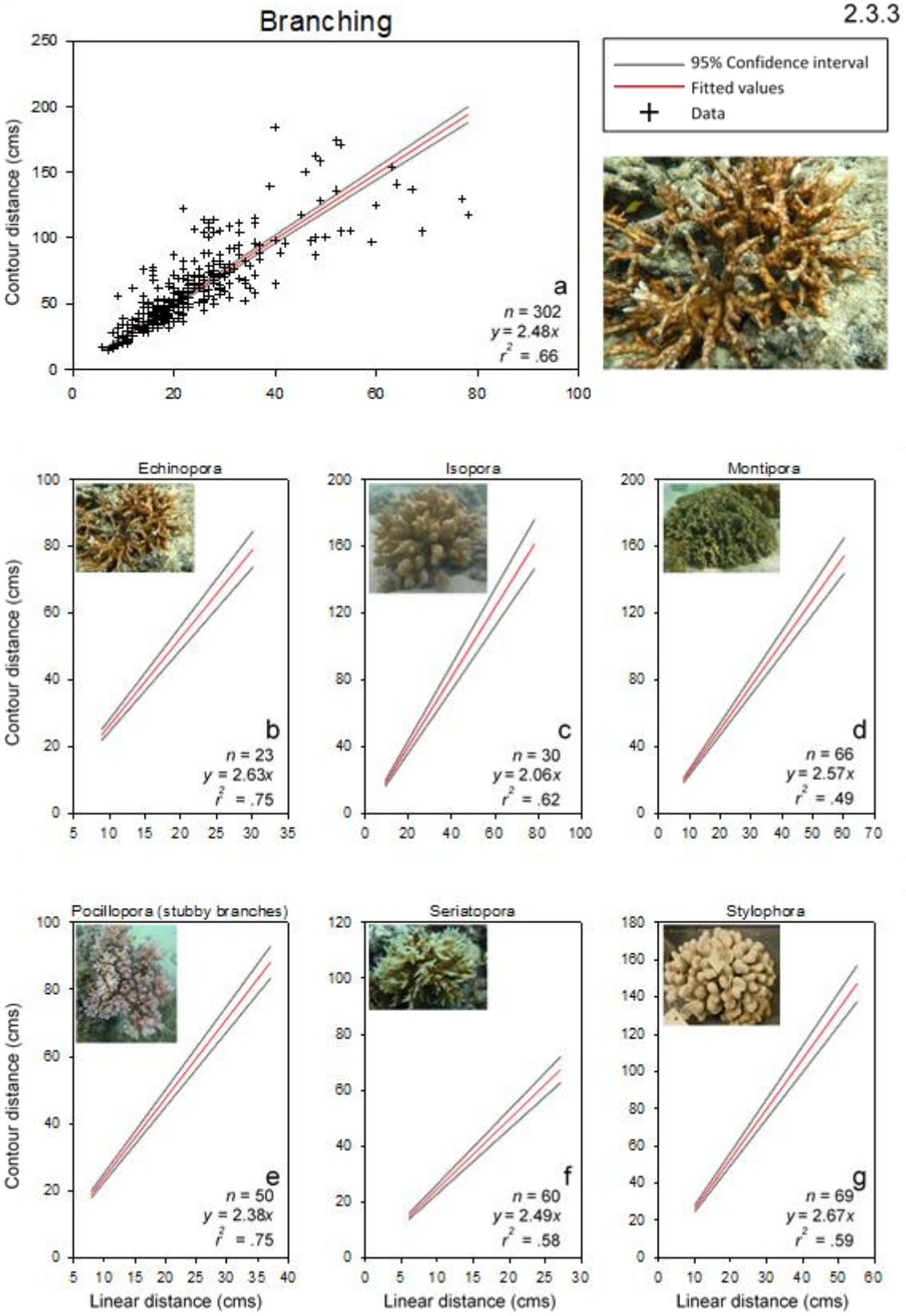
Branching
95% Confidence interval
Fitted values
Data
Contour distance (cms)
a
n = 302
y = 2.48x
r² = .66
Echinopora
b
n = 23
y = 2.63x
r² = .75
Isopora
c
n = 30
y = 2.06x
r² = .62
Montipora
d
n = 66
y = 2.57x
r² = .49
Pocillopora (stubby branches)
e
n = 50
y = 2.38x
r² = .75
Seriatopora
f
n = 60
y = 2.49x
r² = .58
Stylophora
g
n = 69
y = 2.67x
r² = .59
Linear distance (cms)

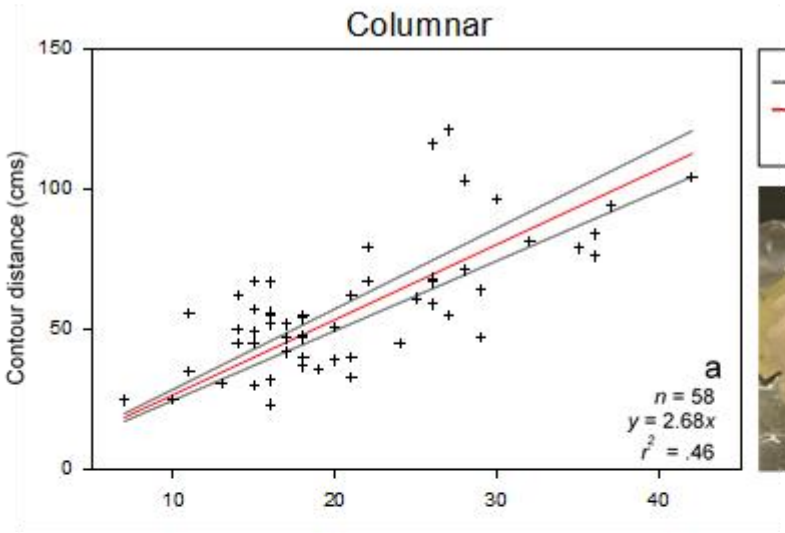
Columnar
Contour distance (cms)
150
100
50
0
10
20
30
40
a
n = 58
y = 2.68x
r² = .46
95% Confidence interval
Fitted values
Data

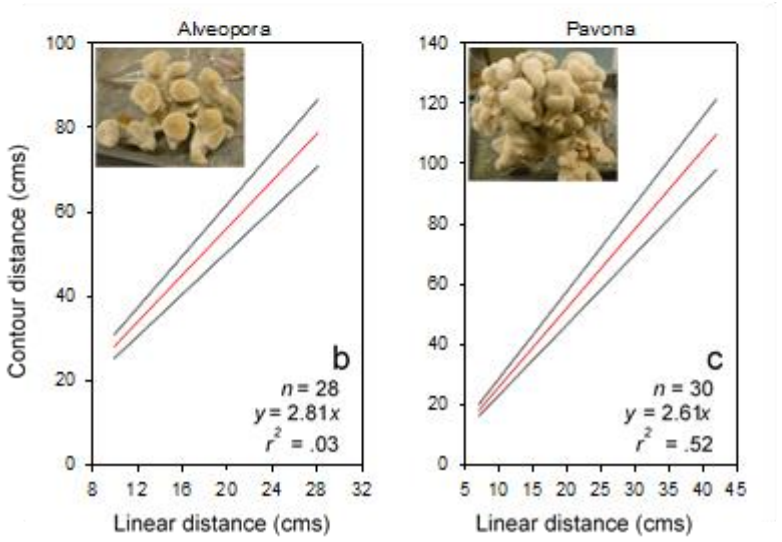
Alveopora
Pavona
Contour distance (cms)
100
80
60
40
20
0
b
n = 28
y = 2.81x
r² = .03
8
12
16
20
24
28
32
Linear distance (cms)
140
120
100
80
60
40
20
0
c
n = 30
y = 2.61x
r² = .52
5
10
15
20
25
30
35
40
45
Linear distance (cms)

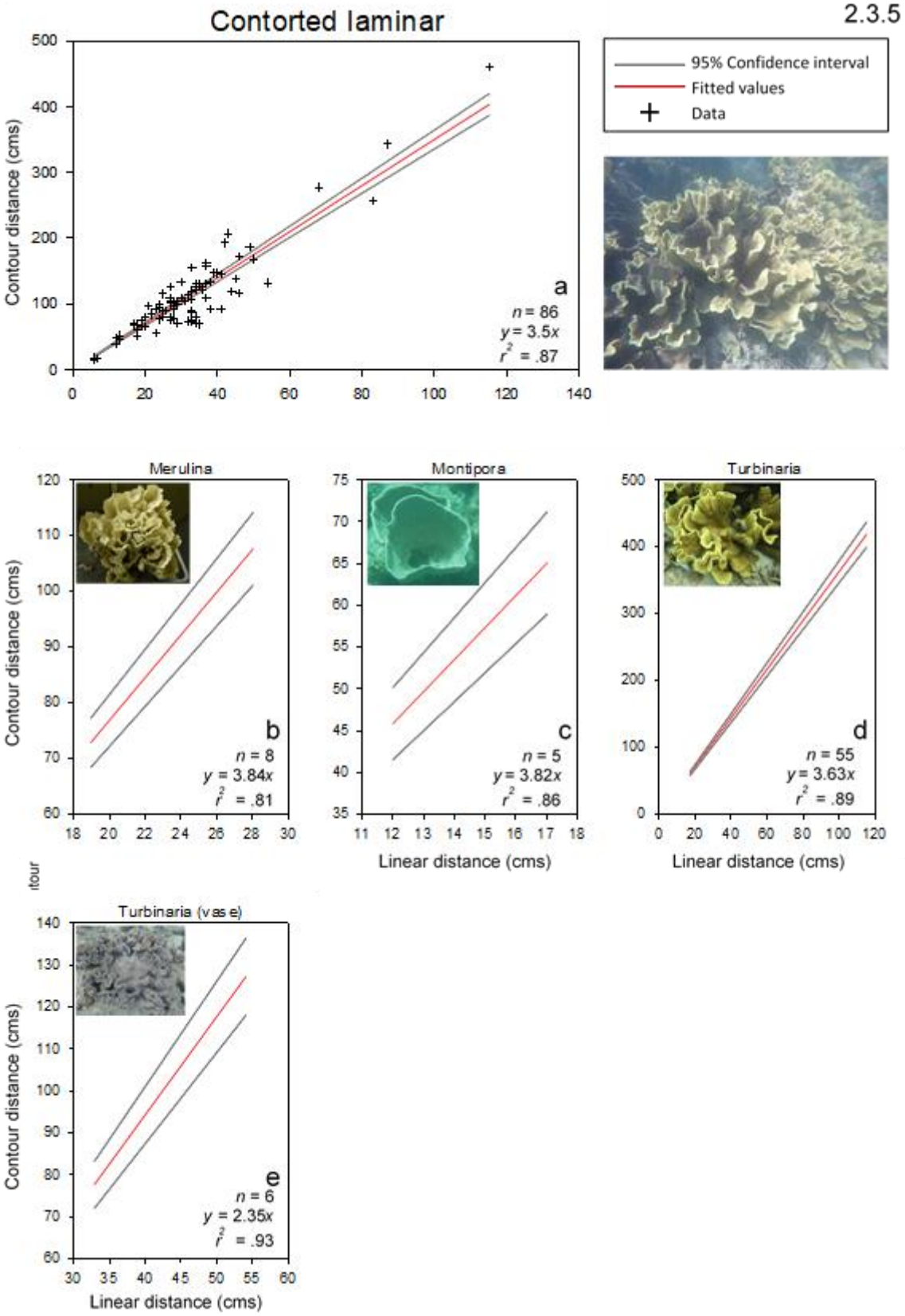
Contorted laminar
95% Confidence interval
Fitted values
Data
Contour distance (cms)
a
n = 86
y = 3.5x
r² = .87
Merulina
b
n = 8
y = 3.84x
r² = .81
Montipora
c
n = 5
y = 3.82x
r² = .86
Turbinaria
d
n = 55
y = 3.63x
r² = .89
Linear distance (cms)
Turbinaria (vase)
e
n = 6
y = 2.35x
r² = .93

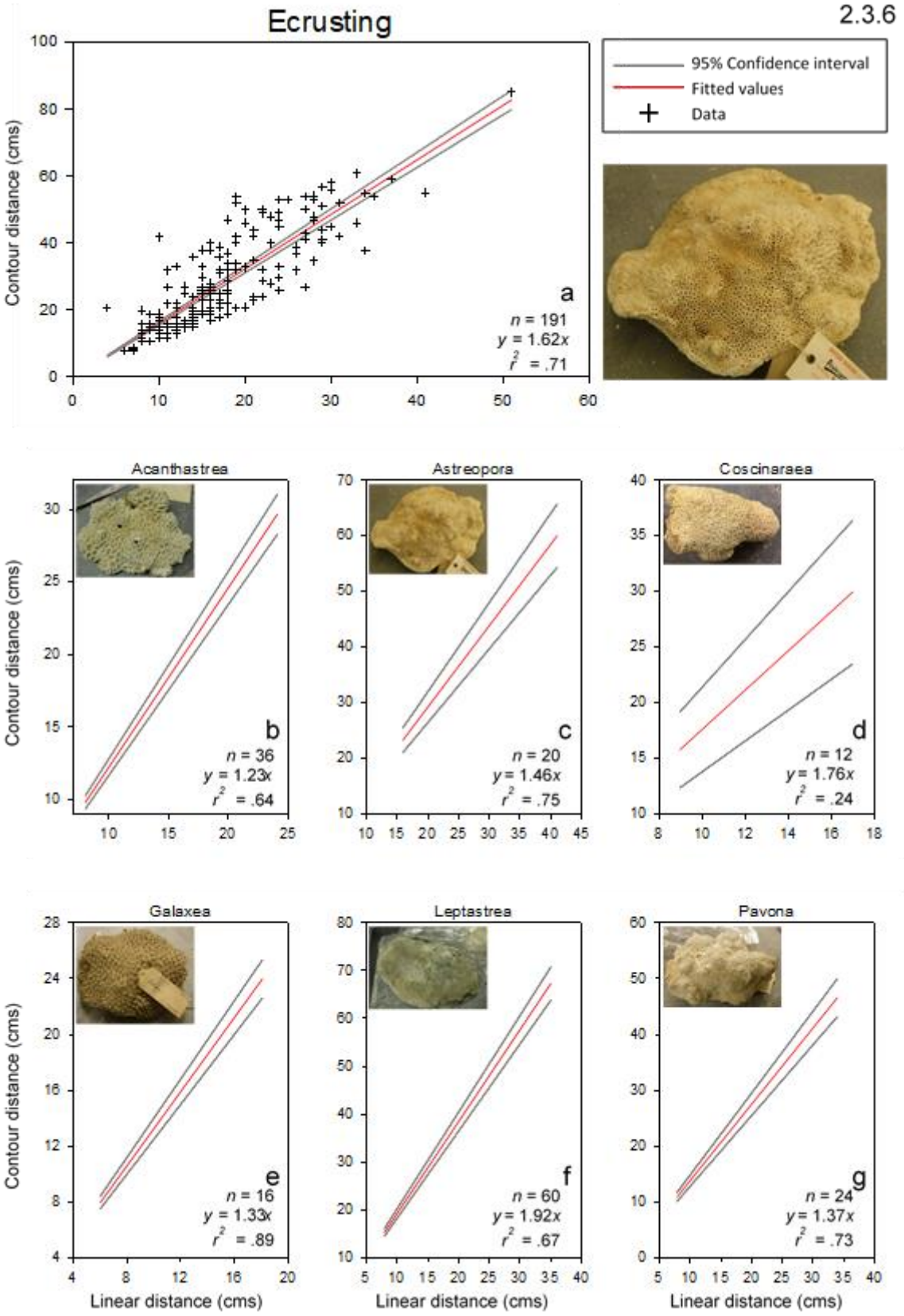
Ecrusting
95% Confidence interval
Fitted values
Data
Contour distance (cms)
a
n = 191
y = 1.62x
r² = .71
Acanthastrea
b
n = 36
y = 1.23x
r² = .64
Astreopora
c
n = 20
y = 1.46x
r² = .75
Coscinaraea
d
n = 12
y = 1.76x
r² = .24
Galaxea
e
n = 16
y = 1.33x
r² = .89
Leptastrea
f
n = 60
y = 1.92x
r² = .67
Pavona
g
n = 24
y = 1.37x
r² = .73
Linear distance (cms)

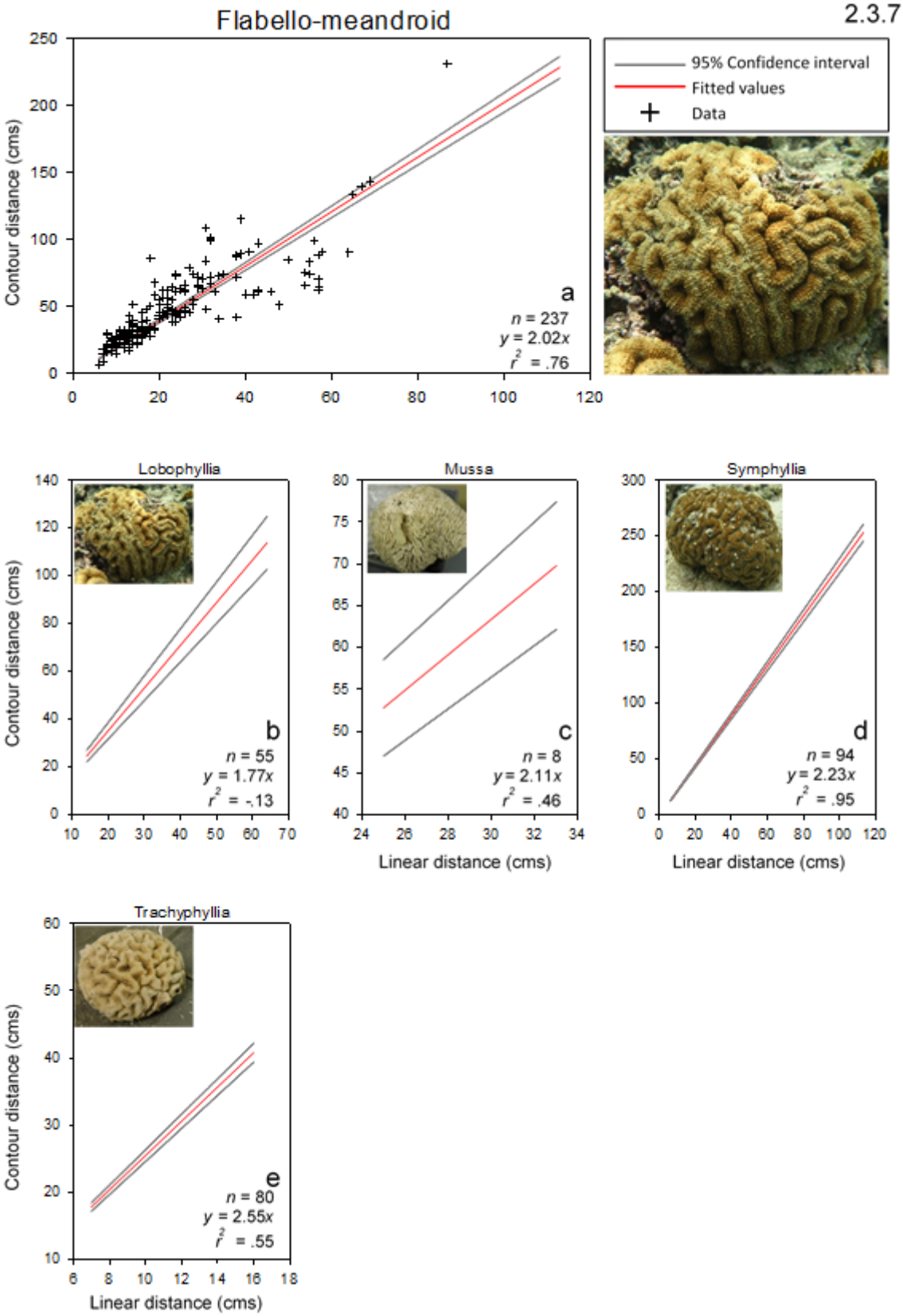
Flabello-meandroid
Contour distance (cms)
95% Confidence interval
Fitted values
Data
a
n = 237
y = 2.02x
r² = .76
Lobophyllia
b
n = 55
y = 1.77x
r² = -.13
Mussa
c
n = 8
y = 2.11x
r² = .46
Symphyllia
d
n = 94
y = 2.23x
r² = .95
Linear distance (cms)
Trachyphyllia
e
n = 80
y = 2.55x
r² = .55

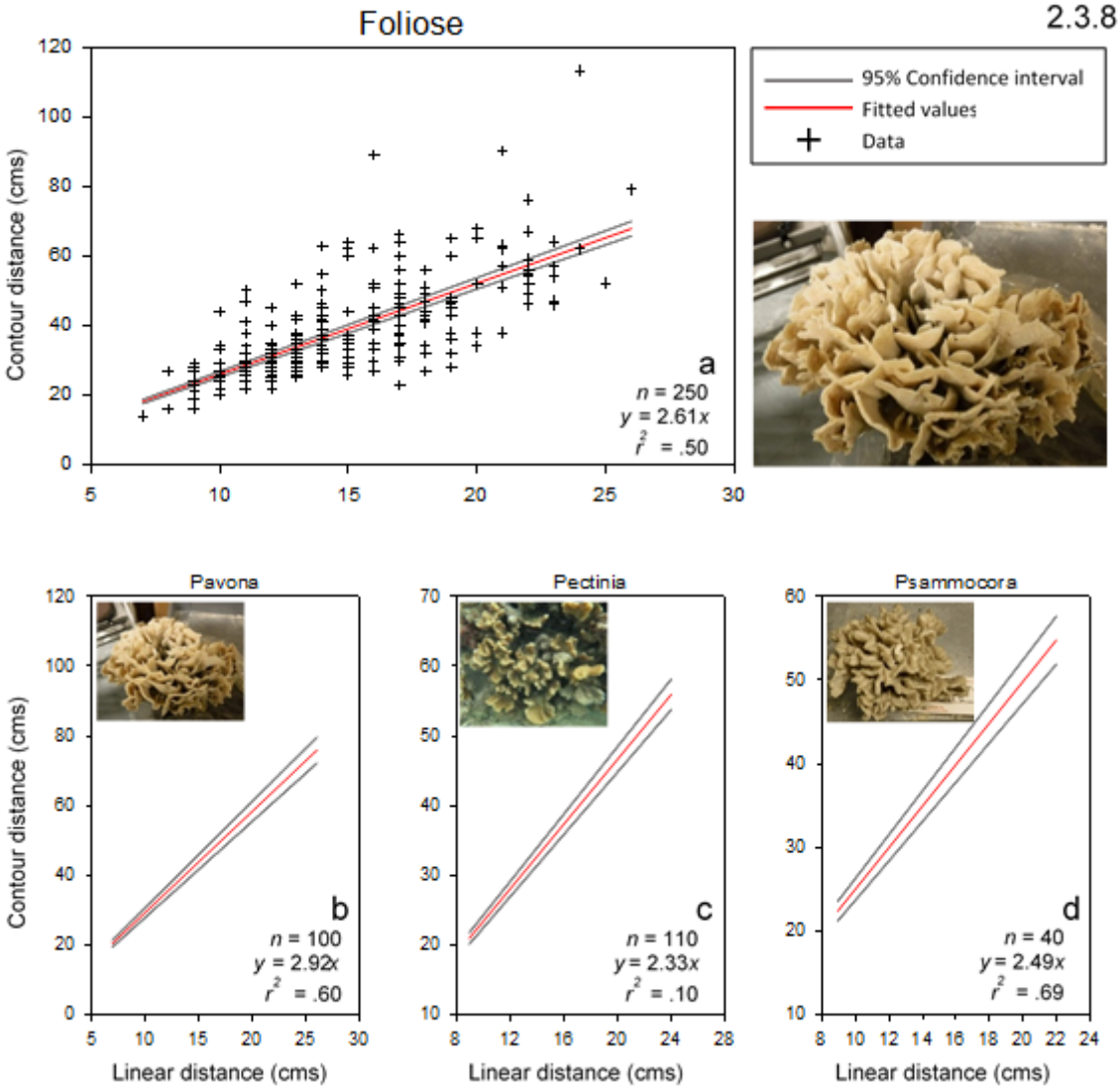
Foliose
95% Confidence interval
Fitted values
Data
Contour distance (cms)
a
n = 250
y = 2.61x
r² = .50
Pavona
b
n = 100
y = 2.92x
r² = .60
Pectinia
c
n = 110
y = 2.33x
r² = .10
Psammocora
d
n = 40
y = 2.49x
r² = .69
Linear distance (cms)

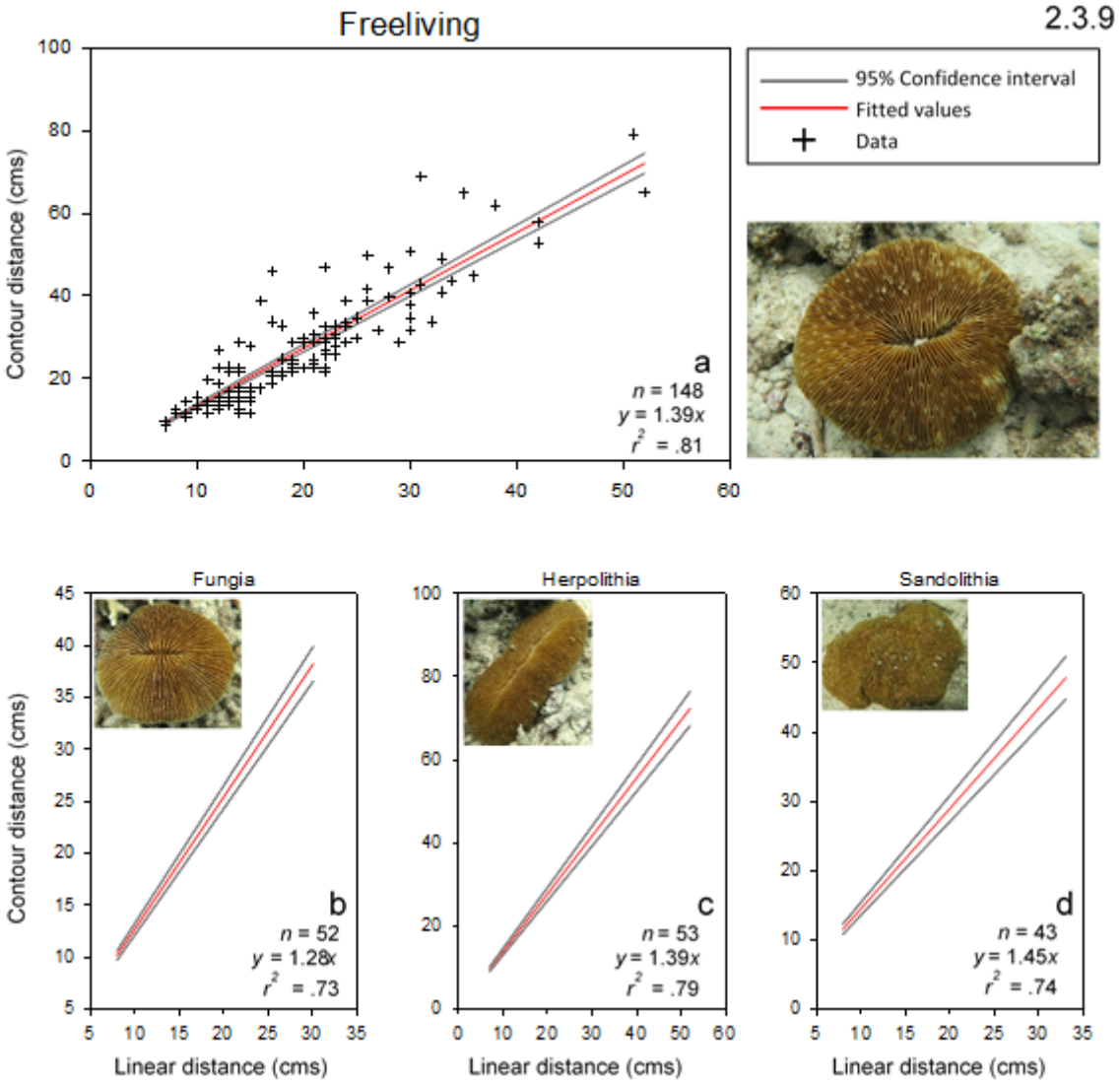
Freeliving
Contour distance (cms)
Linear distance (cms)
95% Confidence interval
Fitted values
Data
a
n = 148
y = 1.39x
r² = .81
Fungia
b
n = 52
y = 1.28x
r² = .73
Herpolithia
c
n = 53
y = 1.39x
r² = .79
Sandolithia
d
n = 43
y = 1.45x
r² = .74

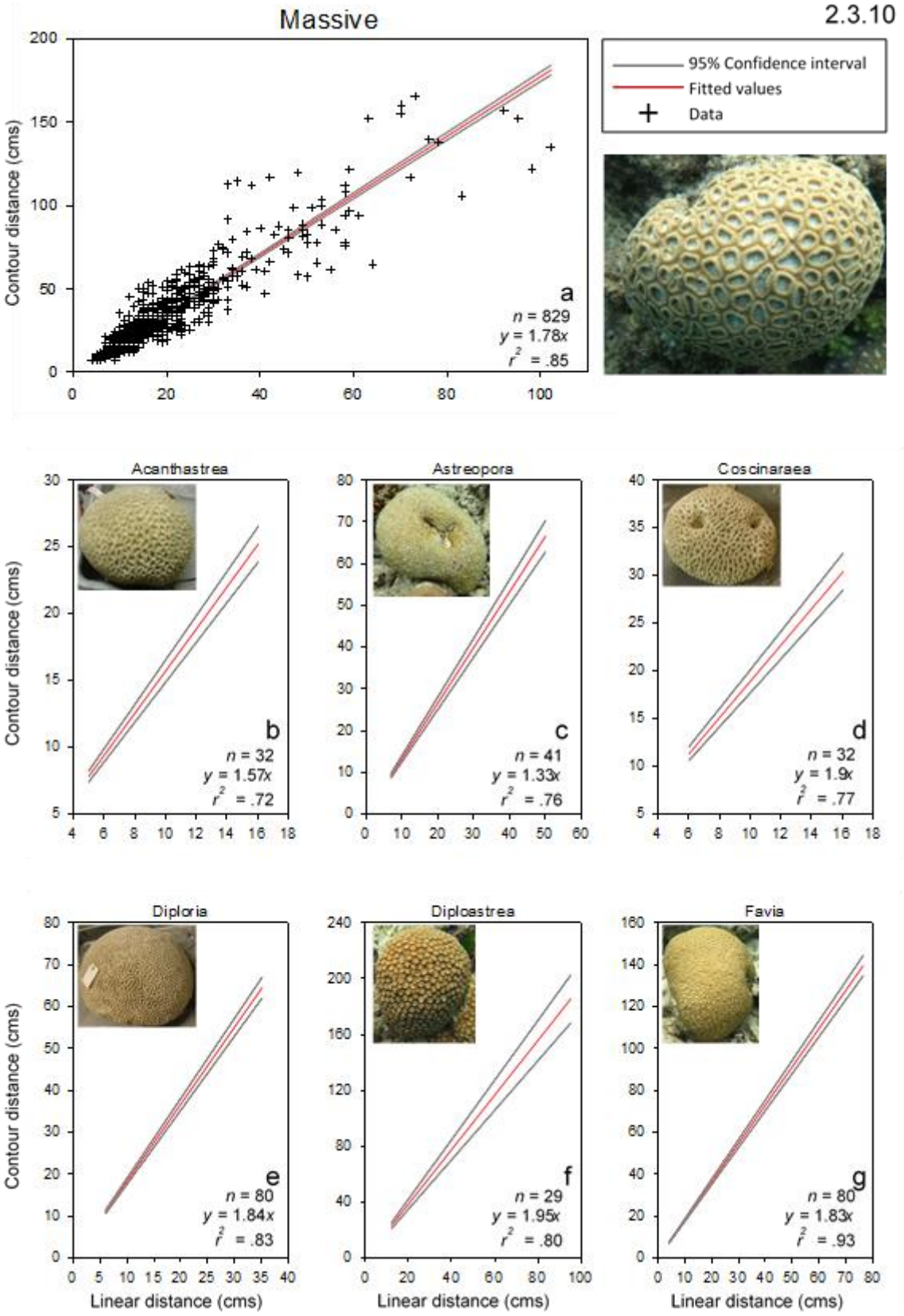
Massive
95% Confidence interval
Fitted values
Data
Contour distance (cms)
a
n = 829
y = 1.78x
r² = .85
Acanthastrea
b
n = 32
y = 1.57x
r² = .72
Astreopora
c
n = 41
y = 1.33x
r² = .76
Coscinaraea
d
n = 32
y = 1.9x
r² = .77
Diploria
e
n = 80
y = 1.84x
r² = .83
Diploastrea
f
n = 29
y = 1.95x
r² = .80
Favia
g
n = 80
y = 1.83x
r² = .93
Linear distance (cms)

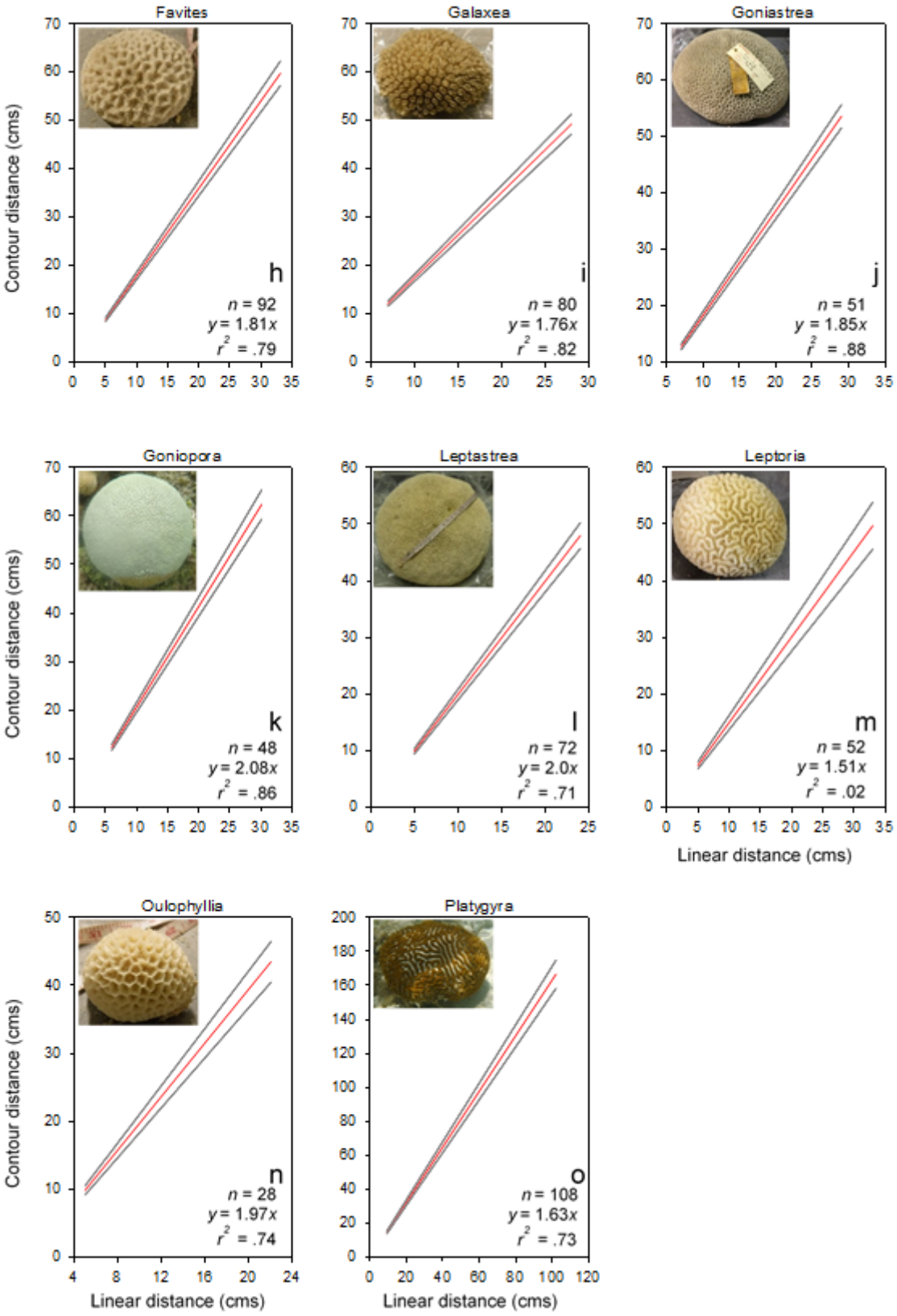
Favites
h
n = 92
y = 1.81x
r² = .79
Galaxea
i
n = 80
y = 1.76x
r² = .82
Goniastrea
j
n = 51
y = 1.85x
r² = .88
Goniopora
k
n = 48
y = 2.08x
r² = .86
Leptastrea
l
n = 72
y = 2.0x
r² = .71
Leptoria
m
n = 52
y = 1.51x
r² = .02
Oulophyllia
n
n = 28
y = 1.97x
r² = .74
Platygyra
o
n = 108
y = 1.63x
r² = .73
Contour distance (cms)
Linear distance (cms)

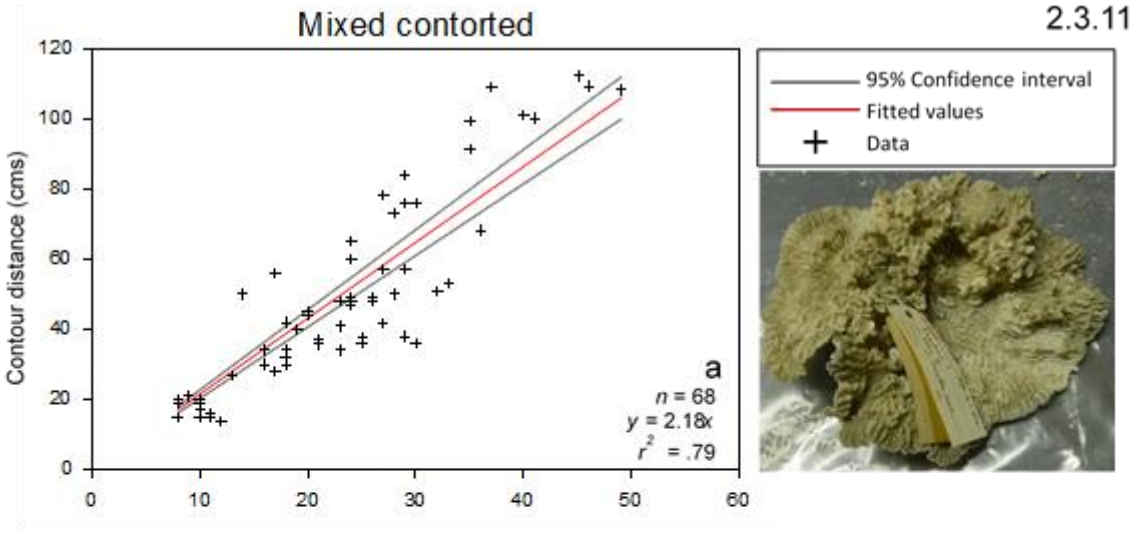
Mixed contorted
Contour distance (cms)
120
100
80
60
40
20
0
0
10
20
30
40
50
60
a
n = 68
y = 2.18x
r² = .79
95% Confidence interval
Fitted values
Data

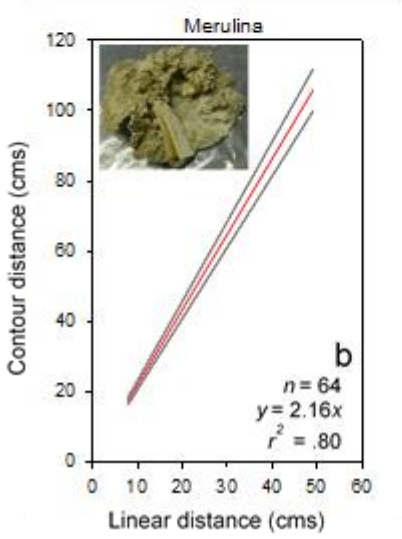
Merulina
Contour distance (cms)
120
100
80
60
40
20
0
0
10
20
30
40
50
60
Linear distance (cms)
b
n = 64
y = 2.16x
r² = .80

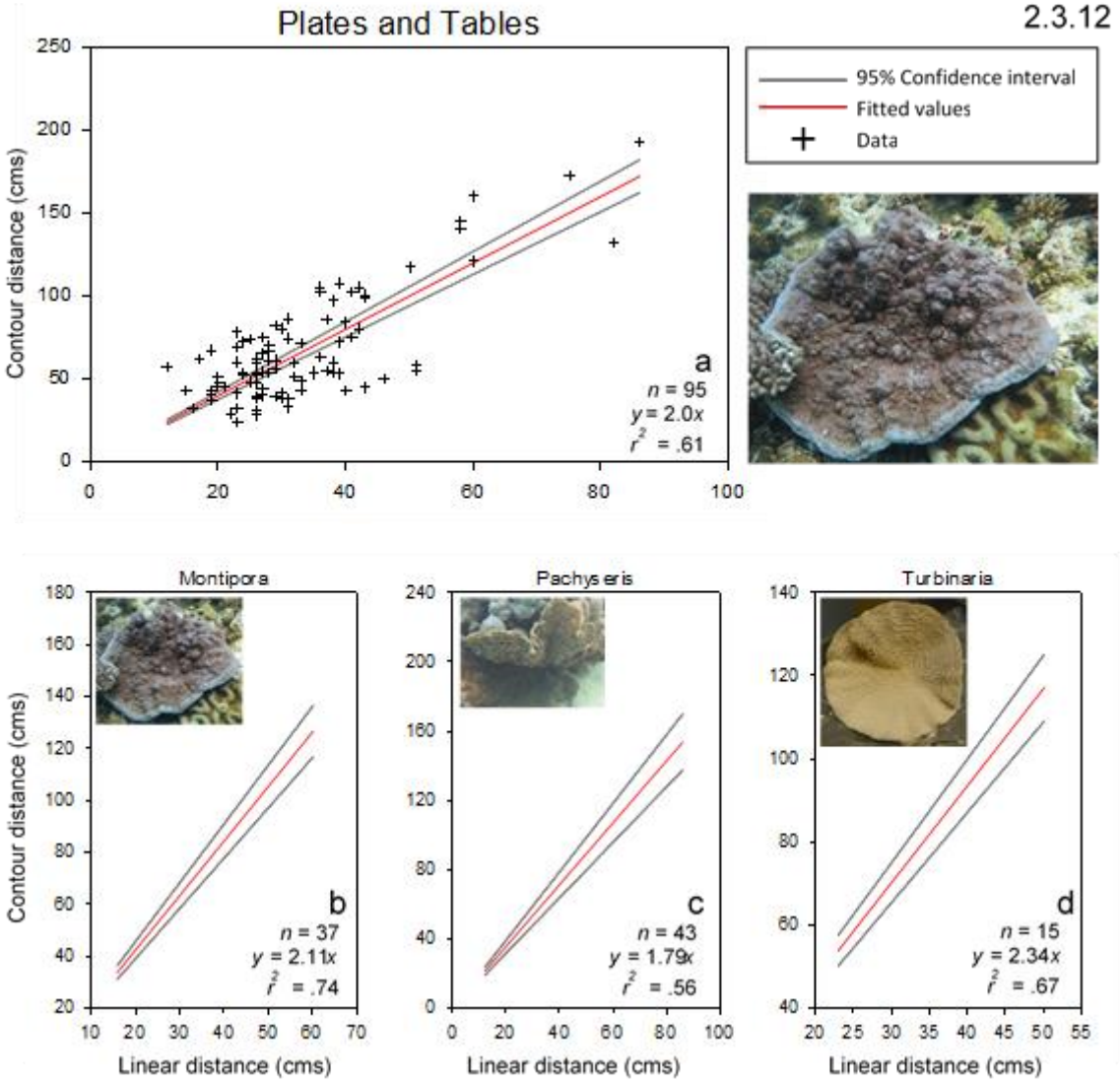
95% Confidence interval
Fitted values
Data
Contour distance (cms)
a
n = 95
y = 2.0x
r² = .61
Montipora
b
n = 37
y = 2.11x
r² = .74
Pachyseris
c
n = 43
y = 1.79x
r² = .56
Turbinaria
d
n = 15
y = 2.34x
r² = .67
Linear distance (cms)

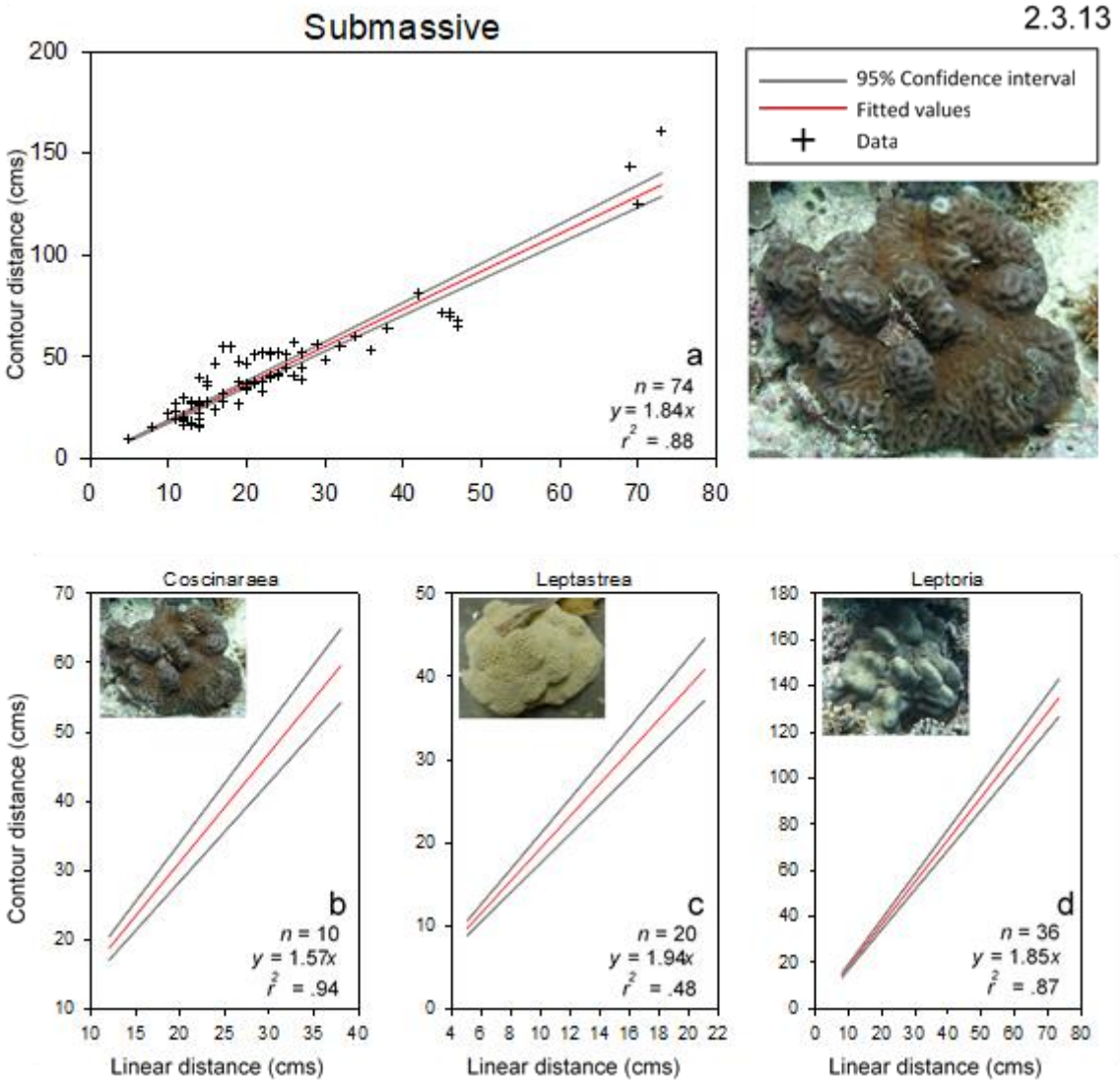
Submassive
Contour distance (cms)
Linear distance (cms)
95% Confidence interval
Fitted values
Data
a
n = 74
y = 1.84x
r² = .88
Coscinaraea
b
n = 10
y = 1.57x
r² = .94
Leptastrea
c
n = 20
y = 1.94x
r² = .48
Leptoria
d
n = 36
y = 1.85x
r² = .87

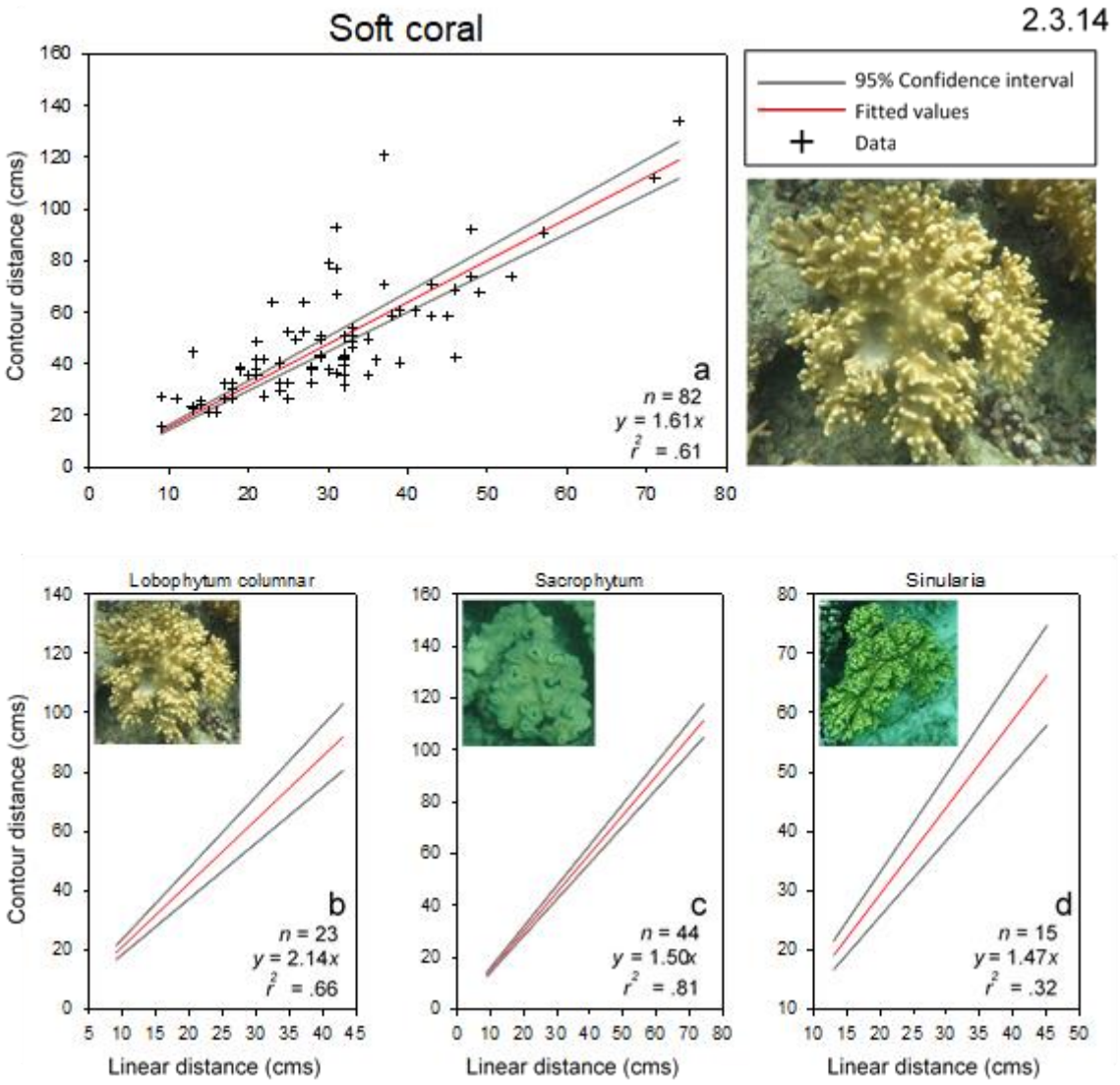
Soft coral
2.3.14
95% Confidence interval
Fitted values
Data
Contour distance (cms)
a
n = 82
y = 1.61x
r² = .61
Lobophytum columnar
b
n = 23
y = 2.14x
r² = .66
Sacrophytum
c
n = 44
y = 1.50x
r² = .81
Sinularia
d
n = 15
y = 1.47x
r² = .32
Linear distance (cms)

Individual genus

2.3.15

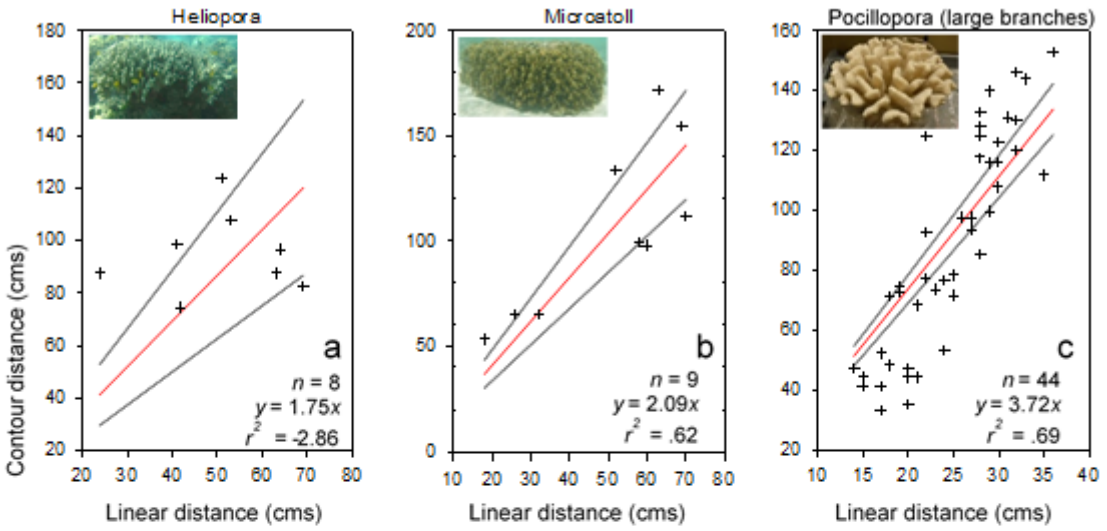

Algae covered coral

2.3.16

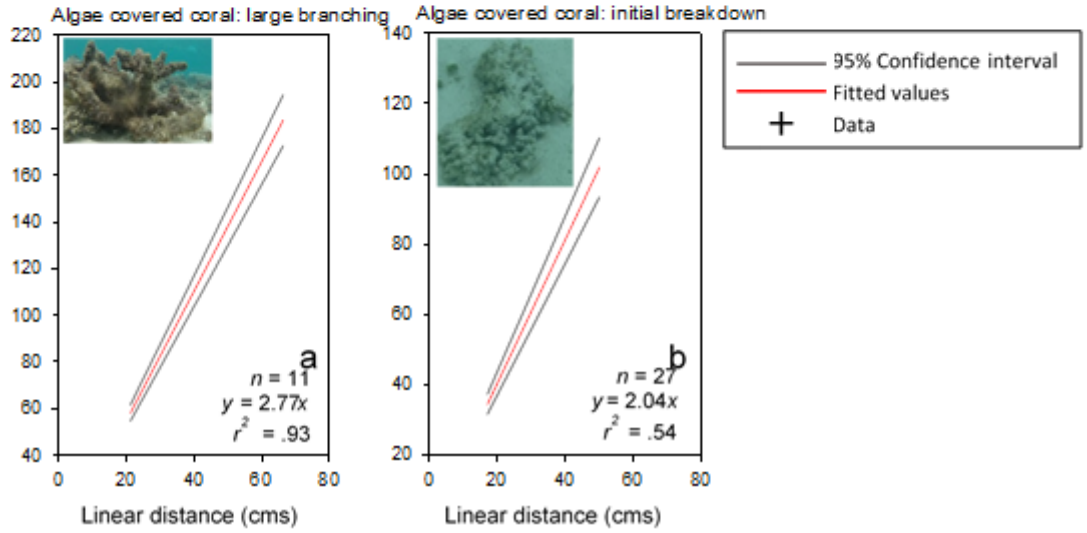

Molluscs

2.3.17

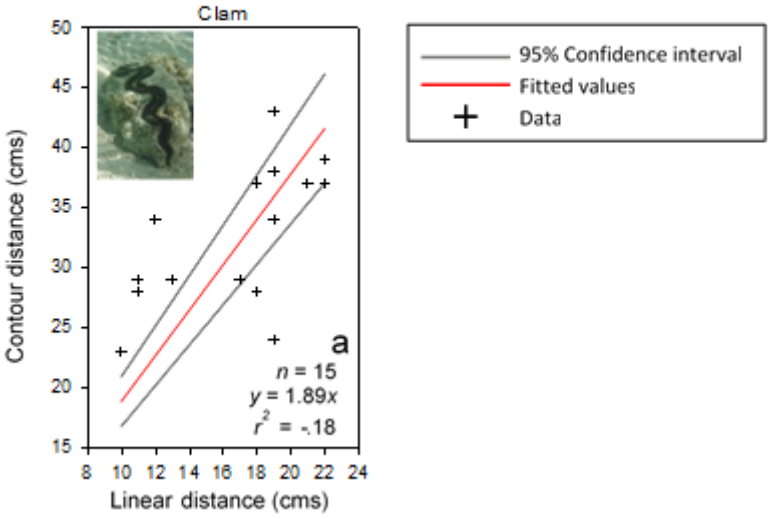

The gradients of the linear regression lines defining the size-rugosity relationships were unique for each coral genus and morphotype and were strongly ($r^2 = 0.95$) correlated with mean rugosity, revealing a strong similarity between these two metrics (figure 2.4). As such, the gradients are representative of coral colony rugosity, ranging from 1.23, for encrusting *Acanastrea* (figure 2.3.6b), to 3.84, for vase shaped *Merulina* (figure 2.3.5b) revealing these genera respectively at the least and most rugose in the rugosity database. For coral morphotypes, the regression gradients ranged from 1.39 for free-living corals (figure 2.3.9a) to 3.50 for contorted laminar corals (figure 2.3.5a), respectively revealing these as the least and most rugose coral morphotypes in the database.

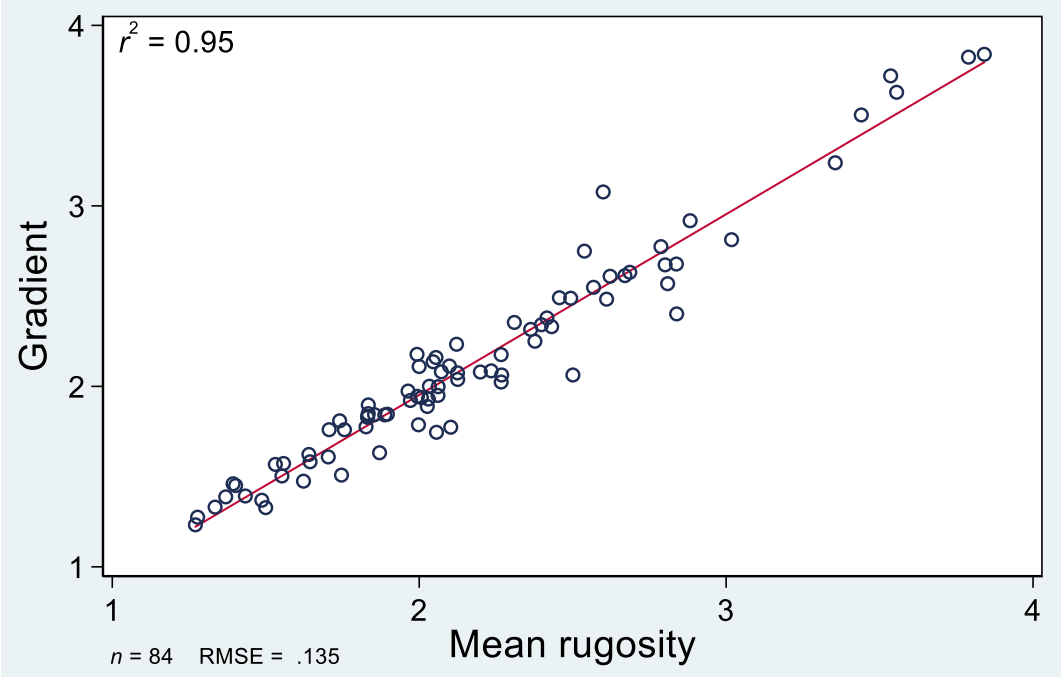

Figure 2.4. Mean rugosity of each coral genus vs the gradients of the coral size-rugosity relationships for the respective corals with linear regression line (red).

Due to this representativeness, the gradients can be used to represent and calculate the rugosity of each coral genus, morphotype and abiotic substrate using the following equations:

Equation 1:

$$y = mx$$

(Where *y* = contour length, *m* = gradient, and, *x* = planar linear length)

Which allows calculation of rugosity as:

Equation 2:

$$Rugosity = calculated\ contour\ length\ /\ planar\ length$$ (Risk, 1972).

As such, the gradients extracted from each linear relationship will be referred to as (coral colony rugosity) conversion factors for the remains of this thesis. These are summarised in full in table 2.2.

Analysis of abiotic substrate

In addition, to corals, numerous other substrates are found on coral reefs and contribute to their structural complexity (Graham and Nash, 2013 and Richardson *et al.,* 2017). To assess the rugosity of these features, two categories of algae covered coral were included in the database: algae covered branching coral (figure 2.3.16a) m = 2.79, S.D. = 0.34, y = 2.77, $r^2 = 0.93$) and other algae covered / eroded coral (figure 2.3.16b) m = 2.13, S.D. =0.44, y = 2.04, $r^2 = 0.54$). These two categories are representative of initial and progressive coral degradation stages, respectively, and also showed strong positive and significant ($p < .05$) correlations between coral size and rugosity (see Appendix A for individual substrata results). For additional rubble and sand abiotic reef substrates, of which boxplots summarise the data in figure 2.5, mean rugosity ranged from 1.02 for homogenous, flat sand patches (figure 2.5g, S.D. = 0.02) to 1.39 for limestone pavement (figure 2.5d, S.D. = 0.05). These data are also summarised in table 2.2. The narrow range of rugosity values measured (y axis) for each abiotic substrate (0.6 for coral rubble (figures 2.5a-d) and 0.2 for sand (figures 2.5e-g)) reveals this data to be highly precise and consequently representative of the respective abiotic features.

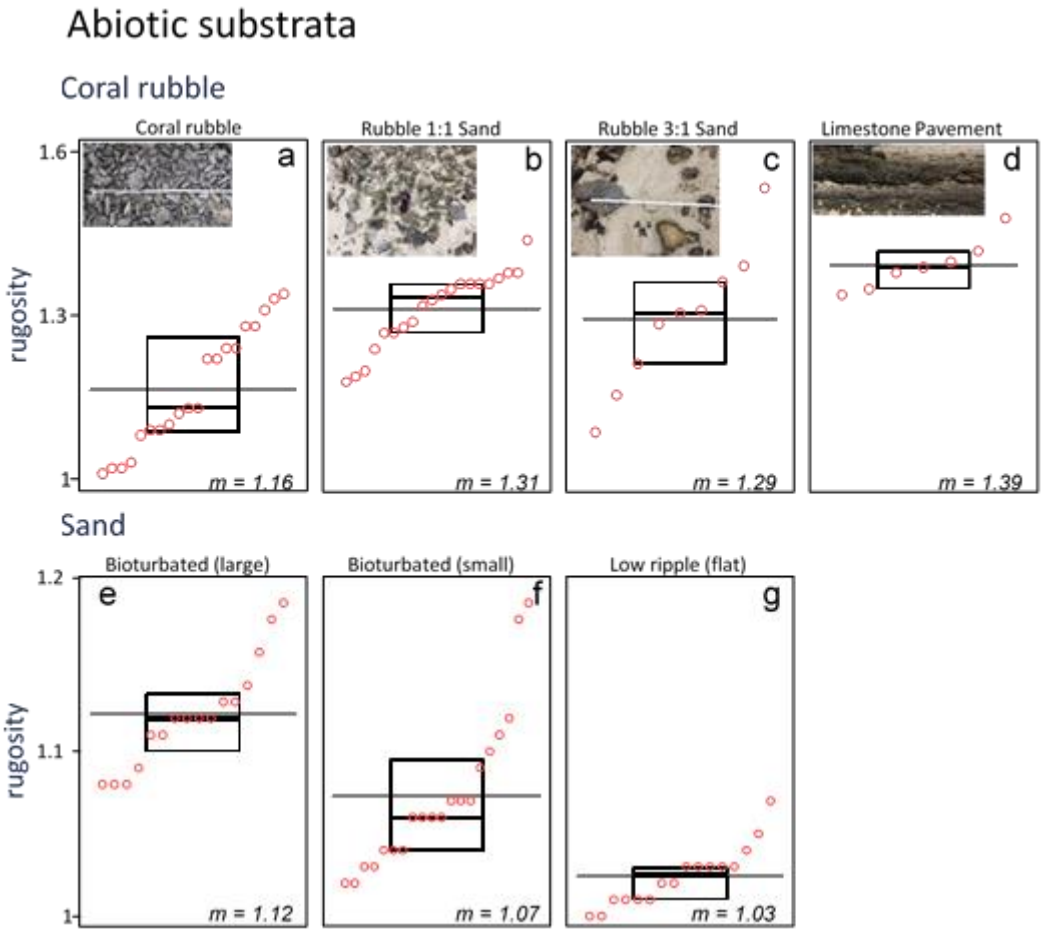

Figure 2.5. The rugosity of rubble and sand abiotic substrates, sampled for inclusion in the rugosity database, represented by box plots. Plots 2.5.a-d represent coral rubble and 2.5.e-g represent sand as specified above each individual graph. The horizontal, black line within each box indicates the median, boundaries of the box indicate the interquartile range and the long, grey line across each boxplot represents the mean rugosity of each reef feature.

Relationship between coral rugosity and life history strategies

When coral genera were grouped by life history strategy, competitive corals had the highest mean rugosity (m = 2.74, S.D. = 0.93), followed by weedy corals (m = 2.39, S.D. = 0.63) and generalist corals (m = 2.33, S.D. = 0.66). Stress tolerant corals had the lowest mean rugosity (m = 1.93, S.D. = 0.62), (figure 2.6). The boxplots, presented in figure 2.6 and each representative of a coral genus, reveal some overlap in the range of rugosity measurements of corals both within and between life history strategy groups. Laminar *Montipora* and *Merulina*, in the generalist category, appear as outliers with the interquartile rugosity range of both genera displaying no overlap with that of other generalist corals.

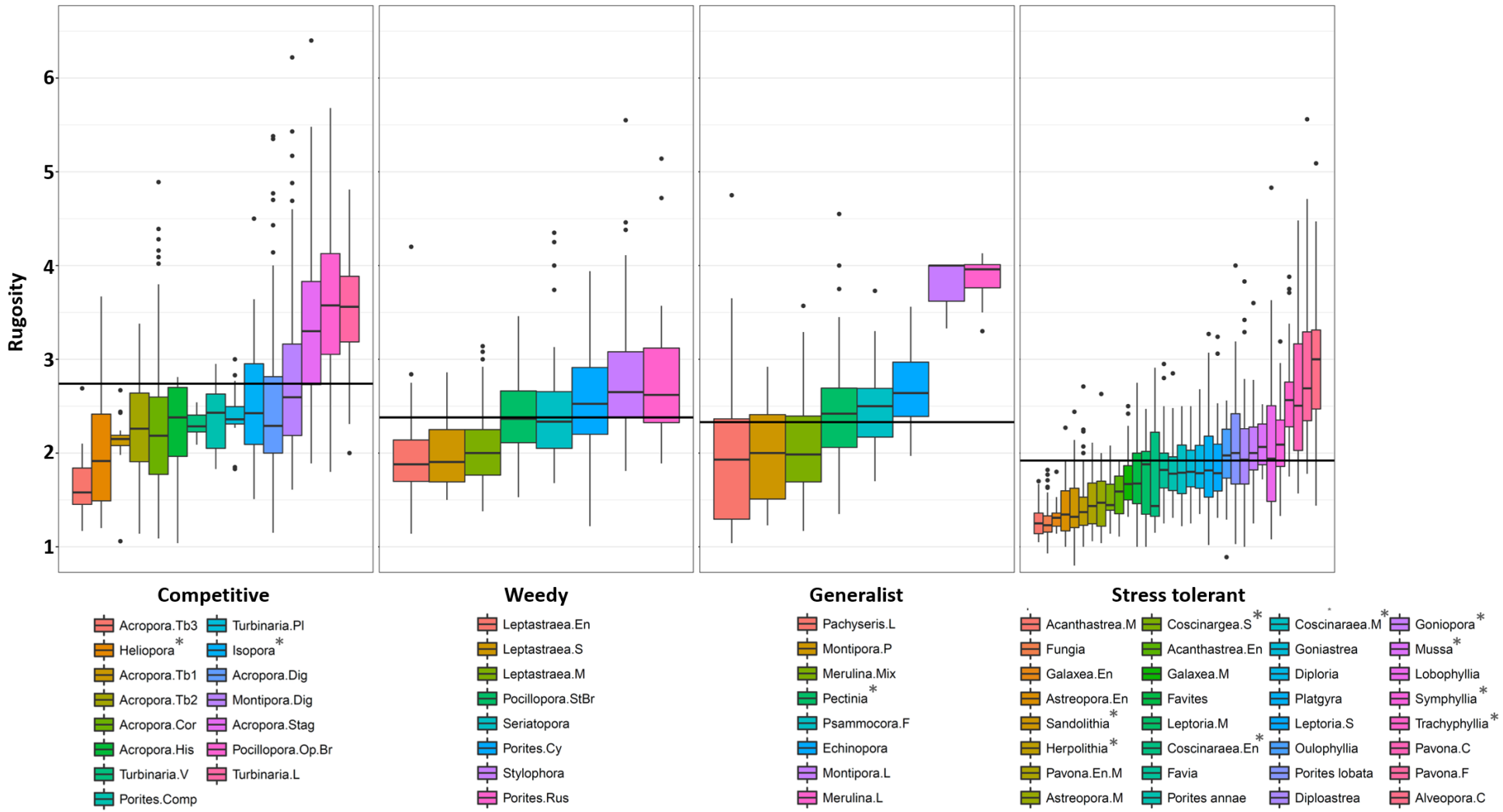

Figure 2.6. Mean rugosity of coral life history strategy groups, left to right representing competitive, weedy, generalist and stress tolerant corals. Boxplots represent the inter-quartile range of data recorded in the rugosity trait database for each coral genus. Black dots represent data points collected outside of this range. Solid, black lines represent the mean rugosity of each coral life history group. Genera marked with a '*' were not included in the original life history strategy analysis by Darling *et al.,* (2012) and have been newly assigned a life history strategy based on morphology.

A one-way ANOVA revealed a statistically significant difference between the mean rugosities of the four life history strategy groups ($F(3, 3023) = 224.9$, $p = 0.00$). Post-hoc Tukey tests revealed that differences between all groups, except between weedy and generalist corals, were significant at the $p = 0.05$ level, (see table 2.3).

Table 2.3. Results of Tukey post-hoc ANOVA tests to determine whether the mean rugosity of competitive, weedy, generalist and stress tolerant corals are significantly different from one another, (* indicates a significant difference).

Comparison (life history strategy)	Tukey test results
Weedy vs competitive*	-0.354 ± 0.044, $p = 0.000$
Generalist vs competitive*	-0.408 ± 0.047, $p = 0.000$
Stress tolerant vs competitive*	-0.812 ± 0.032, $p = 0.000$
Generalist vs weedy	-0.054 ± 0.052, $p = 0.725$
Stress tolerant vs weedy*	-0.459 ± 0.039, $p = 0.000$
Stress tolerant vs generalist*	-0.405 ± 0.043, $p = 0.000$

An additional one-way ANOVA also revealed a significant difference between the mean rugosity of fast (competitive) and slow growing (weedy, generalist and stress tolerant) corals ($F(1, 3025) = 450.31$, $p = 0.00$).

2.4 Discussion

The rugosity trait database

Recent work has recognised a disproportionate and species-specific role of scleractinian corals in building the structural complexity of coral reefs, but to date there has been no accurate means of quantifying this (Alvarez-Filip *et al.,* 2011, 2013 and Bozec *et al.,* 2015). This research has resulted in the creation a new rugosity trait database, built using coral colony level rugosity measurements from a range of coral genera and reef substrate. The database summarises the variable morphotypes and mean rugosity of Indo-Pacific corals which are identified as being highly variable both between and sometimes within coral genera. As would be expected, the database identifies genera with branching and contorted morphologies as the most structurally complex and free-living and massive / plateau corals as the least complex, with corals exhibiting additional morphologies falling in-between (table 2.2, Burns *et al.,* 2015, Richardson *et al.,* 2017, and González-Barrios and Alvarez-Filip, 2018). This initially demonstrates how reef structural complexity is dependent on the morpho-functional traits of coral communities and how the database can be used to recognise and quantify the variable contributions of different coral taxa to reef rugosity (Alvarez-Filip *et al.,* 2011, 2013; Bozec *et al.,* 2015 and Richardson *et al.,* 2017).

One exemption to this may be for soft corals which have a higher mean rugosity than some hard corals included in the rugosity database (summarised in table 2.2). Although unsurprising, considering their complex morphologies in the field (cylindrical), using mean rugosity data to represent the contribution of these corals to reef structural complexity is complex and misleading. This is due to their only partially calcified structure and provision of shorter-term structural complexity than their hard, calcareous counterpart taxa (Richardson *et al.,* 2017 and Ferrari *et al.,* 2016). The database also represents non-coral, abiotic reef features. These abiotic substrates are, on average, much less complex (mean rugosity = 1.48) than the corals (mean rugosity = 2.19), reinforcing the fact that hard-coral cover is the dominant provider of structural complexity on coral reefs (Graham and Nash, 2013, and Alvarez-Filip *et al.,* 2013). In conclusion, the research has provided a much-needed coral taxa specific rugosity trait

database which could be used in future coral reef monitoring and assessment (Balmford *et al.,* 2005).

Coral rugosity importance for coral life history strategies

The broad range of morphologies and rugosity values exhibited by the Indo-Pacific corals are strongly related to coral life history strategies as defined by Darling *et al.,* (2012). The significant differences between the mean rugosity of these categories result from (and are inextricably linked to) coral morphology whereby competitive corals typically exhibit branching or plating morphologies and are more structurally complex than stress tolerant corals with primarily encrusting or massive morphologies (figure 2.6, Darling *et al.,* 2012). Thus, the rugosity database not only allows structural complexity to be quantified, using rugosity as a proxy, but also shows it to be a potential key determinant trait for coral life history strategies. It is therefore suggested that genera mean rugosity, in addition to qualitative coral morphology information, should be considered when assigning coral taxa life history strategies (Darling *et al.,* 2012). This would provide an additional explanatory variable for determining the overall functionality of coral reef ecosystems and response of coral communities to future environmental change, as these, in part, are dependent on coral life history strategy (Alvarez-Filip *et al.,* 2011 and 2013, Darling *et al.,* 2012 and Madin *et al.,* 2016).

The non-significant difference between mean rugosity for weedy and generalist corals is not surprising as generalist corals are known to share traits with corals in other life history strategy groups (Darling *et al.,* 2012). Furthermore, weedy corals have the greatest variation of species traits of all the life history strategies and so are also likely to share characteristics with other genera (Darling *et al.,* 2012). There are two recognisable outliers in the generalist category: laminar *Merulina* and *Montipora* (figure 2.6). These were assigned the same life history strategy as other species within the same genus based on Darling *et al.,* (2012) stating that genus level identification is sufficient to classify coral life histories. These outliers however, with mean rugosity values more similar to competitive corals, show that this is not always appropriate and that coral morphotype must also be considered if variable within a genus.

These results are echoed through the two-group comparison where there is a significant difference between the mean rugosity of fast (competitive) and slow growing (weedy, generalist and stress tolerant corals) (Darling *et al.,* 2012). This shows that competitive corals are not only fast growing, but also contribute the most structural complexity to reefs. This is deeply concerning considering that competitive corals are the most sensitive to physical disruption and environmental change (Darling *et al.,* 2012).

Analysis of the coral size – rugosity relationships

Analysis of the coral size – rugosity relationships revealed that coral rugosity consistently scaled linearly with colony coral size (figure 2.3). The existence of this relationship is unsurprising, given the expectation that a larger coral would have a greater contour length, representative of rugosity, than a smaller colony of the same species (Alvarez-Filip *et al.,* 2013 and Richardson *et al.,* 2017). However, this is the first time this relationship has been quantified individually for a broad range of genera. The relationships for all genera were significant, and, from analysis of r^2 values, were strong for the majority of genera and morphotypes. This supports, builds on and increases the generalisability of this relationship, initially identified by Richardson *et al.,* (2017) for 3 coral species, to a very wide range of common coral morphotaxa in the Indo-Pacific region. While not directly comparable, due to differences in measurement scale, the strength of the relationships for *Porites cyclindrica* and large, open branching *Pocillopora* identified in this research (figure 2.3.2b and figure 2.3.15c respectively) are consistent with those identified by Richardson *et al.,* (2017). The representation of all coral morphotypes, found worldwide, in the database also increases the generalisability of these relationships to coral reef ecosystems worldwide.

Despite their significance it is, however, recognised that the coral size-rugosity relationships were very weak for some genera, especially, *Heliopora*, *Acropora* hispidose and *Lobophyllia*. Of these, *Heliopora* and *Acropora Hispidose* had inadequate sample sizes (8 and 11 respectively) for linear regression and therefore the results are not considered representative or valid for these corals (McCarroll, 2016). Conversely, *Lobophyllia* had a large sample size (n = 55). For this genus, the low correlation coefficient is considered a result of

morphological differences in the valley sizes between individual corallites, for different coral colonies, of which the measurement chain could be poked into some, but not all. The rugosity of colonies with larger valleys will therefore be greater than those with smaller valleys that the chain could not fit into. The same could be true for *Mussa*, which also has an r^2 value below 0.5. Interestingly, the r^2 value for *Lobophyllia* increases from -0.13 to 0.61 when only colonies measured from the NHM are included in the regression analysis. This potentially reveals an issue with *in-situ* measurement of some types of individual coral colonies if they are growing up against other substrates, limiting access for measuring their full diameters (although this was avoided in as many cases as possible in the field).

For other genera, it is unclear why the size-rugosity relationships exhibit low correlation coefficients. There appears to be no association between the strength of the relationships with coral morphology as many genera with the same morphotype exhibit variable r^2 values. It may be that genera presenting low r^2 values show greater variation in colony size and shape, potentially resulting from variable environmental conditions (Richardson *et al.,* 2017). It is hoped that the addition of more rugosity data to the database in the future will improve and help constrain these relationships. In general, however, the data and relationships from this database and analysis are deemed representative of the genera included. This is because any variability considered to occur within genera, especially when sub-divided into genus morphotypes where applicable, is thought to be less than that occurring between them (Alvarez-Filip, *et al.,* 2013).

The rugosity data from this analysis are also considered more accurate than those presented in Richardson *et al.,* (2017) due to being measured at a smaller scale (0.5 cm link chain) which was able to account for the majority of microscale habitats and corrugations present in coral colonies (McCormick, 1994, Knudby and LeDrew, 2007 and Richardson *et al.,* 2017). Furthermore, the rugosity of each coral was measured along four surface profiles as opposed to just the corals diameter which has been used in previous research (Alvarez-Filip, 2013, Richardson *et al.,* 2017 and González-Barrios and Alvarez-Filip, 2018). This increases the representativeness of the mean rugosity values to

entire coral colonies, independent of their orientation on a reef. The chain-tape measurement does still lack the capacity to consider the full 3D structure of a coral colony, including holes throughout the matrix of complex genera such as *Seriatopora*. However, the complex surface of corals is considered to be an accurate representation of the structure within the matrix below, especially when measured using the rugosity index (Commito and Rusignuolo, 2010). This measurement includes many features, such as over and under hangs in the coral that are underestimated or altogether ignored by alternate measurement methods. As such, there is likely to be little bias in the accuracy or error of the chain-tape method between coral genera in this study, consequently providing an urgently required standardised rugosity measurement that is equally representative of surface complexity for all coral genera (Commito and Rusignuolo, 2010). This is in contrast to remote sensing techniques where the accuracy of rugosity measurements is often greatly reduced for more complex corals (Bryson *et al.,* 2013 and Figueira *et al.,* 2015).

Potential of the coral size-rugosity relationships

The linear equations used to determine the coral size-rugosity relationships are consistent for all genera, morphotypes and substrates (y = mx), but with a unique gradient for each (summarised in table 2.2). In the same way that mean rugosity is related to coral life history strategies, this is considered a response to coral morphology whereby the steepest gradients represent corals with the most complex morphologies and the smallest gradients, the least complex corals. This variability is consistent with analysis of mean rugosity from the database and research recognising that the rate of increase of reef structural complexity is dependent on the dominant coral species present on a reef (Alvarez-Filip *et al.,* 2011). It also supports House *et al.,* (2016) whom identified that coral colony surface area and volume scaled with coral planar area, but with conversion parameters specific to coral morphology.

The strong similarity between the linear regression gradients and mean rugosity of respective corals suggests that the gradients could be an accurate proxy for coral colony rugosity, structural complexity and consequently reef functionality (Darling *et al.,* 2012, Alvarez-Filip *et al.,* 2013, Burns *et al.,* 2015 and González-Barrios and Alvarez-Filip, 2018). Even more advantageous, is that when

extracted from the database, the taxa specific linear regression gradients provide conversion factors that can accurately predict coral colony rugosity from the linear lengths of corals, with obvious future applications to coral survey data. The genus level analysis provides the most accurate representation of coral colony scale contributions to rugosity to the overall rugosity of a coral reef. It is also beneficial because coral morphotypes are not always discrete and show variability within groups or genera (House *et al.,* 2016). However, genus level identification can often be difficult and hence occasionally research may require the morphotype level data (Darling *et al.,* 2012). At present, the coral rugosity database also only represents Indo-Pacific coral genera (with exception of *Diploria*) and thus makes an important contribution to ever growing global datasets of coral colony scale rugosity data, such as that recently published for the Caribbean, (González-Barrios and Alvarez-Filip, 2018). The demonstrated use of morphotype equations also increases the applicability of the database to coral reef regions worldwide where such genus specific coral colony level data is not currently available.

Conclusion

The creation of the rugosity trait database has provided a useful resource of coral colony level rugosity information. With additional knowledge of how coral rugosity is related to coral life history strategies, the database is extremely relevant for aiding future understanding of how changes in the composition and richness of coral genera on a coral reef will affect the state (health and function) of coral ecosystems (Hooper *et al.,* 2005 and González-Barrios and Alvarez-Filip, 2018).

The significant coral size-rugosity relationships and genus specific conversion factors are hypothesised to have useful applications for future assessment and monitoring of coral reef rugosity. Calculating ecological characteristics and, in particular, rugosity, from 2D information has thus far had limited success for assessing the health and biodiversity of coral reef ecosystems (Hattori and Shibuno, 2015, and House *et al.,* 2016). In the past, these methods have not had the capability to accurately assess reef structural complexity at a scale that considers the individual contributions of coral colonies, in a time and cost-

effective manner that requires little expert knowledge (House *et al.,* 2016). By providing a dataset that quantifies the contribution of individual corals to the 3D structure of a reef, this research offers an opportunity to examine how the identified conversion factors can be incorporated into coral reef assessment and monitoring programs (Bozec *et al.,* 2015 and Mumby, 2016). This will be explored, in the following chapter on application of the rugosity equations to linear distances measured from three sources of coral reef health data (video transects, line-intercept data and UAV imagery) to show how 3D structural information can be gained from 2D data.

Chapter 3. Applications of the coral rugosity data

3.1 Introduction

In chapter 2, this research developed a rugosity trait-based database containing coral colony scale rugosity data for a range of coral genera, morphotypes and abiotic reef substrates. Analysis of this data revealed mean rugosity as a trait consistent with coral life history strategies and significant relationships between coral colony or substrate size and rugosity for all taxa. The gradients governing these relationships were representative of mean coral rugosity and were proposed for use within equations (1 and 2) as conversion factors; to first enable calculation of coral contour lengths (eq.1) from respective planar lengths, and subsequently, calculation of coral colony rugosity by dividing this calculated contour distance by the planar length of the coral (eq. 2). For abiotic substrates, in the absence of these relationships, mean rugosity was used in-lieu of the gradient in equation 1.

Equation 1:

$$y = mx$$

(Where *y* = contour length, *m* = gradient, and, *x* = planar linear length)

Equation 2:

$$Rugosity = calculated\ contour\ length\ /\ planar\ length$$ (Risk, 1972).

This chapter will investigate the potential of using this database, and the equations determined from it, to gain 3D structural information from 2D reef survey data. It will test whether rugosity calculated using the conversion factors can be consistent with rugosity measured *in-situ*. This will be achieved by applying the aforementioned equations to three types of coral reef survey data: video transects, line intercept data and UAV imagery. Each of these presents a unique opportunity to investigate whether the developed rugosity measurement technique has the potential to derive rugosity information from 2D field data and provide a successful alternative for measuring and monitoring coral reef rugosity.

3.2 Control test: Artificial video transects

Any technique developed to measure rugosity more efficiently, without a need for *in-situ* data collection**,** must do so without any compromise to the accuracy or representativeness of the rugosity measurement (Hobson, 1972, Harris *et al.,* 2015, Ferrari *et al.,* 2016 and Hedley *et al.,* 2016). As a control experiment, the conversion equations derived in chapter 1 were applied to planar lengths of corals measured from video transects of artificial coral reefs built in a controlled setting. This test was set to examine the accuracy of rugosity data calculated using the conversion factors, on a 'reef' transect where hard corals were the only feature contributing to the overall structural complexity. The type of data for this test was selected due to video transects being a well-established method for recording benthic data on coral reefs (AIMS, 2004).

3.2.1 Methods

60 artificial coral reef transects were built using coral colonies from the Natural History Museum dry invertebrate collection. Corals of variable genus and morphotype were placed along a 5 m transect, on the floor, defined by a tape measure. The transects each represented a unique coral community composition and were broadly categorised, by morphotype, as containing only slow growing corals (free-living, encrusting, massive, flabello-meandroid and submassive corals), only fast growing corals (branching, plates, columnar and contorted corals) or a combination of both, in accordance with Darling *et al.,* (2012) life history strategies. Video transects were recorded using a FUJIFILM XP130 camera to capture the corals directly on top of the transect tape, in an identical way to that used for video transects recorded *in-situ* on reefs (Hill and Wilkinson, 2004). A rig system was used to ensure that the height (1 m) and horizontal position (directly above the transect) of the camera remained constant throughout the video recording.

All video transects were analysed using open source Kinovea software (www.kinovea.org). The measurement scale of each transect was calibrated in the first video frame using the visible scale of the tape measure. The planar length of each individual coral colony or 'substrate' along the tape was

measured using the ‘line’ tool and the corals identified to genus level. Where this was not possible, the coral was assigned a morphotype, as in Edwards *et al.,* (2017). The respective rugosity conversation factors for each coral or substrate type were used to calculate the contour length of each measured feature from respective planar lengths, using equation 1. It is noted that for this analysis, the floor, representing the underlying reef substrate, was assigned a rugosity conversion factor of 1 as it showed no variation in height along the transect. The total contour length of each transect was calculated and divided by the respective known planar length (5 m) to determine a rugosity index value for each transect, using equation 2. The mean rugosity of each broad transect category (slow, fast and mixed growing corals, as aforementioned) was also calculated as the sum of rugosity values, divided by the number of transects in each category. The raw data for each individual control transect can be found in Appendix B.

To test whether these calculated transect rugosity values were consistent with *in-situ* measurement, the ‘*in-situ’* rugosity of each transect was also measured using the widely employed rugosity index, chain-tape technique (figure 1.2). For this, the contour distance of each transect was measured, using a 0.5 cm linked chain, with great care taken to capture every coral colony feature in the measurement. This was divided by the transect planar length (5 m) to calculate rugosity (Risk, 1972). These *in-situ* values were plotted against the calculated rugosity of respective transects for comparison and are included in Appendix B.

3.2.2 Results

Analysis of the artificial, control video transects revealed a very strong, positive correlation (figure 3.1, $r^2 = .96$) and significant ($F(1, 58) = 1456.16$, $p = 0.000$) relationship between calculated rugosity, determined using the conversion factors and *'in-situ'* rugosity measured using the rugosity index.

The control reef data also show a clear distinction between the rugosity of transects composed only of slow, fast and both slow and fast growing corals, respectively represented by blue, green and orange data points in figure 3.1. These results are reflected in the mean calculated rugosity values for each category, whereby slow growing coral transects present the lowest mean rugosity of 1.33 (S.D. = 0.2), and fast growing coral transects, the highest mean rugosity of 2.75, (S.D. = 0.41). The mean calculated rugosity of more variable transects, composed of both slow and fast growing corals, falls between these at 1.95, (S.D. = 0.39). A one-way ANOVA revealed that there was a statistically significant difference between these transect categories ($F(2, 57) = 67.15$, $p = 0.000$). A Tukey post-hoc test revealed that the differences between the mean rugosity of the three transect categories (slow, fast and both slow and fast growing corals) were all significantly different from one another at the $p = 0.05$ level: slow and fast growing corals ($1.42 \pm .12$, $p = 0.000$), slow and mixed growing corals ($.62 \pm .12$, $p = 0.000$) and fast and mixed growing corals ($.8 \pm .11$, $p = 0.000$)

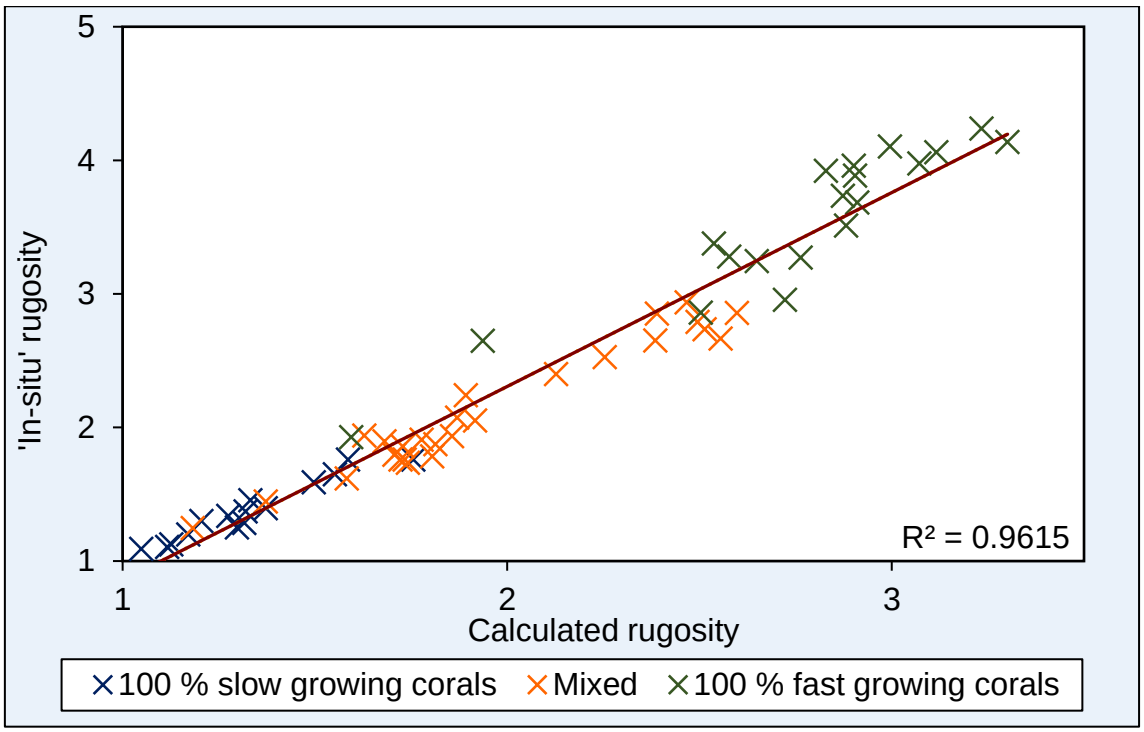

Figure 3.1. Calculated vs *in-situ* rugosity values from analysis of the artificial, control transects from the Natural History Museum, with linear regression line (red). Blue points represent transects composed only of slow growing corals (stress tolerant, weedy and generalist), green points represent transects composed only of fast growing corals (competitive) and orange points represent transects composed of both slow and fast growing corals.

3.2.3 Discussion and conclusion

The very strong and significant correlation between calculated and *in-situ* rugosity, determined from the control video transects, indicates a strong similarity between the two metrics. This shows that rugosity calculated using the conversion factors is consistent with *in-situ* measurements and therefore can provide an accurate proxy of coral reef structural complexity.

The technique and resultant rugosity values were also able to differentiate between transects dominated by corals with variable life history strategies, due to its consideration of the individual and unique contributions of different coral genera, with variable morphotypes, to the overall structural complexity. Figure 3.1 exemplifies this, showing an increase in calculated rugosity as the artificial reefs progress from being dominated by plateau, less complex (slow growing) corals to open branching, plating and contorted (fast growing) corals. This reinforces research recognising that differences in coral reef structural complexity are often a result of the morpho-functional attributes of the dominant coral species present on a reef (Alvarez-Filip *et al.,* 2011 and 2013, Darling *et al.,* 2012, and Perry *et al.,* 2013). These results thus show that the conversion factor technique could be advantageous for accurately distinguishing between reefs of varying coral compositions and complexities and supports the recommendation from chapter 1 that coral morphotype should be considered when assessing reef structure and health (Darling *et al.,* 2012, Burns *et al.,* 2015 and House *et al.,* 2016).

The control data shows the potential of the rugosity trait database equations for calculating rugosity from photo or video imagery. These data are much faster to collect in the field than measurement of the planar and contour lengths of reef transects required to calculate the rugosity index (Risk, 1972). As such, the test initially highlights how the conversion factor technique is more efficient than the traditional chain-tape method for measuring rugosity. The control test also demonstrates how the application of coral conversion factors to measured reef features in video imagery and photographs can aid the constraint of coral colony contributions to reef structural complexity – a scale of rugosity (micro) which has previously eluded the capability of rugosity monitoring methods.

Consequently, the results demonstrate the success of the technique for gaining accurate 3D information from 2D survey data, recorded in a controlled setting, and for being able to distinguish structural differences between naturally heterogeneous reefs with variable coral community compositions.

3.3 Introduction to Field Applications

The artificial coral reef transects provided a unique, control environment in which to test and demonstrate the high accuracy of rugosity data that can be calculated from the application of coral conversion factor equations to 2D video or, hypothetically, photo quadrat imagery. However, for the technique to be successfully considered as a globally applicable, standardised and reliable alternative to *in-situ* rugosity measurement, it must be able to maintain this accuracy when used to calculate rugosity from field survey data, recorded in a natural coral reef environment.

3.4 Field test and Application 1: Video Transects

3.4.1 Methods

The first field survey data, to which the conversion factor technique was applied, were 5, 5 m video transects recorded from the lagoon at Heron Island (figure 2.1) and a further 51, 10 m transects, recorded at sites surrounding three atolls in the Chagos Archipelago; The Great Chagos Bank, Salomon and Peros Banhos (figure 3.2). A videographer used a GoPro or CanonS101 camera to record the coral environment directly below each transect, which was defined by a tape measure that ran in a straight line across the coral reef. As in the control test, the *in-situ* rugosity of each transect was also measured using the rugosity index, where the diver took great care to capture every crack, crevasse and coral colony feature in the contour measurement required for this calculation.

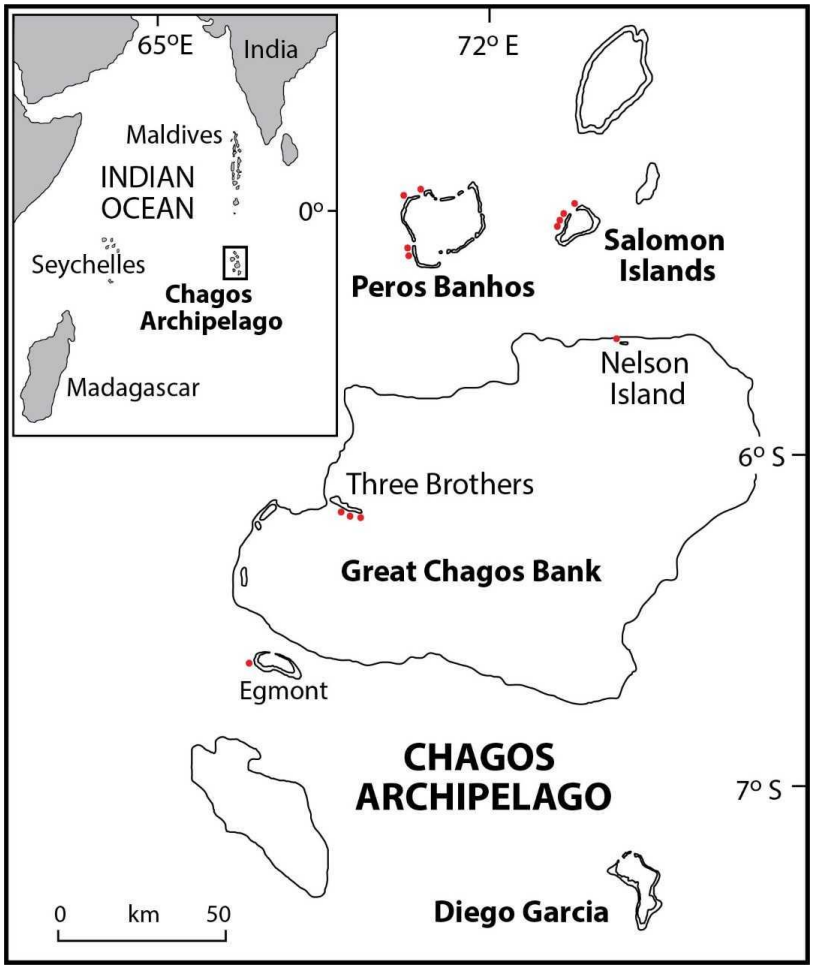

Figure 3.2. Study site locations for video transect data recorded in the Chagos Archipelago. Red dots indicate reefs on which video transects were recorded. Credit to Dr. Ines Lange.

The video transects were analysed in the same way as in the control test, using Kinovea to measure the planar length of every coral reef feature or substrate type directly below each transect. In contrast to the control transects, however, the measurement scale of each video was calibrated in every frame to account for any change in diver height above the substrate throughout the recording. Each coral reef feature measured was identified to a genus or morphotype level. The planar lengths were converted into contour lengths using the rugosity conversion factor equations, noting that for these field transects mean rugosity was used as the coral conversion factor in equation 1 for sand and rubble as opposed to the line gradients used for the coral genera and morphotypes. For each transect, the contour lengths were summed and divided by the respective transect planar lengths to calculate a transect rugosity value.

Corrections factors

Consideration was given to a number of 'holes', peaks and troughs, and undercut areas that were identified throughout these transects, especially those recorded in Chagos, but were not represented in the coral rugosity trait database. To try and account for these features, four categories of 'holes' were defined to represent small, medium, large and very large drops or rises in the reef surface, based on visual observation of these features in the videos. A first correction used values of 20, 30, 50 and 100 cms and a second correction, 25, 50, 100 and 200 cms to respectively represent the holes from small to very large. These values were based on visual estimations of hole sizes, and a six-point scale description of topographic complexity described by Graham *et al.,* (2015) and Polunin and Roberts (1993), that estimates the height of various reef features. The video transects were reanalysed and for each occurrence of these aforementioned features, a respective correction value was added to the overall transect contour length. New rugosity values for each transect were subsequently calculated using these corrected contour lengths.

As in the control transect test, the calculated rugosity values, with and without correction factors, for each transect were compared with the respective *in-situ* values to test for similarity between the two metrics. The raw data for each individual natural, *in-situ* transect, before and after the addition of correction factors, can be found in Appendix C.

3.4.2 Results

Analysis of the video transects recorded in Chagos revealed a very weak correlation (r^2 = .06, figure 3.3a) between *in-situ* rugosity and rugosity calculated from application of the coral conversion factors to planar coral lengths measured in Kinovea (hereafter, calculated rugosity). Linear regression analysis revealed this relationship as non-significant ($F(1, 49) = 3.21$, $p = 0.08$) at a p < .05 confidence level. The addition of two sets of correction factors to the original data slightly increased the correlation coefficients between the two metrics (figures 3.3b and 3.3c). However, these remained weak ($r^2 \leq .02$), despite linear regression analysis revealing that the corrected relationships, between *in-situ* and calculated rugosity, were significant at a $p < .05$ confidence level (see table 3.1).

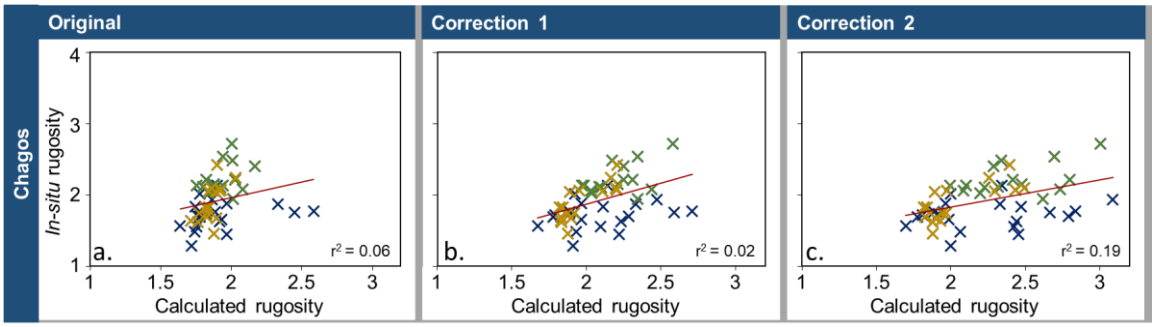

Figure 3.3. Calculated vs *in-situ* rugosity values from analysis of video transects recorded in Chagos. 14a) represents the original data, b) represents the original data with the addition of the first correction factors and c) represents the original data with the addition of the second conversion factors. Green points represent data collected from the Salomon Islands, blue points represent data from the Great Chagos Bank and yellow points represent data from Peros Banhos.

Table 3.1. Results of the regression analysis comparing *in-situ* and calculated rugosity values from analysis of the video transects recorded in Chagos, Heron Island and at the Natural History Museum (included for comparison), (* indicates a significant result).

Dataset	Significance test result
Chagos original	$F(1,49) = 3.29$, $p = 0.076$)
Chagos, correction 1*	$F(1,49) = 12.56$, $p = 0.001$)
Chagos, correction 2*	$F(1,49) = 11.59$, $p = 0.001$)
Heron original	$F(1,3) = 7.71$, $p = 0.0691$)
Heron, correction 1	$F(1,3) = 5.18$, $p = 0.1073$)
Heron, correction 2	$F(1,3) = 3.68$, $p = 0.1511$)
Natural History Museum*	$F(1,58) = 1456.16$, $p = 0.000$)

Conversely, data analysis of the Heron Island video transects showed a strong correlation between *in-situ* and calculated rugosity (figure 3.4a, $r^2 = 0.72$). Furthermore, in contrast to the Chagos transects results, the addition of correction factors to the original data weakened this correlation to $r^2 = 0.63$ and $r^2 = 0.55$ on application of correction factors 1 and 2 respectively (figures 3.4b and 3.4c). Linear regression analysis revealed that neither the original or corrected relationships between *in-situ* and calculated rugosity were significant at a $p < .05$ confidence level. The results of this analysis are presented in table 3.1.

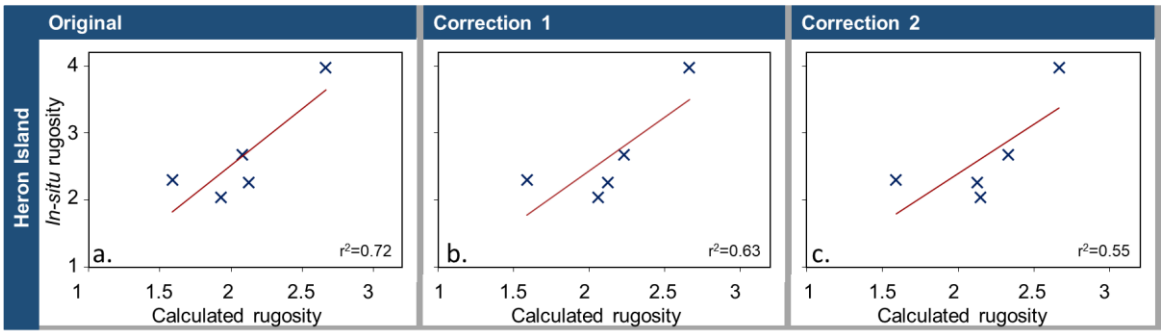

Figure 3.4. Calculated vs *in-situ* rugosity values from analysis of the video transects recorded from Heron Island. 14a) represents the original data, b) represents the original data with the addition of the first correction factors and c) represents the original data with the addition of the second correction factors.

3.4.3 Discussion

Calculated vs *in-situ* rugosity

In contrast to the results from the control video transects (chapter 3.2), for the field survey data there was very little similarity between *in-situ* rugosity and rugosity calculated using the conversion factor technique (calculated rugosity). On initial examination, the strong correlation between these metrics for Heron Island transects (figure 3.4) does appear to show, similar to the control transects, that the application of conversion factors to *in-situ,* field video imagery can provide accurate rugosity information without the need for physical contact with the coral reef. However, the low sample size (n = 5) and statistical insignificance of this relationship greatly reduces the validity of this inference. This positive result is completely negated on subsequent examination of the Chagos transects where a very weak correlation revealed almost no similarity between the calculated and *in-situ* rugosity values. The relationship between these metrics was also insignificant, despite the large increase in sampled transects analysed from Chagos (n = 51) compared to Heron Island.

Consequently, on application of the conversion factor technique to field data, the calculated rugosity values are not consistent with *in-situ* measurements and thus are not accurate representations of natural coral reef structural complexity. These results are in stark contrast to those from the control test (chapter 3.2.2), as well as an array of techniques where rugosity calculated virtually, from alternate survey data, has shown strong agreement with *in-situ* chain-tape rugosity (Brock *et al.,* 2006, Kuffner *et al.,* 2007, Benjarano *et al.,* 2010, Friedman *et al.,* 2012 and Young *et al.,* 2017).

Influence of mesoscale and abiotic reef features

The difference in the accuracy of the calculated rugosity data between the control and field survey transects is considered a result of both the presence of natural, underlying reef substrate on Heron Island and Chagos reefs, and, the use of conversion factors only representative of coral colonies and limited abiotic substrates.

Determining the contribution of coral colonies to reef structural complexity, as demonstrated by the control transects (chapter 3.2), is important for understanding the potential impacts of future coral community change (Harborne *et al.,* 2012, Alvarez-Filip, 2013; and Bozec *et al.,* 2015). However, a large vertical component of coral reef structural complexity also results from natural topographic heterogeneity of the underlying reef substrate, naturally occurring caves and holes, and undercut areas beneath or between coral colonies (Gratwicke and Speight, 2005, Harborne *et al.,* 2012, Friedman *et al.,* 2012 and Richardson *et al.,* 2017). These features contribute to mesoscale rugosity which exerts an important influence on ecosystem biodiversity and functioning at an intermediate scale between structural complexity provided by hard coral skeletons (microscale), and that provided by the seabed (macroscale), (Levin *et al.,* 2000, Mumby and Steneck, 2008, Stier and Osenberg, 2010, and Harborne *et al.,* 2012). The contribution of these features to transect rugosity are captured by the *in-situ* chain-tape measurement. However, they are not accounted for by the calculated rugosity values which only represent the contribution of coral colonies (microscale features), or flat coral rubble and sand patches, to structural complexity (Risk, 1972 and Harborne *et al.,* 2012). This discrepancy in measurement scale invalidates any comparison between the *in-situ* and calculated rugosity values from the field survey video transects. As such, it is not surprising that rugosity measured virtually from alternate remote sensing techniques, at the same scale as the chain-tape method, shows much greater similarity to *in-situ* values, (Hattori and Shibuno, 2015).

The addition of correction factors attempted to account for the rugosity provided by some of the identified mesoscale features (caves and holes, figures 3.3 b and c and 3.4, b and c). However, these had very little effect on increasing the correlation between *in-situ* and calculated rugosity for the Chagos data, and conversely caused the correlation to decrease between these variables for Heron Island data. These mixed results suggest that the (somewhat arbitrary) correction factors did not globally, or accurately represent the mesoscale features intended, and/or, that the natural, underlying heterogeneity of the seabed, which was not accounted for by the correction factors, was also a large contributor to the overall transect rugosity. Consequently, it is concluded that

the methodology, for calculating rugosity from 2D survey data, is well-suited for accurately quantifying coral colony scale rugosity, but is much weaker at measuring overall transect rugosity where the underlying reef substrate is also a contributing factor.

The influence of these mesoscale features, and underlying substrate heterogeneity may also explain why the calculated rugosity for Heron Island data (albeit with only 5 transects) is more accurate than for Chagos. During the 2016 thermal anomaly event, Heron Island reefs did not suffer as extensive coral bleaching or mortality as those in the Chagos archipelago and therefore had a greater proportion of living coral along the transects (Perry and Morgan, 2017a, Sheppard *et al.,* 2017 and AIMS, 2018). This living coral may have masked a proportion of the natural heterogeneity of the underlying reef substrate, from the chain-tape measurement, whereas the dominance of dead, eroded and algae covered coral along the Chagos transects exposed these features to this measurement.

The large proportion of dead coral in Chagos may also have decreased the accuracy of coral colony identification. This is because dead, encrusting coral and underlying reef substrate showed a strong resemblance to one another in the video transects. Any error in identification between these features would have propagative effects through the analysis, as any incorrect assignation of conversion factors would further reduce the accuracy of calculated rugosity, albeit to a small degree. This was not a factor when identifying the corals along the control transects. These issues did, however, highlight the value of having morphotype, as well as genus, conversion factors. This is because, irrespective of the ability to correctly identify a coral to a genus level, coral features could be assigned a conversion factor representative of their rugosity.

Methodological analysis

If considered at the coral colony scale, the ability to calculate rugosity virtually from video imagery will greatly increase the efficiency of dive time. This is because on a single dive, researchers will be able to record video footage and photographs, from which rugosity data can be later extracted, for larger areas than for which rugosity could be measured *in-situ* during the same limited time

period underwater (He *et al.,* 2012). Although new video imagery helps provide a permanent record of reef condition, the technique could also eliminate the need for some dives altogether, if video imagery that the conversion factors can be applied to already exists for a region (Hill and Wilkinson, 2004). Despite this, as is often true for remote sensing techniques, the video analysis, once recorded, was more time consuming, taking ~ 30 minutes to measure, identify and assign the relevant conversion factors to each coral along a 10 m transect. This reduces the time effectiveness of the technique when compared to *in-situ* chain-tape rugosity measurement (Shumway *et al.,* 2007).

Additional methodological issues, identified from analysis of the field transects, resulted from natural ocean swell making it challenging for divers to always maintain their vertical and horizontal position, and camera angle, above the defined transect line. In some videos, this made it difficult to identify the exact coral colonies included in the *in-situ* rugosity measurement. Any discrepancy in the corals measured *in-situ* and identified in the video imagery would greatly reduce the validity of the calculated rugosity. The scale of the video imagery also had to be recalibrated, in Kinovea, each time the camera moved position, adding an extra element of error to the technique. These issues were not identified for the control reef transects (chapter 3.2) where the rig-system maintained the position of the camera above each transect, perhaps aiding the strong similarity between calculated and *in-situ* rugosity for these transects.

3.4.4 Conclusion

The use of the taxa specific rugosity conversion equations to calculate rugosity from both control and ‘real-world’ video imagery, in chapters 3.2 and 3.2, has resulted in the development of a technique that can accurately quantify the variable contribution of individual coral colonies to the overall structural complexity of a coral reef**.** This technique enables more detailed analyses of the relative contribution of these microscale features to reef rugosity than permitted from current techniques and consequently could be highly useful for monitoring the impacts of future coral community change on rugosity through analysis of repeat transects over time (Harborne *et al.,* 2012).

As revealed by analysis of the field transects, the technique is currently limited to calculating coral colony, micro-scale rugosity due to the absence of conversion equations for mesoscale features in the rugosity database. Furthermore, it will only provide representative rugosity information for environments with high living coral cover and little surface heterogeneity. Future work could aim to quantity the contribution of *all* components of a coral reef to its structural complexity and improve the accuracy of meso-scale correction factors, to increase the applicability of the technique for a larger range of reef environments. However, these features are unlikely to be consistent throughout such heterogeneous ecosystems. A more advantageous approach, therefore, is to conclude that the conversion factor technique is successful for quantifying rugosity at the coral colony scale. In this way, this initial application of the conversion factors specifically to control video transect data shows how the technique could be globally useful for monitoring coral colony scale rugosity in all coral reef environments.

3.5 Further applications

The use of the conversion factor equations to convert 2D measurements into 3D structural information from video transect surveys demonstrates the capability of the technique for providing accurate rugosity data, when measured at the coral colony scale. With consideration of this success and to examine the full potential of the technique, this research will hereafter demonstrate two additional applications of the ‘conversion factor technique’ for calculating coral colony scale rugosity from line intercept and UAV imagery survey data.

3.6 Field Application 2: Line Intercept Data

At present a lack of data regarding the baseline condition of coral reefs is limiting the ability of models to accurately predict how reefs will respond to future environmental change (Sweatman *et al.,* 2011). The application of the conversion factors to existing line-intercept data could enable historic reef rugosity information to be gained for areas where this metric of reef health was not previously measured.

3.6.1 Methods

To explore the usefulness of the rugosity trait database for calculating historical rugosity, the rugosity conversion factors were applied to line intercept data from the Seychelles (figure 3.5, from Graham *et al.,* 2015). This pre-existing dataset recorded the linear distance covered by various coral genera and macroalgae along a total of 305, 10 m transects spanning 4 years (2008, 2011, 2014 and 2017) and 21 study sites (7 sites over three habitats / substrates (see Graham *et al.,* 2015 for methods)). These study sites were further categorised as 'recovering' or 'regime shifted' (hereafter shifted) by Graham *et al.,* (2015) based on their recovery after the 1998 bleaching event. The last year of this data (2017) was recorded after the 2016 Indian Ocean coral bleaching event. As such, this application also explores the effects of this disturbance event on selected reefs in the Seychelles, and whether the conversion factor technique can quantify any changes in coral colony scale rugosity resulting from it.

The linear distance of each coral was converted to a contour distance using the conversion factor equations. For corals recorded along these transects not included in the database, a conversion factor was assigned based on morphotype. Macroalgae, for which conversion factors were also not available, were assigned the same rugosity values as coral rubble to ensure subsequent rugosity calculations primarily reflected the differential contributions of hard coral taxa. The rugosity of each transect was calculated as the sum of all contour lengths divided by the planar transect length (10 m) (Risk, 1972). An average rugosity was calculated for each study site, for each of the four years data was collected. This data was plotted as time series and analysed

statistically to asses any change in rugosity through time when reefs were grouped by status (shifted or recovering reefs, defined by Graham *et al.,* 2015*****), site, and by their underlying substrate (sand, coral or granite). The raw data, from conversion of the line intercept data to contour lengths and respective rugosity values, can be found in Appendix D.

*****It is noted that coral reefs previously defined as in a 'recovering' state by Graham *et al.,* (2015), may no longer be in a recovering state if they suffered extensive bleaching during the 2016 Indian Ocean thermal anomaly.

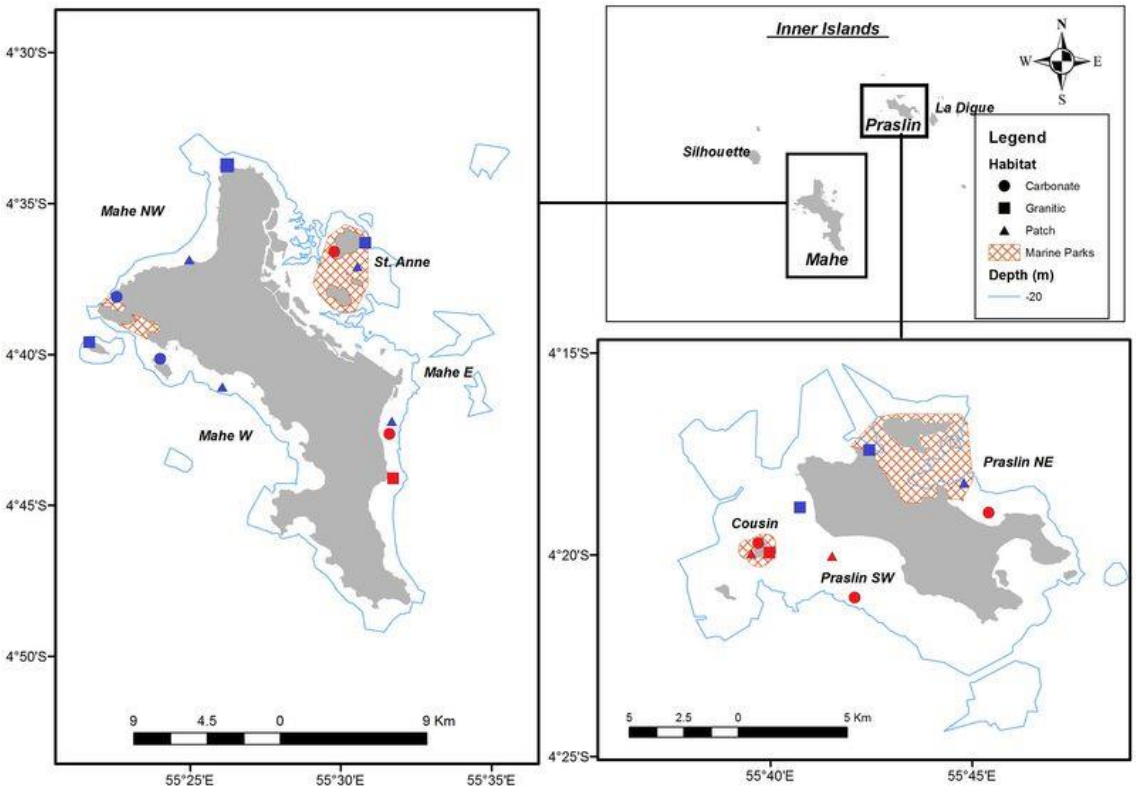

Figure 3.5. Map of study sites in the Seychelles on which the line intercept data was collected. Blue points represent reefs defined as recovering from the 1998 bleaching event and red points represent reefs that were defined as having undergone a regime shift. Taken from Graham *et al.,* (2015), extended data figure 7.

3.6.2 Results

The application of the coral conversion factors to line intercept data shows how coral colony scale rugosity, of variable reefs in the Seychelles, changed between 2008 and 2017. It is noted that hereafter, unless otherwise specified, calculated rugosity will refer to that at the coral colony scale.

Recovering vs regime shifted reefs

Figure 3.6 shows that coral reefs in both recovering and regime shifted states experienced a decline in coral colony rugosity between 2014 and 2017. Over the entire period, the mean rugosity of shifted reefs was more stable then recovering reefs, varying between a minimum of 1.32 (in 2017) and a maximum of 1.40 (in 2014). This is compared with the mean rugosity for recovering reefs which varied between 1.35 (in 2017) and 1.73 (in 2014). The mean rugosity for recovering reefs increased between every period (2008 – 2014) in contrast to the mean rugosity of shifted reefs which decreased between 2008 and 2011. The rugosity of recovering reefs is consistently higher than that of shifted reefs and the greatest and smallest differences between the rugosity of reefs in these stages occurred respectively in 2014 and 2017. This shows that proportionally, recovering reefs experienced much greater declines in rugosity between these years than the shifted reefs (table 3.2). An independent *t*-test revealed that the difference in the mean rugosity of shifted and recovering reefs was statistically significant in 2011 and 2014 ($p<0.05$), but not in 2008 or 2017 (see table 3.3).

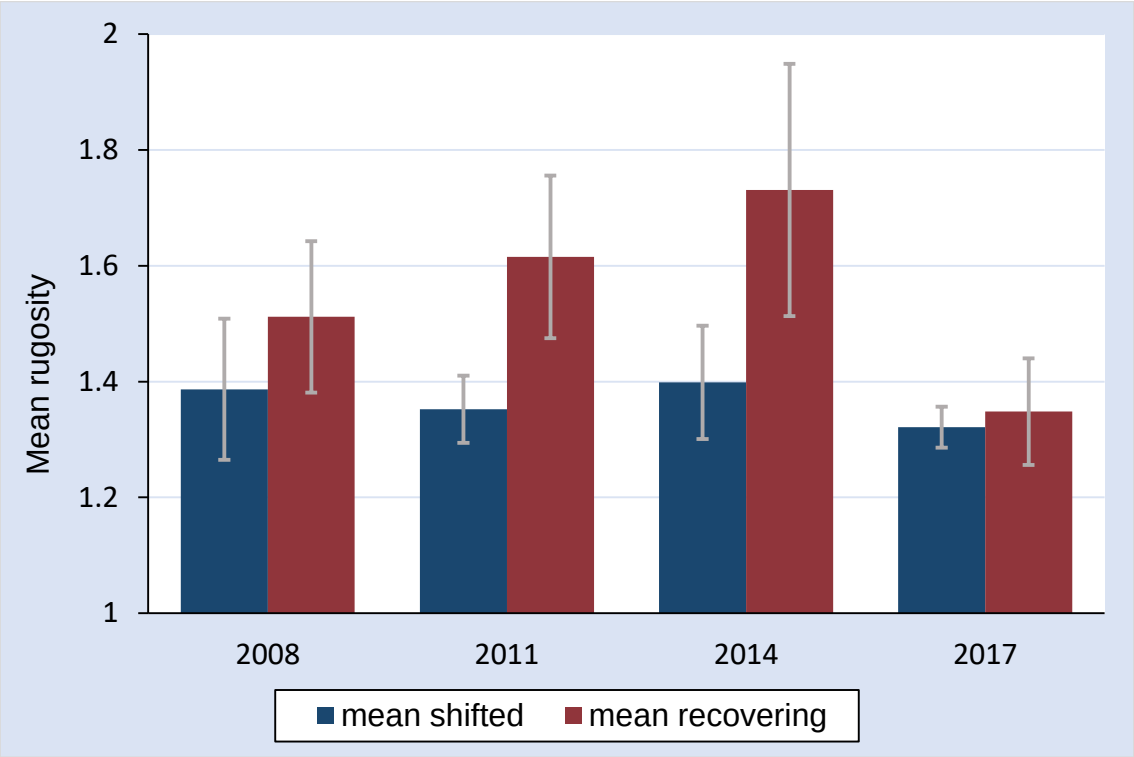

Figure 3.6. Mean rugosity of Seychelles coral reefs, in both regime shifted and recovering states, for four years post the 1998 bleaching event. Error bars represent standard deviation.

Table 3.2. Mean rugosity percentage change of shifted and recovering coral reefs in the Seychelles, for three time periods after the 1998 coral bleaching event.

	Percentage Change: mean rugosity (%)		
	2008-2011	**2011-2014**	**2014-2017**
Shifted reefs	- 1.99	+ 3.44	- 5.21
Recovering reefs	+ 7.18	+ 7.27	- 20.72

Table 3.3. Results of *t*-tests comparing the mean rugosity of shifted and recovering reefs in the Seychelles for four years post the 1998 coral bleaching event, (*indicates a significant difference in the rugosity of shifted and recovering reefs).

Year	**State**	**Mean rugosity**	***t*-test result**
2008	Recovering reefs Shifted reefs	1.51 ± .04 1.39 ± .04	$t(19) = 2.23$, $p = 0.0381$*
2011	Recovering reefs Shifted reefs	1.62 ± .04 1.35 ± .02	$t(19) = 5.27$, $p = 0.0000$*
2014	Recovering reefs Shifted reefs	1.73 ± .06 1.4 ± .03	$t(19) = 4.25$, $p = 0.0004$*
2017	Recovering reefs Shifted reefs	1.35 ± .03 1.32 ± .01	$t(16) = 0.67$, $p = 0.5105$

Inter-site variability

The data, summarised in figure 3.7, reveal inter-site variation in mean rugosity between the four years for which data was collected. The raw data for these results, and rugosity percentage change for individual sites within each reef location, can be found in appendices D and E. All locations, considered irrespectively of whether specific study sites were in a recovering or regime shifted state, experienced a decline in reef rugosity between 2014 and 2017. The magnitude of this decline was greatest in Mahe W (mean site rugosity decline = -27.7 %), and Mahe NW (mean site rugosity decline -23.5%) and smallest in Mahe E (mean site rugosity decline = -6.9 %) and Praslin NE (mean site rugosity decline = -5.5 %). The decline in Cousin Reef rugosity for this period is unknown due to the absence of data for 2017. Praslin NE and Mahe E reefs show additional, smaller rugosity declines of - 3.6 % and - 7.7 % respectively between 2008 and 2011. Between 2011 and 2014 the mean rugosity of all locations increased, ranging from a percentage increase of 0.5 % for Praslin NE to 12.4 % for Mahe NW.

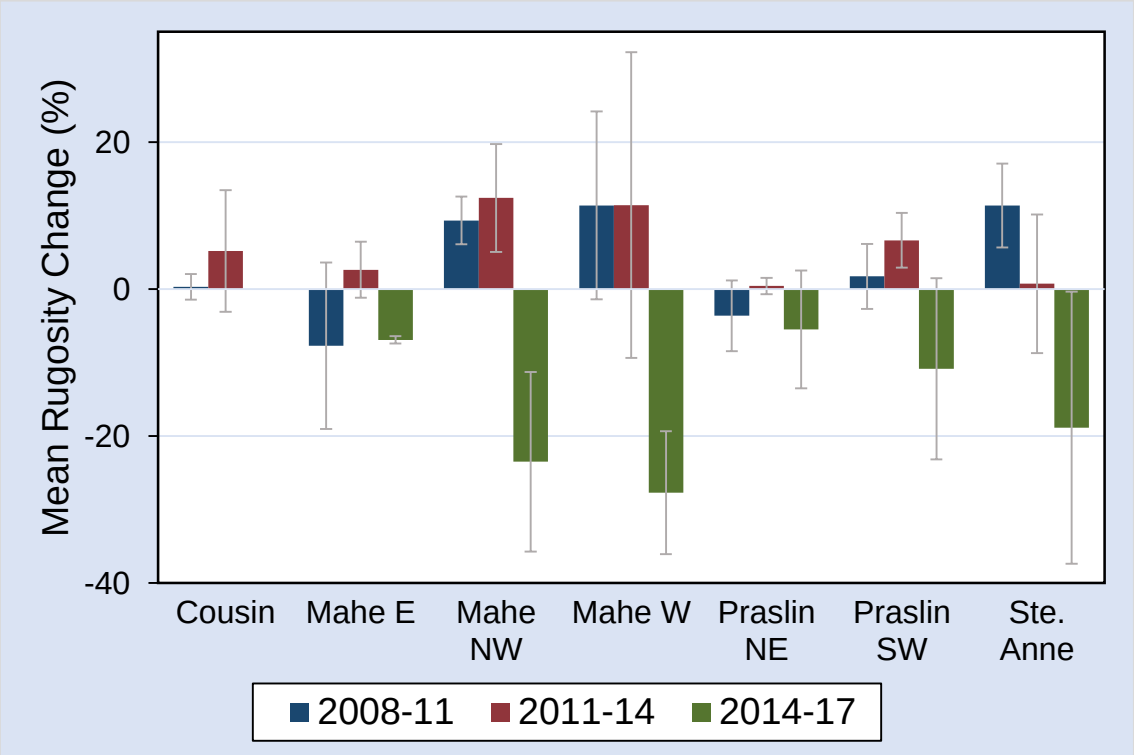

Figure 3.7. Mean rugosity percentage change of 7 reef locations in the Seychelles for three periods between 2008 and 2017. Error bars represent standard deviation.

Habitat differences

Finally, to a lesser degree, the data reveals variability between reefs with either sand, granite or carbonate as the underlying substrate (figure 3.8). In all years - with the exception of 2008, where coral and sand reefs had equal mean rugosity - reefs underlain by granite and sand show higher mean rugosity than reefs underlain by coral. The rugosity of sites underlain by granite and sand also increased during each period prior to 2014 - 2017, whereas sites underlain by coral showed a small decrease in rugosity between 2008 and 2011 before increasing between 2011 and 2014. All reefs, irrespective of underlying substrate, experienced a similar magnitude of rugosity decline between 2014 and 2017 (coral = -15.4 %; granite = -15.05 % and sand = - 16.2 %).

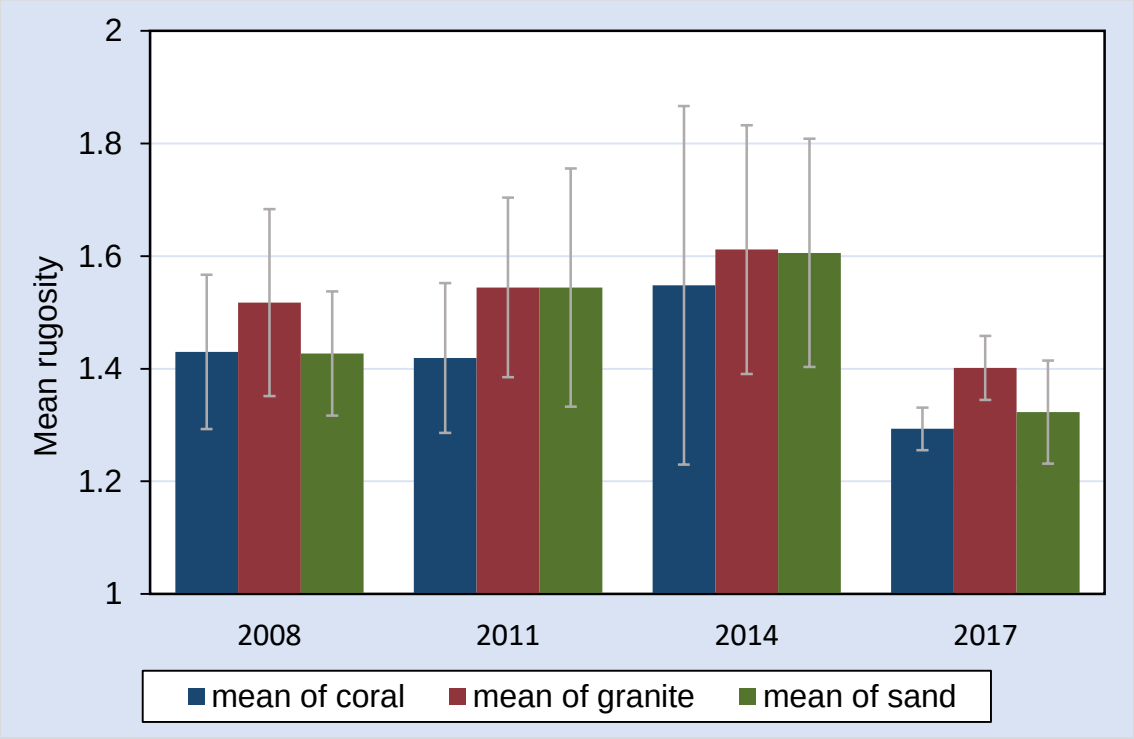

Figure 3.8. Mean rugosity of Seychelles coral reefs, underlain by coral, granite and sand for four years post the 1998 bleaching event. Error bars represent standard deviation.

A one-way ANOVA revealed no statistically significant difference between the mean rugosity of the three coral reef habitats ($p > 0.05$, table 3.4) in 2008, 2011 and 2014, but a significant difference between mean habitat rugosity in 2017

($F(2, 15) = 4.32$, $p = 0.0329$). For this year (2017), a post-hoc Tukey test revealed that the mean rugosity of granite based reefs was statistically, significantly higher than that of coral based reefs (.11 ± .04, p =.031). There were no statistically significant differences between the mean rugosity of granite and sand based reefs (-.08 ± .04, p = .131), or between that of coral and sand based reefs (.03 ± .04, p = .719).

Table 3.4. Results of the ANOVA test comparing the mean rugosity of coral reefs in the Seychelles underlain by coral, granite and sand post the 1998 coral bleaching event, (* indicates a significant result).

Year	Habitat	Mean	ANOVA result
2008	Coral	1.43 ± .14	$F(2, 18) = .94$, $p = 0.4082$
	Granite	1.52 ± .17	
	Sand	1.43 ± .11	
2011	Coral	1.42 ± .13	$F(2, 18) = 1.25$, $p = 0.3096$
	Granite	1.54 ± .16	
	Sand	1.54 ± .21	
2014	Coral	1.55 ± .32	$F(2, 18) = 0.14$, $p = 0.8742$
	Granite	1.61 ± .22	
	Sand	1.60 ± .20	
2017	Coral	1.29 ± .04	$F(2, 15) = 4.32$, $p = 0.0329$*
	Granite	1.40 ± .06	
	Sand	1.32 ± .09	

3.6.3 Discussion

Trajectories of regime shifted and recovering reefs

The application of the conversion factor technique to existing line intercept data has enabled coral colony scale rugosity to be reconstructed for a range of reefs in the Seychelles both before and after the 2016 Indian Ocean bleaching event. It is noted that there was an absence of any relevant scale *in-situ* rugosity data to compare the calculated rugosity values with. However, the success of the conversion factors for accurately quantifying coral colony scale rugosity identified in chapter 3.2, and known responses of the reefs to bleaching events (Graham *et al.,* 2015), permit some interpretations to be made regarding recent, variable changes to coral colony scale reef rugosity in the Seychelles.

Between 2008 and 2017, there was a significant difference in the rugosity of recovering and regime shifted reefs (as defined by Graham *et al.,* 2015) following the 1998 bleaching event, in all years with exception of 2017 (table 3.3). On recovering reefs, with increasing coral cover, coral colony scale rugosity increased year on year between 2008 and 2014. This was much more variable on shifted reefs where rugosity always remained lower than on recovering reefs. These trajectories are consistent with changes in coral cover recorded for reefs in these states by the original line intercept data and consequently, support the well documented (positive) relationship between coral cover and rugosity (Aronson and Precht, 1995, Dustan *et al.,* 2013 and Graham *et al.,* 2015). This is especially true considering that the calculated rugosity predominately reflects the structure provided by coral colonies as opposed to additional reef biota or abiotic substrate.

The rugosity of both shifted and recovering reefs declined between 2014 and 2017, although this decline was of a higher magnitude on recovering reefs. This is consistent with the response of Seychelles reefs, in both states, to the 2016 (and previous) coral bleaching event(s) reported in other sources (Nature Seychelles, 2006 and McGavin *et al.,* 2017). The data therefore show that the 2016 bleaching event reduced the magnitude of rugosity difference between recovering and shifted reefs. This could potentially be due to differences in the morphological functional attributes of dominant corals present on the reefs. For

example, in a hypothetical scenario, with reference to coral life history strategies, fast growing, competitive corals, such as *Acropora,* may have colonised recovering reefs after the 1998 disturbance event, increasing the structural complexity of these reefs compared with shifted reefs. However, these corals are also the least tolerant to environmental change and would have suffered extensive mortality during the 2016 bleaching event, (Darling *et al.,* 2012 and 2013, and Januchowski-Hartley *et al.,* 2017). In contrast, coral communities on shifted reefs may have been dominated by stress tolerant, weedy or generalist corals which are slower growing, but more tolerant to environmental change, thus explaining the much lower variability in coral colony rugosity on these reefs between 2008 and 2017 (Darling *et al.,* 2012, Alvarez-Filip *et al.,* 2013 and Januchowski-Hartley *et al.,* 2017).

These inferences are consistent with observations of Seychelles reefs following the 1998 bleaching event where reefs dominated by branching corals (*Acropora*) underwent significant regime shifts and, in contrast, reefs persistently dominated by massive corals exhibited a much greater recovery (Januchowski-Hartley *et al.,* 2017). The inferences and *in-situ* observations thus highlight the substantial effect that the ecological context and structural complexity of coral reefs pre-disturbance have on reef resilience and recovery post-disturbance (Januchowski-Hartley *et al.,* 2017). Consequently, this application, and the representative inferences made regarding rugosity trajectories, demonstrates an advantage of the conversion factor technique; over the original line-intercept data: the technique has an ability to reconstruct past rugosity and ecosystem community change through consideration of calculated rugosity, coral life history strategies and functional groups. Such reconstruction will aid future prediction of the trajectories of coral reefs after future disturbance events (Ferrari *et al.,* 2016).

A further advantage of calculated rugosity is that, unlike coral cover, it allows consideration of the time-lag between initial coral mortality or weakening following disturbance events and subsequent declines in coral reef structural complexity. This is a well-documented phenomenon where reef structure has been reported as persisting for > 2 years after initial disturbance events (Sheppard *et al.,* 2002 and Graham *et al.,* 2007). This gradual decline in

complexity would not be recognised through an examination of living coral cover data alone, but could be through use of rugosity conversion factors representing differential stages of coral colony structural breakdown (Graham *et al.,* 2007; Alvarez-Filip, 2010 and Lasagna *et al.,* 2010). The addition of coral colony scale rugosity data could thus help constrain the exact nature of the relationship between structural complexity, disturbances and consequently biodiversity, for individual reefs (Mora, 2008, Perry *et al.,* 2013, House *et al.,* 2016 and Harborne *et al.,* 2017). In turn, this will better inform and increase the accuracy of model predictions regarding the recovery capacities of coral reef ecosystems and the risk of reefs undergoing a state or regime shift, of which structural complexity is a key mitigating factor (Alvarez-Filip, 2010, Graham *et al.,* 2015 and Bozec *et al.,* 2015). As such the quantification of colony scale reef rugosity metrics from historical sources, such as the line intercept data, is key for assessing overall coral reef functionality (Graham *et al.,* 2007 and Alvarez-Filip *et al.,* 2009).

Inter-site and habitat variability

Further analysis revealed variability in coral colony structural complexity between individual sites and the three habitat types during the three periods for which data was available (figure 3.8). Graham *et al.,* (2015) did not identify habitat setting (coral, sand or granite) as a key factor that could correctly predict post-bleaching reef trajectories. However, the data here shows that the mean coral colony rugosity on granitic reefs was higher (albeit only significantly in 2017, see table 3.4) than on carbonate and sand reefs in the first year of measurement after the 1998 bleaching event (2008), and, in 2017, one year after the 2016 bleaching event. This potentially reveals that corals with a granitic habitat preference may be more resistant to environmental change (weedy, stress tolerant or generalist corals) than those on sand and carbonate reefs, or that granitic reefs were colonised by fast growing (competitive) corals soon after these two disturbance events (Nature Seychelles, 2006, Darling *et al.,* 2012, and 2013).

3.6.4 Conclusion and methodological consideration

When considered at a coral colony scale, it is likely that these inferences are representative of fluctuations in the structural complexity of Seychelles reefs after two bleaching events in 1998 and 2016. The results demonstrate how the application of conversion factors to historical, quantitative data, originally intended to examine coral cover, can be used to gain rugosity information for areas where the baseline condition of reefs is currently unknown. They also reveal, initially, an ability of the conversion factor technique to quantify changes in coral colony scale rugosity after a disturbance event. This application will therefore enable historical fluctuations in coral reef rugosity to be identified for much greater timescales than has previously been possible. It will also contribute to reducing the shifting baseline effect which currently limits the accuracy of model predictions regarding the future of coral reefs (Jackson *et al.,* 2012 and House *et al.,* 2016).

In a similar way to the video transects, the analysis revealed a limitation of the technique when used in environments where macroalgae is present. The line intercept data included a large number of macroalgae taxa for which conversion factors were unavailable. For this research, all macroalgae were assigned standardised conversion factors to minimise the influence of this feature on the overall coral colony scale rugosity calculation and any rugosity declines caused by changes in coral community composition. However, macroalgae grows over underlying reef substrate or dead coral, covering and concealing the identity of these features. It is unknown therefore whether the macroalgae in this dataset masked any dead coral colonies for which rugosity conversion factors *were* available. Consequently, although the conversion factor technique is successful at quantifying the coral colony scale rugosity of heterogeneous environments, captured in both imagery and line intercept data, consideration must be given to its use in areas where high macroalgae cover conceals any dead or living coral colonies.

3.7 Field Application 3: UAV Imagery

The application of the conversion factors to video imagery and line intercept data is advantageous for providing historical, coral colony scale rugosity data for areas where this information was not previously available. However, these applications remain limited in their capability to monitor rugosity over large areas due to the requirement for initial video image and coral cover data to be recorded *in-situ* (AIMS, 2004, He *et al.,* 2012 and Chirayath and Earle, 2016). Unmanned aerial vehicles (UAV) provide rapid, high resolution and synoptic image surveys of much larger areas than permitted by *in-situ* survey techniques. The application of the conversion factors to available UAV imagery greatly increases the potential of the conversion factor technique for providing large scale assessment of coral reef communities and colony scale rugosity, and for monitoring these as they change over time (Fuad, 2010, Anderson and Gaston, 2013; Goodman *et al.,* 2013, Figueira *et al.,* 2015, and Purkis, 2017).

3.7.1 Methods

To investigate how the coral colony size – rugosity relationship data could be used to assess and monitor coral colony scale rugosity for large areas, the conversion factors (chapter 2) were applied to coral reef features visible in UAV imagery of the Mahutigala reef, in the Maldives (figure 3.9). Multiple images captured by a DJI Phantom 3 Advanced drone, with flying height ranging from 89.2 to 20.5 m, were used to create a georeferenced orthomosaic using Pix4Dmapper. This was imported into ArcMap where three $10m^2$ study sites were defined to represent three environments of variable coral community composition. These were located on the reef crest, reef flat and back reef. Each individual coral colony and abiotic substrate patch, within each site was manually digitised (using shapefiles) and identified to a genus level where possible or, if not, assigned a coral morphotype, with the aid of *in-situ* photographs of the present coral communities on the reef. A new coral category and size-rugosity relationship was developed to include both *Acropora digitate* and *Acropora corymbrose* colonies (results summarised in table 2.2) due to their similar morphologies being difficult to accurately distinguish from the UAV imagery.

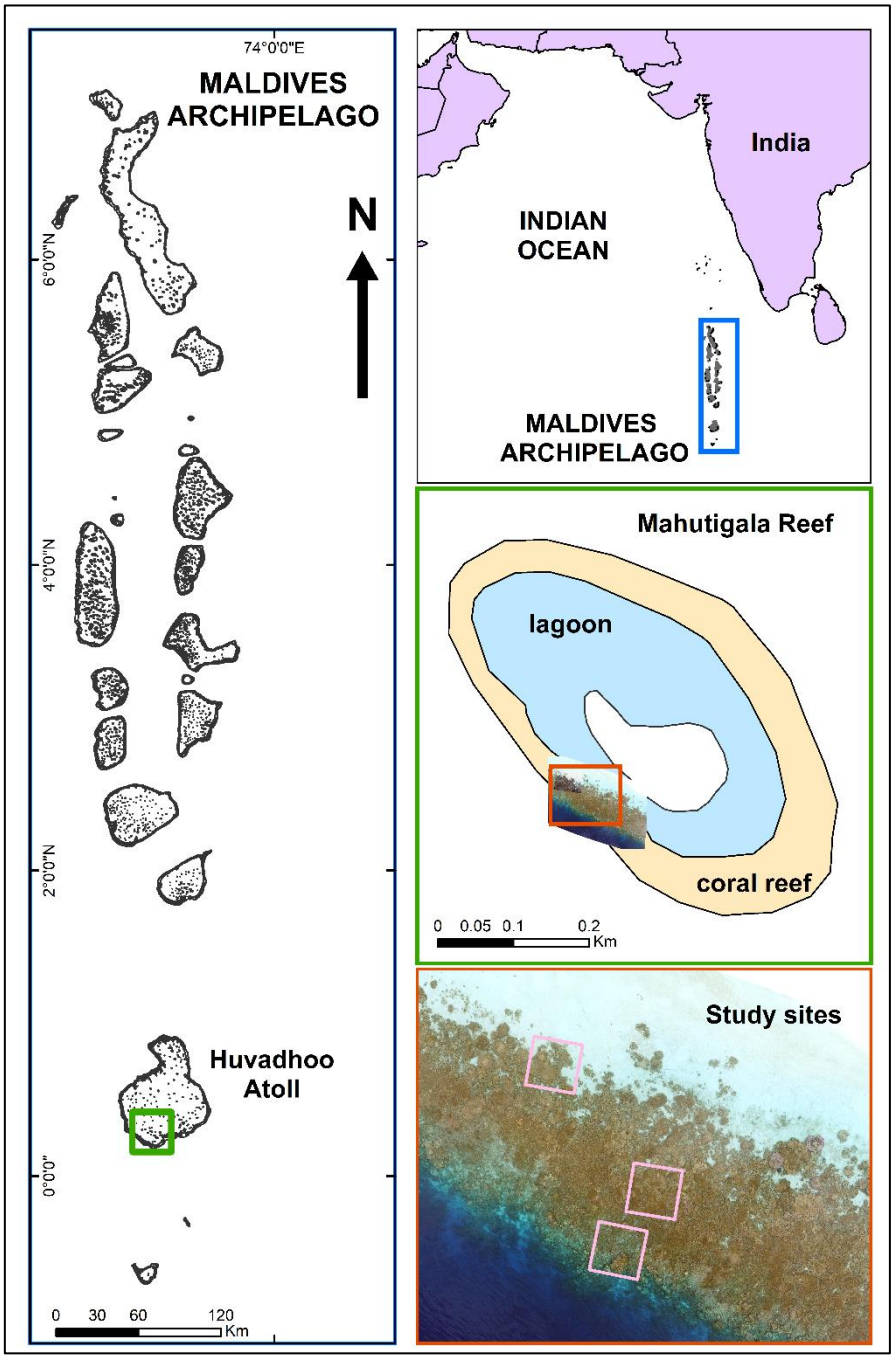

Figure 3.9. The Mahutigala Reef, over which UAV imagery was collected, and its position within the Maldives Archipelago. The map shows the three defined study sites located in on the back reef, reef flat and reef crest.

Twenty-two virtual transects were created over each study site at 1 m intervals (figure 3.10) and intersected (ArcMap tool) with the digitised reef features to measure the planar length of each coral colony or substrate patch directly below it. These were multiplied by the respective rugosity conversion factors to calculate the contour length of each feature (equation 1) and the rugosity of

each transect subsequently calculated as the sum of all contour lengths divided by 10 m – the planar transect length (equation 2, Risk, 1972). The rugosity of each study site was calculated at three scales, as the mean rugosity of transects placed every 1, 2 and 5 m throughout each study site. As an additional scale, overall surface area (m^2) rugosity was also determined by calculating the area of each reef feature, multiplying this by the respective conversion factor to calculate a contour area, and diving the sum of these by 100 m^2 - the planar area of each study site. It is noted that all recognisable coral was assumed to be living for this analysis unless obvious from visual recognition that the coral was bleached or dead.

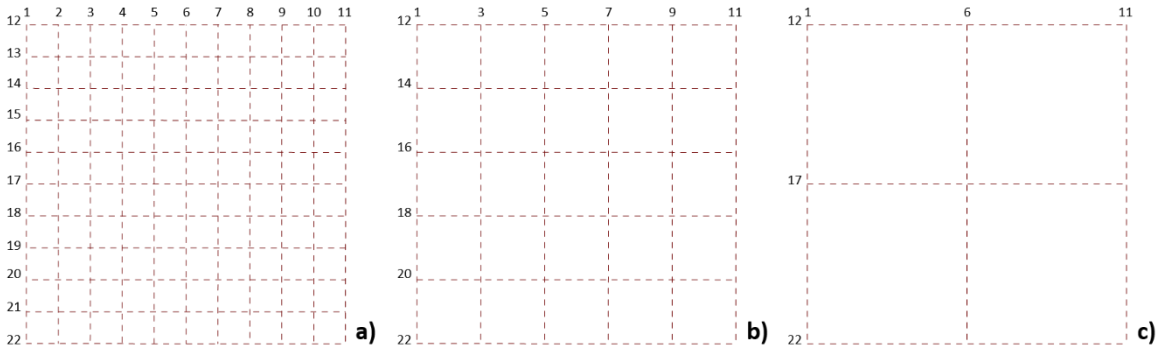

Figure 3.10. Representation of the three scales at which mean rugosity was calculated for three 10m^2 study sites on the Mahutigala reef. 3.10. a) shows transects placed every 1 m, b) every 2 m and c) every 5 m.

Projecting change in community composition

To show how the conversion factor technique could predict and monitor rugosity through time, the digitised 'present, baseline' coral communities were manipulated to represent two stages of coral reef degradation. These stages were based on data collected following the 1998 Maldivian coral bleaching event as: i) the initial colonisation of the reef by algae, 1-2 years post-bleaching, and ii) subsequent erosion of the coral to rubble, 2-3 years post-bleaching (Schuhmacher *et al.,* 2005, Bianchi *et al.,* 2006 and Lasagna *et al.,* 2010). Using previously assigned life history strategies and known, community level, degradation pathways of Maldivian reefs, the status of each digitised coral and abiotic feature in each degradation stage was predicted, and new rugosity

conversion factors assigned (if applicable) to the corals, to represent any change in structure. These predicted pathways for the variable reef features are summarised in table 3.5.

Table 3.5. The predicted degradation trajectories of coral genera, morphotypes and abiotic substrate, 1-2 and 2-3 years, after a coral bleaching disturbance event.

Coral / life history strategy		
Present **Competitive corals**	**Phrase 1 decline (1-2 years post-disturbance)**	**Phrase 2 decline (2-3 years post-disturbance)**
Acropora Branching	Branching algae covered coral	Coral rubble
Acropora plates and tables	Algae covered plate	Limestone pavement
Acropora digitate or corymbrose	Algae covered coral	Coral rubble
Branching	Algae covered coral	Coral rubble
Plates and tables	Algae covered plate	Limestone pavement
Micro-atoll (Acropora)	Algae covered coral	Coral rubble
Stress tolerant corals		
Porites lobata Massive Flabello-meandroid	No Change	No Change
Stress tolerant / weedy corals		
Submassive	Algae covered other coral	Coral rubble
Abiotic substrate / algae covered coral		
Coral rubble Boulder Algae covered coral Branching algae covered coral Limestone pavement Sand 1:1 rubble Sand (low ripple)	No Change	No Change

*N.B. Algae covered plates are given the same rugosity conversion as healthy plates. Limestone pavement is used to represent plates that have broken down due to the similarity in their morphology.

New coral contour lengths and, consequently, site transect and surface area rugosity values were recalculated for each degradation phrase using the reassigned rugosity conversion factors (and equations 1 and 2). These predicted pathways were visually mapped and statistically analysed to show how the structural complexity of the study sites might change with time.

3.7.2 Results

Coral digitisation and reef composition

On importing UAV imagery into ArcMap, it was possible to digitise all corals and substrate present in the selected sites. In total 430 corals and substrate patches were digitised from the back reef, 768 from the reef flat and 1085 from the reef crest. These represented a variety of coral genera, morphotypes and abiotic substrates (see column two ('present') in figure 3.11). All corals were identifiable to a minimum of a genera/morphotype level and some more obvious corals, such as *Porites lobata*, identifiable at a species level.

Under 'present' conditions (column two, figure 3.11), represented by the status of the reef in the original drone imagery, the back reef site has a greater proportion of sand (36.22 %) and abiotic substrate (9.01 %) compared with the reef flat which is dominated by branching Acropora (64.12 %). The reef crest has a more variable coral composition, dominated by *Acropora* digitate and Corymbrose (37.27 %) *Porites lobata* (20.03 %), and branching corals (25.86 %). These community compositions are reflected in the calculated mean rugosity of the three sites where at all measurement scales (1 m, 2 m, 5 m and total area (m^2)) the reef flat is the most rugose (m = 2.78, S.D. = .08), followed by the reef crest (m = 2.28, S.D. = .04). The back reef is the least rugose of the three sites with a mean rugosity of 2.02 (S.D. = .06). Table 3.6 presents a summary of the mean rugosity of each study site, measured at all spatial scales. The calculated contour lengths and rugosity data, used in these calculations, for each individual transect can be found in Appendix F and the raw data for the coral community composition of each study site is presented in Appendix G.

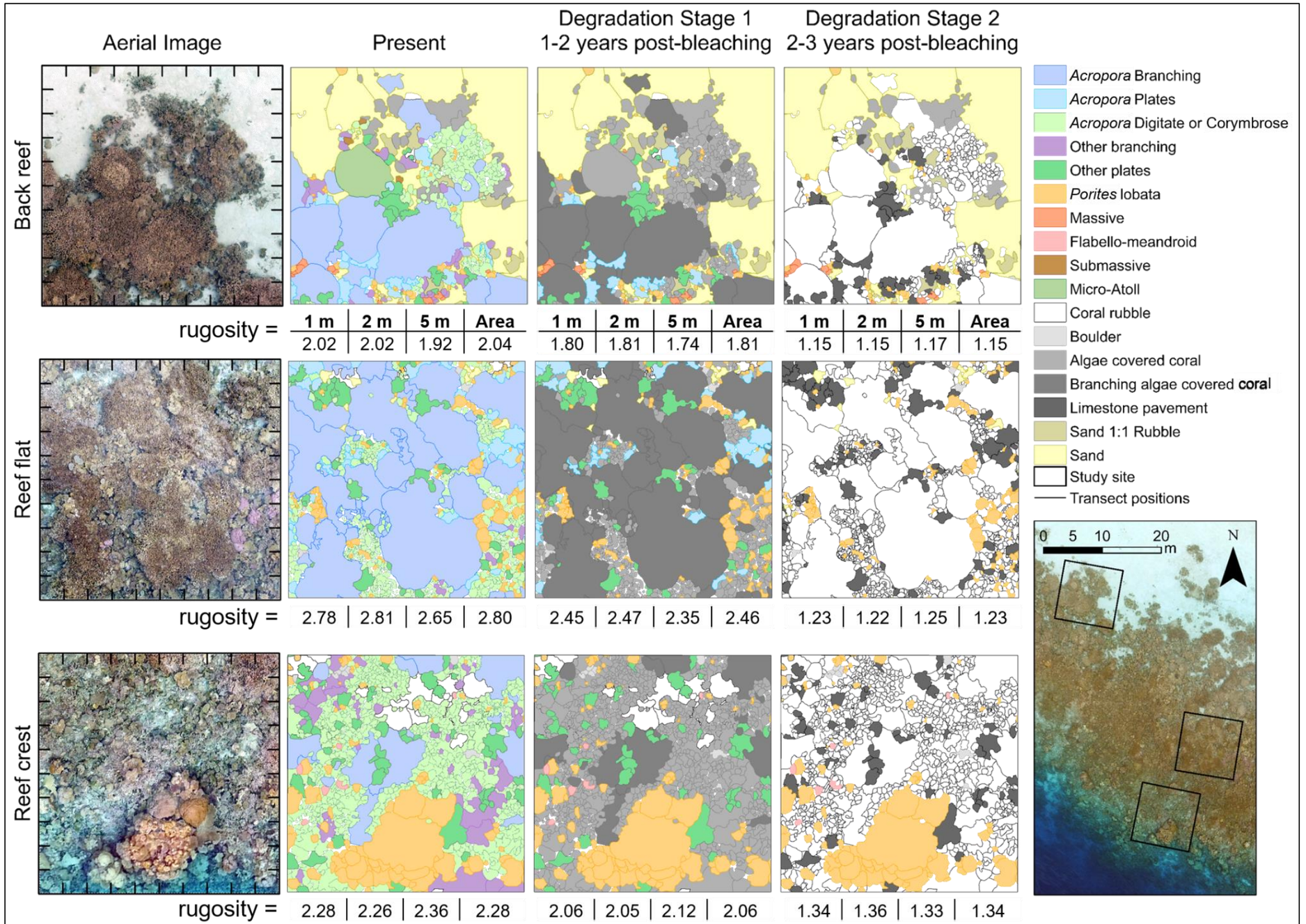

Figure 3.11. Digitisation of present coral communities and abiotic substrate in three study sites (back reef, reef flat and reef crest) from a UAV image of the Mahutigala reef and predicted trajectories of how the coral compositions change 1-2 years and 2-3 years after a coral bleaching event. The mean rugosity of each study site, in each time period (present, degradation stage 1 and degradation stage 2) is presented, calculated as the mean rugosity of transects places every 1 m, 2 m and 5 m throughout the sites, as well as, the overall surface area rugosity. Inset map shows the position of the three study sites on the Mahutigala Atoll reef (see figure 3.9 for greater locational context).

Table 3.6. Mean rugosity of each Mahutigala reef study site during three time periods: at present, degradation stage 1 (1-2 years post-bleaching) and degradation stage 2 (2-3 years post-bleaching). For each site, rugosity is calculated as the mean of transects placed every 1 m, 2 m, 5 m throughout the 100 m^2 study site and as overall surface area rugosity.

		Mean Rugosity					All scales		Excluding 5 m	
		1 m	2 m	5 m	Area	Mean	Range	S.D.	Range	S.D.
Back reef	**Present**	2.02	2.02	1.92	2.04	2.00	0.12	0.06	0.02	0.01
	Degradation stage 1	1.80	1.81	1.74	1.81	1.79	0.07	0.04	0.01	0.00
	Degradation stage 2	1.15	1.15	1.17	1.15	1.15	0.02	0.01	0.00	0.00
Reef flat	**Present**	2.78	2.81	2.65	2.80	2.76	0.17	0.08	0.03	0.02
	Degradation stage 1	2.45	2.47	2.35	2.46	2.43	0.12	0.05	0.02	0.01
	Degradation stage 2	1.23	1.22	1.25	1.23	1.23	0.03	0.01	0.01	0.00
Reef crest	**Present**	2.28	2.26	2.36	2.28	2.30	0.10	0.04	0.03	0.01
	Degradation stage 1	2.06	2.05	2.12	2.06	2.07	0.07	0.03	0.02	0.01
	Degradation stage 2	1.34	1.36	1.33	1.34	1.34	0.02	0.01	0.01	0.01

Reef degradation

Predicted reef degradation, based on the aftermath of the 1998 bleaching event, is represented by colour scheme changes to the digitised corals (see columns 3 and 4, figure 3.11). As the reef degrades in stage 1 (column 3, figure 3.11), 1-2 years after the bleaching event, the sites become dominated with algal covered dead coral (reef crest = 72.96 %, reef flat = 90.42 %, and back reef = 58.10 %), even though many coral colonies remain structurally in place. By stage 2 (column 4, figure 3.11), 2-3 years after the event, the algae covered coral has eroded to coral rubble in all three study sites. Coral plates and tables remain structurally intact through stage 1 despite being overtaken by algae, but lose some structure in degradation stage 2. *Porites lobata* and massive corals dominate the reefs as the only living hard corals remaining in stage 2. This process is reflected in continuous decreasing rugosity values at all sites through stages 1 and 2, when measured at all scales. The reef flat shows the largest overall decrease in rugosity between 'present' conditions and stage 2 (mean change = - 1.53) and the back reef shows the least overall rugosity decrease (m change = - 0.85), (see table 3.6). The reef crest showed a rugosity degrease of 0.96.

In degradation stage 2, the reef crest (mean rugosity = 1.34, S.D. = .01) surpasses the reef flat (mean rugosity = 1.23, S.D. = .01) as the most structurally complex site and the back reef remains the least structurally complex (mean rugosity = 1.15, S.D =.01). As sites degrade, there is much less inter-site variability in mean rugosity which ranges from m = 0.76, in the present condition, to m = 0.19 in degradation stage 2. There was a much greater decrease in rugosity between degradation stages 1 and 2 (mean decline = 0.85) than between present conditions and degradation stage 1 (mean decline = 0.25), (see table 3.6).

Measurement scale

There was very little variability in mean site rugosity when calculated at each of the four scales (1m, 2m, 5m and surface area (m^2)), within each reef state stage (present, degradation stage 1 and degradation stage 2), summarised in table 3.6. No site or stage showed more than 0.17 variability in rugosity between

scales. In stage 2, the back reef and reef crest showed just 0.02 variability in rugosity values calculated at different scales, represented by the range (see table 3.6). Rugosity measured at the 5 m transect scale did show slightly more variability than the other scales; across all three sites and stages, there was a mean range of 0.08 (S.D. = 0.04) between rugosity calculated at the different scales when the 5 m measurements were included. This reduced to just 0.02 (S.D. = 0.01) when the 5 m measurements were excluded (see table 3.6).

3.7.3 Discussion

The use of the conversion factor technique enabled coral colony scale rugosity to be (virtually) assessed and projected through time, from 2D planar measurements of coral reef features identifiable in UAV imagery.

Initial quantification of present state rugosity

The high resolution drone imagery allowed individual coral colonies and abiotic reef patches, forming the 'present' coral community within three, 100 m^2 study areas of the Mahutigala reef, to be digitised and identified, to a minimum of a genera-morphotype level (figure 3.11, 'present'). Some more distinctive or larger coral colonies were able to be identified to species level, and, to an extent, through colour comparison with living counterparts, as dead or algae covered. The development of morphotype conversion equations, additionally to the genus equations, was shown to be advantageous for this application, as the rugosity of digitised features could be calculated irrespective of whether genus identification was possible from the imagery. The use of these morphotype equations here also demonstrates how their development allows the conversion factor technique to quantify rugosity for regions where specific coral genus rugosity data is not yet available.

Although there was no *in-situ* data available to test the accuracy of the 'present' condition calculated rugosity values, the mean rugosity of each study site is reflective of the dominant substrate, coral morphotype and overall coral community present in each reef zone (Goatley and Bellwood, 2011). For example, the back reef, with a high proportion of sand, is the least rugose site, and the reef flat, dominated by branching corals, the most rugose. The mean rugosity of the reef crest, with a more mixed community composition of complex and plateau corals, consequently falls between the rugosity of these sites. Considering this and the known accuracy of the conversion factors for measuring colony scale rugosity (chapter 3.2), it is inferred that the calculated rugosity values are representative of the natural structural complexity of the study sites. Consequently, the application of the conversion factors to the drone imagery initially shows how the technique can successfully and accurately

quantify the contribution of coral colonies and abiotic substrate to reef rugosity over large areas, without a need for *in-situ* measurements.

Temporal rugosity monitoring

The second half of figure 3.11 (columns three and four) illustrates the predicted pathways of how individual corals and whole study sites might respond to a disturbance event, in two stages of degradation, based on the 1998 Maldivian bleaching event. This demonstrates how the application of the conversion factors to repeat drone surveys could successfully monitor microscale (coral colony) structural complexity over large scales through time (Schuhmacher *et al.,* 2005, Lasagna *et al.,* 2010 and Madin *et al.,* 2016). After the hypothetical bleaching event, the rugosity of all three study sites declines between present conditions and degradation stage 2, in a progression from healthy, complex reefs (present), to algae covered reefs (degradation stage 1), and finally to a homogenous and eroded reef (degradation stage 2). These predicted trajectories are of consistent magnitude with indicative trends of declining rugosity measured in the 2-3 m, shallow fore reef zone of the Mahutigala Reef. Here, rugosity has been observed to decline from 2.80 to 2.48 in the 6 month initial period after the 2016 Maldivian coral bleaching event, and even further to 2.0 and 1.7, 12 and 22 months respectively after this event (Perry and Morgan, 2017a and 2017b). As such, the application shows how the technique can help identify and monitor the structural degradation of coral reefs when exposed to environmental stressors. For example, in this scenario, mature reefs, identified in present conditions with a high proportion of hard coral cover (figure 3.11), transform to regressive reefs, with a high proportion of rubble and sand in stage two; this is a transition process observed on many Maldivian reefs after the 1998 bleaching event (Schuhmacher *et al.,* 2005 and Lasagna *et al.,* 2010).

Furthermore, the calculated rugosity values illustrate how, in monitoring rugosity, the technique can consider and recognise the time-lag between an environmental disturbance event, coral mortality and a decline in structural complexity. This phenomena, initially discussed in chapter 3.6.3, has been observed throughout southern Maldivian reefs, including on the Mahutigala reef, following the 2016 coral bleaching event. Small and insignificant declines in

rugosity on these reefs, recorded initially 6 months after the 2016 bleaching event, increased in both magnitude and significance 12 months later as dead coral skeletons began to collapse (Sheppard *et al.,* 2002 and Graham *et al.,* 2007 and Perry and Morgan 2017b). In the predicted pathways in figure 3.11, this trend is replicated by an initial, small, decline of rugosity in stage 1, as algae colonises dead corals which maintain part of their 3D structure, compared with a much greater decline in rugosity as coral skeletons erode to rubble in degradation stage 2 (Schuhmacher *et al.,* 2005 and Lasagna *et al.,* 2010). These consistencies with measured data for the same reef, albeit at different study sites, increases the validity of the predicted rugosity trajectories of future coral communities and reductions in structural complexity on the Mahutigala reef.

The variable magnitude of rugosity declines for the three study sites further highlights the importance of coral morphological traits in determining the response of individual coral colonies, and consequently, the overall reefs to environmental change or anthropogenic disturbance. In the hypothetical scenario, after the ‘bleaching event’, competitive, complex corals died, were colonised by cyanobacterial turfs or algae and eventually eroded to rubble. This resulted in the reef flat, dominated by these competitive and stress sensitive corals, experiencing the greatest loss of rugosity of the three sites. This too is consistent with observations of Maldivian reefs dominated by branching and tabular *Acropora* experiencing the largest rugosity (and carbonate budget) declines after the 2016 bleaching event (Perry and Morgan 2017a). In contrast, massive, stress tolerant corals suffered less mortality and eroded *in-situ*, retaining their structure (Sheppard *et al.,* 2002 and Bianchi *et al.,* 2006). As such, it is no surprise that in stage 2, the reef crest, dominated by massive, stress tolerant corals becomes the most structurally complex (highest mean rugosity) of the three reef sites (Darling *et al.,* 2012).

These results reveal how coral genus specific rugosity data can be useful for quantifying changes to the structural complexity of coral reef ecosystems. They illustrate the importance of considering coral morphotype, a functionally significant trait that is key to mediating species response to disturbance, when predicting coral degradation pathways. This reinforces the advantage of

extracting both genus and morphotype conversion factors from the rugosity database. Consequently, this application shows how trait based physiological data, such as that in the coral rugosity database, can be used to make meaningful generalisations about 3D reef structure and coral ecosystem function and evolution from patterns of coral biodiversity identified in UAV imagery (Madin *et al.,* 2016).

Methodological analysis

This application demonstrates the distinct advantages UAV aerial imagery has over other image based coral rugosity monitoring methods, despite not always permitting identification of corals in the imagery to a genus level. It also shows the benefits of the conversion factor technique for quantifying the 3D nature of coral colonies, including any overhangs and under hangs typical of different coral genera, from imagery – a feature that has currently limited the use of 2D, top-down, photographic, methods for reef structure monitoring (Commito and Rusignuolo, 2000). UAV imagery has greater spatial resolution than alternate large-scale imagery from satellite and plane based sensors, thus allowing more accurate digitisation and identification of corals, and allocation of coral rugosity conversion factors (Chirayath and Earle, 2016 and Hattori 2017). It also has greater spatial coverage than manually operated cameras, allowing for a more representative assessment of overall reef rugosity, (Anderson and Gaston, 2013 and House *et al.,* 2016).

Further methodological advantages are that once digitised, the linear distances of the corals along each transect can be automatically measured by ArcMap spatial analysis tools. This reduces human error that may result from manual measurement, such as for the video transect analysis in Kinovea (chapter 3.2 and 3.2). The image collection and digitisation process also provides a permanent record of individual colony coral cover at a site as a complimentary product to rugosity for assessing overall reef health (Leujak and Ormond, 2007 and Sweatman *et al.,* 2011 and Naughton *et al.,* 2015). This will allow any change in structure of individual colonies to be quickly identified through reassignment of relevant conversion factors to the existing digitised corals, in repeat drone imagery at specified intervals through time or immediately after a

disturbance event (Naughton *et al.,* 2015, Ferrari *et al.,* 2016, Chirayath and Earle 2016 and Casella *et al.,* 2017).

The technique is also valuable due to its flexibility for measuring rugosity at variable, user-defined scales which can be decided post data collection. This is demonstrated by the virtual placement of transects 1 m, 2m and 5 m throughout the study sites in figure 3.11. Measurement scale flexibility is a feature offered by many remote sensing techniques, especially those that measure rugosity virtually from DEM's (Brock *et al.,* 2006, Kuffner *et al.,* 2007, Knudby *et al.,* 2007, Wedding *et al.,* 2008 and Purkis *et al.,* 2007). However, the accuracy of these measurements for microscale rugosity is often scale dependent and limited by DEM model resolution, issues which are eliminated by the use of the accurate, standardised conversion factors to calculate rugosity (Storlazzi *et al.,* 2016).

The greatest advantage of this application, however, results from the ability to calculate the surface area rugosity of each study side. This composite rugosity measurement is much more robust and representative than that calculated as the mean of multiple transects due to its complete consideration of every digitised feature in each reef site as opposed to single coral diameters (Storlazzi *et al.,* 2016). Calculating surface area rugosity increases the efficiency of dive and/or analysis time by reducing the time required to determine the most representative locations to survey on reefs and the incremental distances over which to place transects (Storlazzi *et al.,* 2016). It also reduces the scale dependency of rugosity values calculated from the technique, as demonstrated by the slightly greater variability of rugosity calculated at the 5 m scale, than that at the smaller 1 m, 2 m scales. This issue is eliminated by the use of area based rugosity.

Despite these advantages, the global use of the technique is limited by the conditions under which UAVs can be deployed and gain imagery of sufficient quality and resolution to enable accurate coral digitisation and identification. These include calm atmospheric conditions, low wind or turbulence and clear waters (Beijbom *et al.,* 2012, Anderson and Gaston, 2013 and Casella *et al.,* 2017). Large waves or ripple on the water surface or high turbidity cause optical

distortion and reflections which reduce image resolution and introduce error into photo alignment processes required to create ortho-mosaics of large reef areas (Leon *et al.,* 2015 and Casella *et al.,* 2017). Light absorption by the water also results in recognition of coral features being precluded below critical depths, limiting the use of this technique to imagery of shallow water reefs. These depth effects are highlighted in figure 3.12 whereby the slope of the reef crest, and water ripple distort the imagery, increasing the difficulty of coral identification. Continually developing fluid lensing technologies have had some success in minimising the effect of surface waves on image quality and increasing image observational capacity. At present this experimental technology is limited by the intrinsic optical properties of the water column and irradiance effects and has only produced imagery at 5 cm resolution. This is not yet sufficient for detecting small changes in the size of corals which often have annual growth rates of < 1 cm a year (Edinger *et al.,* 2000, De'ath *et al.,* 2009 and Chirayath and Earl, 2016). It is hoped that future improvements to this technology will enable higher resolution UAV imagery to be captured in both optimal and non-optimal conditions.

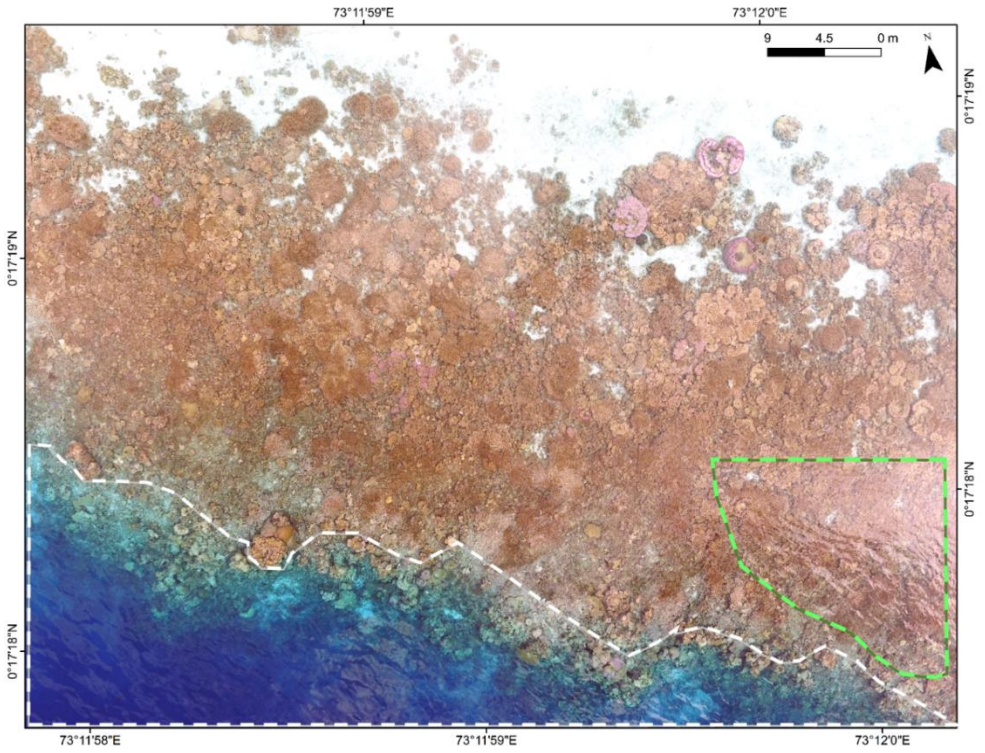

Figure 3.12. UAV image of the Mahutigala Reef, in the Maldives Archipelago (see figure 3.9) showing the effect of surface water ripples (green dotted shape), water depth and reef crest slope (white dotted shape) on image clarity and ability to accurately digitise and identify corals.

3.7.4 Conclusion

Previously, optical remote sensing techniques have been limited in their ability to resolve the vertical component of coral reef structure or precisely monitor reef rugosity at small ecological scales (Purkis *et al.,* 2007 and Dustan *et al.,* 2013). Surveying individual corals from UAV imagery may present more challenges than *in-situ* field methods in terms of the limited conditions in which imagery can be collected. However, this application shows that quantifying the 3D structure of individual coral colonies is becoming more feasible as UAV technology improves and provides high quality survey data from which coral genera and morphotypes can be identified. Furthermore, the use of the conversion factors to gain rugosity data from this UAV imagery, has demonstrated the additional advantage of being able to survey the rugosity of coral communities over much larger scales than permitted by *in-situ* methods. Furthermore, it does this with a much higher accuracy than currently permitted by many remote sensing techniques.

Although fine scale measurement (mm scale) remains challenging, as coral reef communities and landscapes continue to rapidly change, it is considered that the advantages of UAV imagery for providing fast, repeat observations outweigh the current limitations posed by image resolution (Goatley and Bell, 2011 and Figueira *et al.,* 2015). The growing use of UAV options, both to researchers and the public, will greatly increase the access to georeferenced imagery of coral reefs worldwide and thus the available data from which the unique contributions of coral colonies to reef rugosity can be calculated using the conversion equations (Carbonneau and Dietrich, 2017). It is hoped that this will translate into a great capability to document the consequences of global community change on coral reefs to reef structural complexity resulting from future environmental change and disturbance events.

Chapter 4. Analysis of overall technique and recommendations

In the previous chapter, this research demonstrated how the application of taxa-specific, conversion factor equations, to three types of 2D coral survey data, can accurately quantify the coral colony scale rugosity of coral reef environments. It is noted that this is with exception of the application of the equations to field video transects which revealed the technique as less successful at quantifying meso-scale or overall transect scale rugosity. Thus far, this 'conversion factor' technique has been discussed with reference to the many advantages and methodological issues associated with the application of the equations to each of the three mediums of coral survey data (control and *in-sit* video transects (chapters 3.2 and 3.4), line intercept data (chapter 3.6) and UAV imagery (chapter 3.7)). To evaluate the technique as a whole, it will now be analysed with reference to criteria set out by Hobson, (1972) and Ferrari *et al.,* (2016), presented in table 1.1, to consider whether it is useful for both measuring surface (structural) complexity and accurately monitoring coral reef framework. This evaluation is summarised in table 4.1 which also compares the conversion factor technique with aforementioned, alternative methods of measuring rugosity from chapter 1.

Table 4.1. Summary of the capability of different techniques for quantifying and monitoring the structural complexity or rugosity of coral reefs, with reference to criteria set out by Hobson, (1972) and Ferrari *et al.,* (2016), (table 1.1). An 'x' indicates that a criterion has been met by any particular method.

		Hobson (1972)			Ferrari *et al.,* (2016)					
Method / Sensor	**Correlation with rugosity index**	**Conceptually descriptive (rugosity)**	**Easily measured in the field**	**Measurable at many scales**	**Efficient and cost-effective***	**Useable by non-experts**	**Applicable to historical data**	**Applicable in shallow waters**	**Measures coral colony scale**	**Additional considerations**
Rugosity index McCormick, (1994) and Knudby and LeDrew (2007).		x	x	x		x		x	x	Scale dependent relationship with biodiversity. Environmental damage caused by chain.
Visual assessment Sheppard, *et al.,* (2002), Long, *et al.,* (2004) and Wilson, (2007).	r^2 = 0.85, (Wilson, 2007)	x	x		x	x	x	x		Subjectivity reduces validity. Inter-observer bias.
Patch reef volume (rugosity proxy, a *x* h) (Hattori and Shibuno, 2015).	N/A	x	x			x	x	x		Considers only meso-scale rugosity. Assumes all reefs to have a 3D cylindrical shape.
Reef structural components (rugosity proxy, e.g. no. of corals and coral height). Hardborne and Mumby (2012) and Newman *et al.,* (2015).	N/A		x			x	Some structures.	x	Some structures.	Each structure has a relative, non-linear and complex relationship with biodiversity. Does not summarise rugosity as an individual characteristic.
Optical intensity analysis Shumway *et al., (*2007).	r^2 = 0.52 (Shumway *et al.,* 2007)	x		x			x	x		Only distinguishes broad scale habitats.
Digital pressure gauge (seafloor bathymetry) Dustan *et al.,* (2013).	N/A	x	x	x				x	Resolution would suggest so.	Measurement accuracy dependent on wave swell and human error whilst diving.

Acoustic bathymetry (RoxAnn backscatter) White *et al.,* (2003) and Benjarano *et al.,* (2010).	r^2 = 0.66 (Benjarano *et al.,* 2010)	x		x				Not when attached to vessel.		Acoustic sensor performance dependent on reef slope, depth, distance from reef edge and sediment type.
IKONOS imagery and Acoustic bathymetric data Riegl and Purkis (2005) and Purkis *et al.,* (2008).	N/A	x		x				x		Scale dependency of LiDAR point spaces and DEM grid cell size. Acoustic sensor performance dependent on environment.
LiDAR bathymetric data Wright and Brock, (2002) and Brock *et al.,* (2004).	N/A	x		x				x		LiDAR measurement scale depends on subjective laser beam spacing.
Virtual rugosity from EAARL LiDAR DEMs Brock *et al.,* (2006), Kuffner *et al.,* (2007) and Wedding *et al.,* (2008).	r^2 < 0.2 (but significant, (Kuffner *et al.,* 2007) r^2 = 0.61 (Wedding *et al.,* 2008)	x		x				x		Output rugosity is scale dependent on LiDAR point spaces and DEM grid cell size. Accuracy dependent on coral environment.
Virtual rugosity from SfM models Friedman *et al.,* (2012), He *et al.,* (2012), Leon *et al.,* (2015), Burns *et al.,* (2015), Storlazzi *et al.,* (2016) and Young *et al.,* (2017).	r^2 = 0.89 (Friedman *et al.,* 2012) r^2 = 0.85-87 (Young *et al.,* 2017)	x		x			x	x	x	Rugosity measurement scale dependent on model resolution. Morphotype effect on model accuracy. Multiple, subjective processing decisions. Trade-off between model accuracy and resolution with processing time.
Virtual rugosity from UAV derived DEMs. Chirayath and Earle, (2016), Dietrich, (2017) and Casella *et al.,* (2017).	N/A	x		x			x	x	Research suggests the method has potential to.	UAV use limited to clear, calm and non-turbid and calm atmospheric conditions. SfM propagative processing errors.
Conversion factor technique This research	r^2 = 0.95	x	N/A	x	x	x	x	x	x	Difficult to use accurately in macroalgae dominated environments.

*with reference to measuring large areas of coral reef ecosystems.

4.1 Is the technique a useful measure of surface complexity? (Hobson *et al.,* 1972)

Hobson (1972) proposed that for a measure of surface complexity to be useful it must be conceptually descriptive, able to measure rugosity at a number of scales and easily measurable in the field. The development of the rugosity database here provides **conceptually descriptive** information regarding the rugosity of variable coral genera, morphotypes and reef abiotic substrates, which is related to coral life history strategy and coral colony size (Darling *et al.,* 2012). Consequently, as demonstrated in chapter 3.2, any rugosity measurement gained from the use of the conversion factors, extracted from this database, will accurately describe the contribution of these reef features to the overall structural complexity for the area in question.

For analysing whether the technique can **measure rugosity at a number of scales**, (Hobson's second criteria) there are two factors that must be considered. The first is the spatial scale at which rugosity is measured, and this for the conversion factor technique, is dependent on the medium of data to which the conversion factors are applied. For example, video transects and line intercept data record coral cover along single line transects which limits the application of conversion factors to these surfaces (AIMS, 2004). In contrast, the use of UAV imagery increases the flexibility of the spatial scale virtual rugosity can be measured at. This allows rugosity to be calculated as a mean of multiple transects, of variable distance apart or for the entire study site using surface area coverage, thus meeting this criterion.

The second factor is the scale of the actual rugosity measurement, which does highlight a drawback of the technique which only quantifies rugosity at the coral colony scale (microscale). There is an urgent need for techniques that can isolate the contribution of different reef features to structural complexity, and this technique is advantageous in its success of quantifying one of these components. However, the technique does not consider meso- and macro-scale features, such as holes and natural surface heterogeneity in the underlying reef substrate that also contribute to the overall structural complexity of a coral reef (Komyakova *et al.,* 2013). To improve the technique in the future, the rugosity

database could be expanded to include rugosity data for a greater variety of abiotic substrates and macroalgae, and include rugosity data for mesoscale features such as caves and holes etc. Although these features are naturally heterogeneous, the addition of this data to rugosity monitoring programs is imperative given the increasing rate at which coral reefs are progressing towards macroalgae and abiotic substrate dominated states (McCook, 1999, Hoegh-Guldberg *et al.,* 2007, Montefalcone *et al.,* 2011, Alvarez-Filip *et al.,* 2013 and GBRMPA, 2014). Unless these features are represented in the database, there will remain a need for *in-situ* measurement to assess the structural complexity of coral reefs at all ecologically relevant spatial scales.

Despite this, the use of the conversion factors do show how micro-scale rugosity measurement can be standardised for any medium of data. This is hugely advantageous for allowing valid comparisons between past, present and future coral reef rugosity survey data and assessments which have previously been limited by a multitude of differences in measurement scale between rugosity monitoring techniques (Knudby and LeDrew, 2007, Alvarez-Filip, 2011, Jackson, Alexandre and Sala*,* 2012, González-Rivero *et al.,* 2014, Burns *et al.,* 2015, Leon *et al.,* 2015, House *et al.,* 2016 and Hedley *et al.,* 2016, see table 4.1). The ability to produce high resolution, standardised and accurate rugosity information, from new or previously collected data, also increases the efficiency of monitoring benthic habitats temporally by facilitating repeat observations of the same reefs. This is vital for detecting how coral foundation species are changing in response to environmental and anthropogenic stressors, and predicting the consequences of this for the overall ecosystem structure and function (Goatley and Bell, 2011, Figueira *et al.,* 2015, Ellison *et al.,* 2005 and Storlazzi *et al.,* 2016). As a result, the standardization of coral colony scale rugosity measurement offered by this technique, will help improve assessment of present reef rugosity and any future changes to this experienced by coral reefs worldwide (Balmford *et al.,* 2005 and Knowlton and Jackson, 2008).

Hobson's final (1972) criteria, that a measure of surface complexity should be **easily measured in the field**, is not appropriate to consider for this or future techniques that use remote sensing and computer analysis to measure ecological characteristics**.** A key goal of this research, and other wider

research, is to develop a rugosity monitoring technique that drastically reduced or altogether removed the need for *in-situ* measurement (Fuad, 2010 and House *et al.,* 2016). The resulting method quantifies colony scale rugosity, using virtual coral measurements and equations, from existing data sources. Consequently this research has been successful in its goal to eliminate the need for *in-situ* rugosity measurement. Although some mediums of survey data - for example, video transects and line intercept data - still require human presence in the water, the technique increases the efficiency of dive time, removes the need for any physical contact with the coral and, as such, is more time efficient and less invasive to reefs and their associated communities than traditional techniques (e.g. the chain-tape method, Risk, 1972, He *et al.,* 2012 and Hedley *et al.,* 2016). With advancement in remotely operated vehicle technology, for automated image collection underwater, expected to continue, the requirement for human presence even in the data collection stage is expected to decrease. These technologies will also increase the spatial coverage and depth at which imagery, that rugosity conversion factors can be applied to, can be captured (Shihavuddin *et al.,* 2013 and Beijbom *et al.,* 2015, Naughton *et al.,* 2015). Thus, when considered in terms of coral colony scale structural complexity, this technique exceeds Hobson's (1972) criteria by altogether eliminating a need for *in-situ* rugosity measurement and can overall be considered as a useful measure of surface complexity (summarised in table 4.1).

4.2 Is the technique useful for accurately measuring coral reef framework? (Ferrari *et al.,* 2016)

More recent criteria outlined by Ferrari *et al.,* (2016) do take into consideration progress made in remote sensing techniques, stating that for any method aiming to quantify structural complexity to be useful, it must be cost-effective and useable by non-experts. In contrast to many methods that use remote sensing to measure rugosity, the technique developed in this paper is **cost-effective** as it requires no specialist or costly computer software. Analysis of the video and drone imagery was completed using freely available, open source Kinovea software, and ArcMap which is readily available in research institutions. Subsequently, calculation of rugosity took place in Excel. The use of consumer grade software also increases the accessibility of the technique to **non-experts,** thus additionally meeting this criteria. The technique requires no complex computer processing knowledge that is often required for measuring rugosity using Structure from Motion or from DEM based techniques (see table 4.1). Although identification of corals to the genus level, and, basic ArcMap skill would benefit from some expert knowledge, this can be readily gained with access to coral identification guides and ArcMap tutorials.

For this technique, even the initial survey data can be collected with little expert knowledge or expensive technology as demonstrated by the use of consumer grade devices (CanonS101 and DJI Phantom 3 Advanced drone) to record the video transects and UAV imagery. The development of such consumer grade equipment, with digital geo-referencing, offers a cost-effective alternative to professional sensors for providing high quality imagery (Goodman *et al.,* 2013). At present, the growing production of topographic data from sub-metric resolution imagery from these sources is transforming Earth topographic survey and disaster management (Dietrich and Carbonneau, 2017). This is causing a shift in topographic mapping whereby non-expert individuals can produce *in-situ* or airborne imagery of sufficient resolution that the coral conversion factors can be applied to, providing a permanent record of coral reef communities and rugosity (Beijbom *et al.,* 2015 and Carbonneau and Dietrich, 2017, Young *et al.,* 2017, and Casella *et al.,* 2017). This is especially true, considering the recent development of similar rugosity datasets for other coral reef regions worldwide,

such as the Caribbean (González-Barrios and Alvarez-Filip, 2018). It is thus considered that the conversion factor technique has provided a cost-effective, consumer level tool for measuring rugosity which, due to its standardised measurement, will be applicable to an ever-increasing bank of coral reef imagery and rapidly help build a global scale view of coral colony scale rugosity.

That the technique is applicable to a wide range of data sources also highlights its ability to be applied to **historical data** - an extra 'ideal' criteria set by Ferrari *et al.,* (2016). This is specifically demonstrated by the application of conversion factors to line intercept data recorded between 2008 and 2017 and to UAV data collected in 2016. The recent development of UAVs will limit the amount of large scale 'historical' data the conversion factors can be applied to. However, the successful use of equations for calculating rugosity from video and still imagery of coral reefs shows how the technique can enable past changes in coral ecosystem rugosity to be quantified for greater areas and periods than has ever been possible before. This data will help minimise the shifting baseline effect that has hindered previous rugosity data comparisons (Beijbom *et al.,* 2012 and Burns *et al.,* 2015). It will also allow reconstructions as to how coral reefs previously responded to environmental change with regard to specific community compositions as demonstrated in figure 3.11 (UAV). This will improve the accuracy of predictions regarding how reefs will respond to future disturbance (Ferrari *et al.,* 2016). Historical rugosity has been measured before, using 3D, SfM and DTM models (e.g. He *et al.,* 2012 and Storlazzi *et al.,* 2016 (see table 4.1)). However, reconstructed rugosity from this new technique will be much more valid due to its accurate and standardised measurement of microscale rugosity - a scale too small to be accounted for by many current remote sensing techniques (Burns *et al.,* 2015, table 4.1).

The final criteria set by Ferrari *et al.,* (2016) is that the monitoring technique must be **efficient**. As aforementioned, the application of conversion factors to alternate data sources requires no *in-situ* rugosity measurement which greatly increases the techniques efficiency compared with the chain-tape technique (Risk, 1972). Even if new survey data is required, the growing use of UAVs will make this much faster to acquire than *in-situ* data for large reef areas (Chirayath and Earle, 2016). Furthermore, the technique requires no complex or

time consuming computer processing which increases its efficiency even more. Thus, from consideration of these factors, it is pertinent to conclude that the technique meets this and all other criteria set out by Ferrari *et al.,* (2016) and consequently is useful for accurately measuring and monitoring coral reef structural complexity (summarised in table 4.1).

4.3 Ongoing methodological challenges

One current drawback of the technique is the time taken to measure, identify and assign conversion factors to each coral colony along a video transect or within defined study sites in UAV imagery. Manual annotation of one 10 m video transect took 30 minutes and digitisation of every coral colony within a 10 m^2 study area in ArcMap took 7-8 hours. These processes greatly reduce the time efficiency of calculating rugosity, even if acquisition of the initial survey data is rapid, or more efficient than *in-situ* measurement* (Shumway *et al.,* 2007, table 4.1).

*These disadvantages do not apply to line intercept data where coral lengths and genus are already recorded.

Manual digitisation has been a longstanding technique used for annotating coral habitats using both paper and pen and more recently computer software, such as ArcMap (Goodman *et al.,* 2013, Hedley *et al.,* 2016 and Edwards *et al.,* 2017). However, with the development of consumer grade camera equipment and remotely operated vehicles, the capacity for image acquisition has now outpaced the resources used to manually annotate them, making the process unfeasible for large areas (Beijbom *et al.,* 2012, Shihavuddin *et al.,* 2013 and Naughton *et al.,* 2015). The 100 Island Challenge project is a prime example of this, using advanced large scale imaging techniques to map the benthic communities of 100, 100 m^2 reef areas worldwide using manual annotation of orthomosaics. Whilst the acquisition of > 3000 photos required to create the orthomosaic is relatively fast (approx. 2 hours / one diver) the annotation process is inefficient, taking up to 60 hours (Lirman *et al.,* 2007, Naughton *et al.,* 2015 and Edwards *et al.,* 2017). As such, although the technique developed in this research is more efficient than previous methods, there remains improvement to be made with regard to the tedious and time consuming image annotation process required for calculation of *in-situ* rugosity.

4.4 Towards the future

Automated annotation

Recent advancements in computer supervised and unsupervised classification technologies may hold the key to replacing this manual image annotation with an automated approach (Gleason *et al.,* 2007, Shihavuddin *et al.,* 2013 and Naughton *et al.,* 2015). Computer classification uses algorithms to gain reflectance information from imagery, often on a pixel by pixel basis, and uses this to automatically classify features as polygons with similar spectral signatures. More recently, OBIA (object based image analysis) has increased the accuracy of classification by also considering image texture, location, pixel group shape and the relationship of annotated features to externally derived factors, such as depth, on top of spectral reflectance properties in the automation process (Goodman *et al.,* 2013 and Hedley *et al.,* 2016).

Classification has been used to map coral habitats since the 1990s (e.g. Mumby *et al.,* 1997 and Pican *et al.,* 1998) and today, with higher resolution imagery, has been successful in classifying a variety of reef features, including bleached, medium and dark coral and areas dominated by *Acropora* and *Porites* (Leiper *et al.,* 2009, Scopélitis *et al.,* 2010 and Parsons *et al.,* 2018). Morphological filtering algorithms have also increased the identification accuracy of some coral morphotypes (overall accuracy of 85.5 %, Shihavuddin *et al.,* 2013). However, these technologies remain limited in their ability to classify individual coral colonies compared with manual annotation and as such, the image outputs are not of sufficient accuracy for the application of the rugosity conversion factors (Scopélitis *et al.,* 2010 and Parsons et al, 2018). The most challenging aspect of automated classification is the ability to distinguish between different coral genera (Naughton *et al.,* 2015) as all corals have ambiguous reflectance signatures and host photosynthetic zooxanthellae in their tissues (Beijbom *et al.,* 2012 and Purkis, 2017). Due to this, all corals have a dominant chlorophyll-a spectral peak at 400 nm which makes it near impossible to classify different coral species and consequently assign annotated corals the correct rugosity conversion factors (Beijbom *et al.,* 2012).

It is hoped that increasing manual annotation of coral communities, such as that completed in the application of the conversion factors to UAV imagery (chapter 3.7), will eventually provide comprehensive training data from which classification algorithms, with the ability to distinguish between different coral genera, can be generated (Beijbom *et al.,* 2012 and Naughton *et al.,* 2015). Development of aforementioned fluid lensing algorithms are also increasing the capacity of classification techniques to recognise individual coral colonies (NASA, 2018). Until these advancements progress at a rate equal to that of image acquisition, there will remain a bottleneck between available scientific and consumer grade imagery, to which the rugosity conversion factors could be applied, and actual large scale quantitative rugosity data required for coral reef management (Naughton *et al.,* 2015, Beijbom *et al.,* 2015). Only when this is resolved will the full potential of the conversion factor technique be revealed through its ability to quantify rugosity from the rapidly growing datasets of high resolution coral reef imagery (Shihavuddin *et al.,* 2013).

4.5 Implications for coral reef management and conservation

Even before the aforementioned technological advancements, the application of the rugosity conversion factors to imagery to determine past, present and future coral colony scale rugosity still has significant implications for reef monitoring, management and conservation efforts (Alvarez-Filip *et al.,* 2011). This is especially true considering that the technique meets all criteria set by Hobson (1972), Ferrari *et al.,* (2016) and additional criteria from this study, summarised in table 4.1. Consequently, the conversion factor technique is identified as the most successful rugosity monitoring technique thus far developed to measure coral colony scale rugosity. Furthermore, although at present, the rugosity database developed in this research is only representative of coral genera from the Indo-Pacific, the use of coral morphotype conversion factors allows the technique to be applied to any line intercept or image data recorded for global coral reefs.

The rugosity data provided by the conversion factor technique will be hugely advantageous for predicting the long term resilience and capacity of reefs, over large scales, to sustain positive carbonate budgets and for aiding assessment as to which reefs are most at risk from future environmental change and anthropogenic stressors (Perry and Morgan 2017a). The data will help constrain and improve the parameterization and calibration of models aiming to predict how coral reefs will respond to ongoing coral reef community change (Bozec *et al.,* 2015, House *et al.,* 2016 and Hedley *et al.,* 2016). This is especially true if the rugosity data, on application to historical imagery, can determine how coral reefs previously responded to historic, disturbances and stressors, analogous to those at present (Aronson and Precht, 1995, Alvarez-Filip, 2011 and Darling *et al.,* 2012 and 2013). Better constrained models will produce more accurate susceptibility predictions regarding coral community change and regime shifts which will be useful for reef mangers determining the likelihood that a reef will move from a phase of net accretion to net erosion (Bozec *et al.,* 2015, House *et al.,* 2016; and Hedley *et al.,* 2016). These will subsequently help inform reef management under variable climate change scenarios, (Hughes *et al.,* 2010) and help triage reefs for the most appropriate conservation action (Dustan *et al.,*

2013). Hopefully this will contribute to an overall aim of coral reef conservation, of being able to sustain the ability of reefs to provide ecosystem goods and services into the future, which current management practices are failing to do at global scales (Bellwood *et al.,* 2004).

4.6 Conclusion

This research has led to the development of a new (conversion factor) technique for remotely assessing and monitoring the rugosity of coral reefs at an ecologically relevant, coral colony scale and demonstrated how it can quantify the structural complexity of coral reefs from a variety of coral survey data sources. In doing this, the research has established a new coral taxa specific rugosity database. Subsequent analysis of this led to recognition that mean rugosity is a key trait relevant to determining coral life history strategies and identification of significant, generalizable relationships between coral size and rugosity for all coral taxa and abiotic substrate.

The application of coral genus, morphotype and abiotic substrate specific conversion factors, extracted from this database, to control and field video transects, line intercept data and UAV imagery demonstrated how 3D ecosystem characteristics can be determined from 2D data. Most importantly, the technique has shown how rugosity trait data can accurately quantify the relative and individual contributions of different coral genera to the overall structural complexity of a coral reef ecosystem. This is vital for improving current understanding of how microscale rugosity influences the ecological community dynamics, overall functioning of and services provided by coral reefs, as well as, the predicted trajectories of coral reefs under environmental and anthropogenic stressors (Graham and Nash, 2013 and González-Barrios and Alvarez-Filip, 2018).

Using coral conversion factor equations to calculate and monitor rugosity revealed many advantages over alternate and traditional methods. The conversion factors can be applied to a plethora of existing data sources, allowing prediction as to how coral reefs responded historically to previous disturbance events. The technique provides a standardised rugosity measurement which allows valid comparisons of rugosity data across global scales and multiple surveys. Due to its applicability to UAV imagery, the technique can also provide rapid response surveys post-disturbance events and rugosity information for large areas of coral reef. The key advantage of this technique, however, is its elimination of the need for any *in-situ* rugosity

measurement or complex processing technology, making it much more time and cost-effective than traditional techniques. It is hoped that growing rugosity trait databases, representative of all coral reef regions worldwide, alongside these advantageous features, will make the conversion factor technique globally available for use by both researchers and communities. This will result in more accurate identification of which reefs are most at risk and predictions of how the structural complexity of coral reef ecosystems will respond to ongoing environmental change in the future.

Appendices

Appendix A. Results of the linear regression analysis run to test the statistical significance of the coral size - rugosity relationships for all coral genera and morphotypes in the rugosity database.

Reef taxa or substrate		
Acropora	**Morphotype**	**Regression analysis result**
Acropora branching	Branching	$F(1, 140) = 3603.65$, $p = 0.000$
Acropora (stubby branches)	Plates and tables	$F(1, 20) = 1116.40$, $p = 0.000$
Acropora (flat plate)	Plates and tables	$F(1, 39) = 521.22$, $p = 0.000$
Acropora (outwards branching)	Plates and tables	$F(1, 27)$, = 892.86, $p = 0.000$
Acropora corymbrose	Corymbrose	$F(1, 129) = 1146.68$, $p = 0.000$
Acropora digitate	Digitate	$F(1, 78) = 445.57$, $p = 0.000$
Acropora hispidose	Hispidose	$F(1, 10) = 103.03$, $p = 0.000$
Porites		
Porites compressa	Branching	$F(1,5) = 219.97$, $p = 0.000$
Porites cyclindrica	Branching	$F(1, 75) = 2604.46$, $p = 0.000$
Porites lobata	Massive	$F(1, 104) = 1315.83$, $p = 0.000$
Porites unknown	Stubby branching	$F(1,36) = 8,26,62$, $p = 0.000$
Porites rus	Contorted branching	$F(1,17) = 205.04$, $p = 0.000$
Coral Genera		
Acanthastrea	Encrusting	$F(1,35) = 1921.40$, $p = 0.000$
Acanthastrea	Massive	$F(1,31) = 1504$, $p = 0.000$
Alveopora	Columnar	$F(1,27) = 417.50$, $p = 0.000$
Astreopora	Encrusting	$F(1,19) = 491.84$, $p = 0.000$
Astreopora	Massive	$F(1,40) = 1306.72$, $p = 0.000$
Coscinaraea	Encrusting	$F(1,11) = 105.41$, $p = 0.000$
Coscinaraea	Massive	$F(1,31) = 1039$, $p = 0.000$
Coscinaraea	Submassive	$F(1,9) = 641.49$, $p = 0.000$
Diploastrea	Massive	$F(1,29) = 491.19$, $p = 0.000$
Diploria	Massive	$F(1,79) = 2693.79$, $p = 0.000$
Echinopora	Branching	$F(1,22) = 951$, $p = 0.000$
Favia	Massive	$F(1,79) = 3319.84$, $p = 0.000$
Favites	Massive	$F(1,91) = 2208.13$, $p = 0.000$
Fungia	Free-living	$F(1,51) = 2113.65$, $p = 0.000$
Galaxea	Encrusting	$F(1,15) = 1403.76$, $p = 0.000$
Galaxea	Massive	$F(1,79) = 2295.82$, $p = 0.000$
Goniastrea	Massive	$F(1,50) = 2760.37$, $p = 0.000$
Goniopora	Massive	$F(1,47) = 1735.14$, $p = 0.000$
Heliopora	Fossil branching	$F(1,7) = 73.64$, $p = 0.000$
Herpolitha	Free-living	$F(1,52) = 1242.31$, $p = 0.000$
Isopora	Branching	$F(1,29) = 504.41$, $p = 0.000$
Leptastrea	Encrusting	$F(1,59)$, 1512.64, $p = 0.000$
Leptastrea	Massive	$F(1,71) = 1775.23$, $p = 0.000$
Leptastrea	Submassive	$F(1,19) = 525.42$, $p = 0.000$
Leptoria	Massive	$F(1,51) = 586.61$, $p = 0.000$
Leptoria	Submassive	$F(1,35) = 1122.46$, $p = 0.000$
Lobophyllia	Flabello-meandroid	$F(1,54) = 425.54$, $p = 0.000$
Merulina	Mixed	$F(1,63) = 1246.67$, $p = 0.000$
Merulina	Contorted laminar	$F(1,7) = 1539.83$, $p = 0.000$
Montipora	Branching	$F(1,65) = 850.7$, $p = 0.000$
Montipora	Plates and tables	$F(1,36) = 676.08$, $p = 0.000$

Montipora	Contorted laminar	$F(1, 4) = 882.16$, $p = 0.000$
Mussa	Flabello-meandroid	$F(1, 7) = 473.45$, $p = 0.000$
Oulophyllia	Massive	$F(1, 27) = 889.88$, $p = 0.000$
Pachyseris	Plates and tables	$F(1, 42) = 368.84$, $p = 0.000$
Pavona	Encrusting	$F(1, 23) = 801.40$, $p = 0.000$
Pavona cactus	Foliose	$F(1, 99) = 1649$, $p = 0.000$
Pavona clavus	Columnar	$F(1, 29) = 370.54$, $p = 0.000$
Pectina	Foliose	$F(1, 109) = 2573.26$, $p = 0.000$
Platygyra	Massive	$F(1, 107) = 1584.31$, $p = 0.000$
Pocillopora	Stubby branches	$F(1, 49) = 1384.96$, $p = 0.000$
Pocillopora	Large open branches	$F(1, 43) = 1022.24$, $p = 0.000$
Psammocora	Foliose	$F(1, 39) = 1493.85$, $p = 0.000$
Sandolithia	Free-living	$F(1, 42) = 987.40$, $p = 0.000$
Seriatopora	Branching	$F(1, 59) = 848.73$, $p = 0.000$
Stylophora	Branching	$F(1, 68) = 913.15$, $p = 0.000$
Symphyllia	Flabello-meandroid	$F(1, 93) = 4426.39$, $p = 0.000$
Trachyphyllia	Flabello-meandroid	$F(1, 79) = 3321.23$, $p = 0.000$
Turbinaria (*vase)*	Contorted laminar	$F(1, 5) = 1273.96$, $p = 0.000$
Turbinaria	Contorted laminar	$F(1, 54) = 1975$, $p = 0.000$
Turbinaria	Plates and tables	$F(1, 14) = 983.56$, $p = 0.000$
Soft Coral		
Sinularia	Columnar	$F(1, 14) = 287.17$, $p = 0.000$
Lobophytum - Sacrophyton	Lettuce like	$F(1, 43) = 1223.30$, $p = 0.000$
Lobophytum	Columnar	$F(1, 22) = 284.71$, $p = 0.000$
Coral Morphotypes		
Branching		$F(1, 301) = 4056.54$, $p = 0.000$
Acropora Plates and Tables		$F(1, 88) = 1681.50$, $p = 0.000$
Columnar		$F(1, 57) = 762.76$, $p = 0.000$
Contorted laminar		$F(1, 85) = 2373.90$, $p = 0.000$
Encrusting		$F(1,190) = 3246.99$, $p = 0.000$
Flabello-meandroid		$F(1, 236) = 3064.43$, $p = 0.000$
Free-living		$F(1, 147) = 3565$, $p = 0.000$
Foliose		$F(1, 249) = 4053$, $p = 0.000$
Massive		$F(1, 828) = 15077.43$, $p = 0.000$
Mixed contorted		$F(1, 67) = 1329.53$, $p = 0.000$
Micro-atoll		$F(1, 8) = 170.61$, $p = 0.000$
Plates and tables		$F(1, 94) = 1194.33$, $p = 0.000$
Submassive		$F(1, 73) = 2195$, $p = 0.000$
Soft coral		$F(1, 81) = 1104.17$, $p = 0.000$
Digitate and Corymbrose		$F(1, 208) = 1418.83$, $p = 0.000$
Algae covered coral		
Branching coral		$F(1, 26) = 618.93$, $p = 0.000$
Other colonies		$F(1, 10) = 1410.48$, $p = 0.000$
Giant clam		
Clam		$F(1,14) = 386.79$, $p = 0.000$

Appendix B. Calculated and *in-situ* contour lengths and rugosity values measured for artificial, control transects from the Natural History Museum. Transects are grouped by coral community as composed of only slow growing corals, only fast growing corals and both slow and fast growing corals.

		Calculated virtually		*In-situ* measurement	
Transect composition:		**Contour length (m)**	**Transect rugosity (c / 5)**	**Contour length (m)**	**Transect rugosity (c / 5)**
Slow growing corals					
Transect No.	1	7.49	1.50	7.96	1.59
	2	7.93	1.59	8.80	1.76
	3	7.76	1.55	8.25	1.65
	4	6.66	1.33	7.28	1.46
	5	6.03	1.21	6.50	1.30
	6	5.24	1.05	5.46	1.09
	7	5.85	1.17	6.00	1.20
	8	5.63	1.13	5.63	1.13
	9	6.60	1.32	6.87	1.37
	10	6.37	1.27	6.70	1.34
	11	6.58	1.32	6.43	1.29
	12	6.86	1.37	6.99	1.40
	13	6.49	1.30	6.27	1.25
	14	5.58	1.12	5.53	1.11
	15	8.78	1.76	8.80	1.76
Slow and fast growing corals					
Transect No.	1	5.91	1.18	6.24	1.25
	2	6.86	1.37	7.24	1.45
	3	8.41	1.68	9.49	1.90
	4	8.14	1.63	9.70	1.94
	5	8.67	1.73	8.80	1.76
	6	8.71	1.74	8.69	1.74
	7	9.03	1.81	8.93	1.79
	8	9.07	1.81	9.38	1.88
	9	9.29	1.86	9.68	1.94
	10	7.92	1.58	8.10	1.62
	11	8.53	1.71	8.99	1.80
	12	8.64	1.73	9.30	1.86
	13	9.58	1.92	10.27	2.05
	14	9.46	1.89	11.22	2.24
	15	8.62	1.72	8.80	1.76
	16	9.35	1.87	10.37	2.07
	17	8.89	1.78	9.55	1.91
	18	10.64	2.13	12.01	2.40
	19	11.27	2.25	12.64	2.53
	20	11.93	2.39	13.26	2.65
	21	12.48	2.50	13.96	2.79

	22	12.57	2.51	13.68	2.74
	23	12.99	2.60	14.29	2.86
	24	12.78	2.56	13.33	2.67
	25	12.33	2.47	14.69	2.94
	26	11.95	2.39	14.27	2.85
Fast growing corals					
Transect No.	1	13.61	2.72	14.78	2.96
	2	13.24	2.65	16.24	3.25
	3	12.52	2.50	14.30	2.86
	4	13.81	2.76	16.37	3.27
	5	14.41	2.88	17.57	3.51
	6	14.55	2.91	18.43	3.69
	7	14.52	2.90	19.43	3.89
	8	14.51	2.90	19.81	3.96
	9	14.98	3.00	20.52	4.10
	10	14.14	2.83	19.62	3.92
	11	15.58	3.12	20.31	4.06
	12	16.17	3.23	21.20	4.24
	13	16.51	3.30	20.69	4.14
	14	15.36	3.07	19.89	3.98
	15	14.37	2.87	18.68	3.74
	16	12.69	2.54	16.89	3.38
	17	12.89	2.58	16.40	3.28
	18	9.69	1.94	13.25	2.65
	19	7.97	1.59	9.65	1.93

Appendix C. *In-situ* rugosity and calculated contour lengths, planar lengths and rugosity for natural coral reef transects measured on Heron Island (Great Barrier Reef) and from three atolls in the Chagos Archipelago. Calculated rugosity is shown as originally calculated and with the addition of two correction factors.

			***In-situ* measurement**	**Calculated virtually**				
Location	**Site**	**T. no.**	**Rugosity**	**Contour length (cms)**	**Planar length (cms)**	**Rugosity (c / p)**	**Rugosity Correction 1**	**Rugosity Correction 2**
Heron Island (Great Barrier Reef)		1	2.04	888.86	460.98	1.93	2.06	2.15
		2	2.26	969.98	456.67	2.12	2.12	2.12
		3	2.30	735.32	462.78	1.59	1.59	1.59
		4	2.68	823.69	396.23	2.08	2.23	2.33
		5	3.98	1110.46	416.66	2.67	2.67	2.67
Peros Banhos (Chagos)	Ile de la Passe	1	2.10	1679.93	904.50	1.86	2.20	2.49
		2	1.63	1592.83	929.69	1.71	1.83	1.93
		3	2.06	1669.25	870.71	1.92	1.95	1.97
		4	1.67	1770.62	933.20	1.90	1.90	1.90
	Ile de la Diamante	1	1.75	1811.58	1022.96	1.77	1.88	1.94
		2	2.05	1781.73	942.70	1.89	1.89	1.89
		3	1.62	1566.15	887.96	1.76	1.83	1.88
		4	1.82	1734.46	953.59	1.82	1.82	1.82
	Ile Gabrielle	1	2.07	1909.02	989.74	1.93	2.20	2.43
		2	2.05	1721.21	934.86	1.84	2.11	2.30
		3	2.25	1807.63	890.46	2.03	2.16	2.25
		4	1.82	1672.97	908.98	1.84	1.84	1.84
	Ile Poule	1	1.75	1627.49	890.43	1.83	1.92	1.97
		2	2.42	1734.68	912.02	1.90	2.21	2.40
		3	1.69	1763.97	965.06	1.83	1.83	1.83
		4	1.46	1885.98	1003.98	1.88	1.88	1.88

Salomon (Chagos)	Ile Anglaise Middle	1	2.15	1811.03	963.62	1.88	2.21	2.48
		2	2.11	1747.10	908.39	1.92	2.10	2.23
		3	2.41	1790.62	826.72	2.17	2.25	2.29
		4	2.72	1705.17	850.39	2.01	2.58	3.00
	Ile Anglaise North	1	2.03	1803.55	979.79	1.84	2.03	2.20
		2	2.14	1768.23	1008.85	1.75	1.97	2.10
		3	1.95	1981.74	992.54	2.01	2.35	2.62
		4	2.13	1896.13	976.65	1.94	1.98	1.99
	Ile Anglaise South	1	2.22	1685.60	924.32	1.82	2.31	2.80
		2	2.48	1832.04	912.76	2.01	2.17	2.34
		3	2.08	1911.26	918.22	2.08	2.44	2.73
		4	2.22	1822.02	903.17	2.03	2.25	2.42
	Ile du Passe	1	2.54	1671.78	863.86	1.94	2.35	2.69
		2	2.11	1752.51	973.08	1.80	2.09	2.31
		3	2.06	1835.15	976.44	1.88	2.03	2.08

Great Chagos Bank (Chagos)	Egmont North West	1	1.87	2124.76	911.77	2.33	2.33	2.33
		2	1.88	1814.37	922.95	1.97	1.97	1.97
		3	1.77	2039.51	789.14	2.58	2.71	2.84
		4	1.75	2284.58	932.31	2.45	2.59	2.66
	Middle Brother	1	1.72	1616.93	920.40	1.76	1.79	1.81
		2	2.13	1508.76	793.24	1.90	2.14	2.34
		3	1.70	1576.84	887.80	1.78	2.28	2.79
		4	1.94	1672.99	898.47	1.86	2.47	3.09
	Nelson	1	1.70	1665.96	937.52	1.78	1.78	1.78
		2	2.02	1592.12	895.85	1.78	1.92	2.00
		3	1.84	1549.73	896.01	1.74	2.11	2.47
		4	1.55	1701.39	969.90	1.75	2.09	2.42
	South Brother East	1	1.57	1390.00	848.35	1.64	1.67	1.70
		2	1.77	1129.15	598.26	1.89	1.89	1.89
		3	1.45	1621.74	824.51	1.97	2.22	2.45
		4	1.63	1649.87	860.59	1.92	2.23	2.44

	South Brother West	1	1.73	1436.01	776.92	1.82	1.88	1.92
		2	1.66	1797.43	929.66	1.93	1.97	1.99
		3	1.49	1625.23	934.31	1.74	1.93	2.06
		4	1.28	1535.25	892.81	1.72	1.91	2.00

Appendix D. Calculated contour lengths and rugosity values for 305 transects in the Seychelles calculated from the application of the rugosity conversion factors to line intercept data. The data spans four years and is grouped into 21 study sites from 3 habitat types in 7 reef locations. Each individual site is identified as in a regime shifted or recovering state following the 1998 coral bleaching event.

Site:		2008			2011			2014			2017		
	Transect number	Contour (m)	Rugosity (c / 10)	Mean	Contour (m)	Rugosity (c / 10)	Mean	Contour (m)	Rugosity (c / 10)	Mean	Contour (m)	Rugosity (c / 10)	Mean
Cousin, Granite (regime shifted)	1	13.57	1.36	1.32	12.72	1.27	1.30	13.09	1.31	1.30			
	2	13.11	1.31		13.04	1.30		13.67	1.37				
	3	13.04	1.30		12.82	1.28		12.91	1.29				
	4	12.76	1.28		13.26	1.33		12.88	1.29				
	5	13.02	1.30		13.47	1.35		12.75	1.28				
	6	12.95	1.29		13.69	1.37		12.92	1.29				
	7	13.28	1.33		12.51	1.25		12.98	1.30				
	8	13.23	1.32		12.82	1.28		13.00	1.30				
	9	13.16	1.32										
	10	14.02	1.40										
	11	12.77	1.28										
	12	13.68	1.37										
	13	13.74	1.37										
	14	13.49	1.35										
	15	13.10	1.31										
	16	12.72	1.27										
Cousin, Sand (regime shifted)	1	13.58	1.36	1.36	13.29	1.33	1.38	17.67	1.77	1.59			
	2	13.11	1.31		12.92	1.29		14.09	1.41				
	3	13.32	1.33		12.96	1.30		19.06	1.91				
	4	13.27	1.33		13.07	1.31		16.53	1.65				
	5	13.03	1.30		13.66	1.37		16.23	1.62				
	6	13.02	1.30		14.34	1.43		14.39	1.44				
	7	13.57	1.36		15.41	1.54		15.06	1.51				
	8	13.05	1.30		15.04	1.50		13.98	1.40				
	9	13.66	1.37										
	10	13.06	1.31										
	11	12.99	1.30										
	12	14.37	1.44										
	13	14.47	1.45										

	14	14.32	1.43								
	15	13.87	1.39								
	16	14.23	1.42								
Cousin, Coral (regime shifted)	1	14.71	1.47	1.31	13.16	1.32	1.31	13.14	1.31	1.32		
	2	13.13	1.31		13.13	1.31		13.24	1.32			
	3	12.20	1.22		13.26	1.33		13.01	1.30			
	4	13.65	1.37		13.00	1.30		13.39	1.34			
	5	13.50	1.35		12.95	1.29		13.17	1.32			
	6	12.87	1.29		13.04	1.30		13.27	1.33			
	7	12.82	1.28		13.02	1.30		13.22	1.32			
	8	12.48	1.25		13.25	1.32		13.37	1.34			
	9	12.43	1.24									
	10	12.74	1.27									
	11	12.60	1.26									
	12	12.87	1.29									
	13	13.17	1.32									
	14	13.51	1.35									
	15	13.12	1.31									
	16	13.15	1.32									
Mahe E, Granite (regime shifted)	1	14.26	1.43	1.50	13.41	1.34	1.34	13.08	1.31	1.39	13.05	1.31	1.30
	2				13.00	1.30		16.79	1.68		12.80	1.28	
	3				13.06	1.31		14.97	1.50		12.64	1.26	
	4				12.92	1.29		13.32	1.33		13.11	1.31	
	5	14.54	1.45		14.80	1.48		13.25	1.33		13.13	1.31	
	6				13.40	1.34		13.38	1.34		13.14	1.31	
	7				12.77	1.28		13.56	1.36		13.06	1.31	
	8				13.69	1.37		13.17	1.32		13.19	1.32	
	9	15.35	1.54										
	13	15.65	1.57										
Mahe E, Sand (recovering)	1	13.92	1.39	1.45	15.08	1.51	1.52	14.80	1.48	1.49	13.54	1.35	1.40
	2				15.11	1.51		14.03	1.40		13.69	1.37	
	3				15.54	1.55		14.95	1.50		13.76	1.38	
	4				14.79	1.48		14.17	1.42		14.07	1.41	
	5				16.11	1.61		14.14	1.41		14.01	1.40	
	6	15.50	1.55		15.25	1.52		15.00	1.50		13.91	1.39	
	7				15.08	1.51		17.95	1.80		14.32	1.43	

	8				14.73	1.47		14.54	1.45		14.37	1.44	
	9	14.56	1.46										
	12	14.11	1.41										
Mahe E, Coral (regime shifted)	1	16.43	1.64		13.12	1.31		15.54	1.55		13.22	1.32	
	2				13.42	1.34		13.76	1.38		13.44	1.34	
	3				13.35	1.34		16.49	1.65		13.49	1.35	
	4	14.31	1.43		13.20	1.32	1.38	14.36	1.44	1.45	13.26	1.33	1.34
	5			1.67	13.47	1.35		14.66	1.47		13.70	1.37	
	6				13.22	1.32		13.37	1.34		13.79	1.38	
	7				15.15	1.51		14.46	1.45		13.30	1.33	
	8				15.34	1.53		13.62	1.36		13.33	1.33	
	9	20.93	2.09										
	12	15.08	1.51										
Mahe NW, Granite (recovering)	1	14.39	1.44		14.90	1.49		16.71	1.67		14.48	1.45	
	2	14.34	1.43		14.58	1.46		17.84	1.78		14.31	1.43	
	3	14.74	1.47		15.68	1.57		18.36	1.84		14.74	1.47	
	4	14.54	1.45		15.41	1.54	1.56	16.71	1.67	1.72	15.08	1.51	1.47
	5	14.81	1.48		15.10	1.51		16.78	1.68		14.91	1.49	
	6	14.40	1.44		17.77	1.78		16.49	1.65		14.93	1.49	
	7	14.48	1.45		16.32	1.63		16.19	1.62		14.27	1.43	
	8	15.36	1.54	1.44	15.38	1.54		18.24	1.82		14.62	1.46	
	9	14.98	1.50										
	10	14.17	1.42										
	11	14.34	1.43										
	12	14.09	1.41										
	13	13.63	1.36										
	14	13.91	1.39										
	16	13.64	1.36										
Mahe NW, sand (recovering)	1	14.69	1.47		17.04	1.70		17.36	1.74		14.38	1.44	
	2	14.35	1.44		15.88	1.59		22.21	2.22		13.12	1.31	
	3	13.56	1.36		15.59	1.56		16.72	1.67		13.84	1.38	
	4	13.80	1.38	1.51	15.11	1.51	1.61	15.29	1.53	1.72	14.87	1.49	1.40
	5	15.01	1.50		15.57	1.56		17.10	1.71		14.39	1.44	
	6	17.15	1.71		17.16	1.72		16.07	1.61		14.35	1.44	
	7	13.96	1.40		16.57	1.66		14.91	1.49		14.60	1.46	

	8	13.53	1.35		15.64	1.56		17.58	1.76		12.31	1.23	
	9	17.23	1.72										
	10	16.93	1.69										
	11	13.55	1.36										
	12	13.78	1.38										
	13	16.78	1.68										
	14	16.24	1.62										
	15	16.47	1.65										
	16	14.53	1.45										
Mahe NW, Coral (recovering)	1	12.79	1.28	1.45	16.30	1.63	1.63	22.92	2.29	1.97	11.68	1.17	1.23
	2	13.04	1.30		17.54	1.75		23.54	2.35		11.81	1.18	
	3	14.64	1.46		14.72	1.47		22.96	2.30		12.09	1.21	
	4	13.92	1.39		16.09	1.61		20.99	2.10		12.42	1.24	
	5	14.77	1.48		18.09	1.81		17.36	1.74		11.92	1.19	
	6	13.69	1.37		15.46	1.55		22.65	2.26		12.48	1.25	
	7	15.58	1.56		16.21	1.62		14.43	1.44		13.08	1.31	
	8	16.40	1.64		16.35	1.64		12.96	1.30		13.23	1.32	
	9	15.55	1.56										
	10	14.44	1.44										
	11	14.11	1.41										
	12	13.81	1.38										
	13	14.85	1.49										
	14	15.39	1.54										
	15	15.09	1.51										
	16	13.70	1.37										
Mahe W, Granite (recovering)	1	15.99	1.60	1.51	15.47	1.55	1.66	17.78	1.78	1.84	14.13	1.41	1.43
	2	15.55	1.55		15.88	1.59		16.98	1.70		14.20	1.42	
	3	14.60	1.46		17.12	1.71		17.25	1.72		14.57	1.46	
	4	14.54	1.45		17.78	1.78		18.39	1.84		14.95	1.49	
	5	14.84	1.48		16.00	1.60		17.94	1.79		14.46	1.45	
	6	15.05	1.50		16.55	1.65		18.27	1.83		14.00	1.40	
	7	15.13	1.51		17.32	1.73		21.55	2.16		13.68	1.37	
	8	15.17	1.52		16.80	1.68		19.31	1.93		14.60	1.46	
	9	16.54	1.65										
	10	14.94	1.49										
	11	14.45	1.44										

	12	14.30	1.43								
	13	13.41	1.34								
	14	15.34	1.53								
	15	16.14	1.61								
	16	15.23	1.52								
Mahe W, Sand (recovering)	1	15.47	1.55	1.51	16.47	1.65	1.88	17.73	1.77	1.71	13.21	1.32	1.31
	2	12.41	1.24		30.86	3.09		20.04	2.00		12.21	1.22	
	3	12.99	1.30		16.03	1.60		20.35	2.04		13.05	1.31	
	4	16.53	1.65		17.54	1.75		14.35	1.43		12.38	1.24	
	5	13.26	1.33		17.87	1.79		14.69	1.47		14.96	1.50	
	6	17.83	1.78		18.12	1.81		14.69	1.47		12.99	1.30	
	7	14.85	1.49		16.36	1.64		17.66	1.77		12.80	1.28	
	8	16.61	1.66		17.16	1.72		17.15	1.71		13.00	1.30	
	9	13.48	1.35										
	10	14.23	1.42										
	11	13.37	1.34										
	12	14.50	1.45										
	13	20.62	2.06										
	14	16.91	1.69										
	15	11.91	1.19										
	16	16.24	1.62										
Mahe W, Coral (recovering)	1	15.73	1.57	1.55	15.12	1.51	1.54	18.71	1.87	2.04	12.64	1.26	1.28
	2	14.49	1.45		14.52	1.45		20.25	2.02		13.44	1.34	
	3	14.45	1.44		15.22	1.52		23.85	2.38		13.40	1.34	
	4	16.01	1.60		15.97	1.60		20.31	2.03		13.48	1.35	
	5	12.88	1.29		16.08	1.61		19.69	1.97		12.96	1.30	
	6	15.12	1.51		14.88	1.49		20.92	2.09		12.27	1.23	
	7	14.60	1.46		14.91	1.49		18.80	1.88		11.95	1.19	
	8	16.59	1.66		16.46	1.65		20.62	2.06		12.12	1.21	
	9	16.10	1.61										
	10	19.91	1.99										
	11	15.79	1.58										
	12	12.30	1.23										
	13	13.72	1.37										
	14	17.55	1.75										
	15	17.60	1.76										

	16	15.47	1.55								
Praslin NE, Granite (recovering)	1	18.63	1.86	1.77	15.39	1.54	1.61	17.19	1.72	1.62	13.79	1.38	1.38
	2	16.11	1.61		16.91	1.69		14.55	1.46		13.76	1.38	
	3	20.27	2.03		14.81	1.48		17.37	1.74		13.54	1.35	
	4	19.45	1.94		15.32	1.53		16.82	1.68		13.13	1.31	
	5	23.59	2.36		16.07	1.61		15.18	1.52		13.61	1.36	
	6	18.89	1.89		17.26	1.73		14.94	1.49		14.00	1.40	
	7	19.06	1.91		16.38	1.64		16.94	1.69		14.39	1.44	
	8	16.78	1.68		16.84	1.68		16.48	1.65		14.18	1.42	
	9	18.83	1.88										
	10	14.77	1.48										
	11	15.95	1.60										
	12	17.94	1.79										
	13	16.47	1.65										
	14	14.62	1.46										
	15	15.63	1.56										
	16	16.79	1.68										
Praslin NE, Sand (recovering)	1	12.16	1.22	1.30	12.94	1.29	1.30	14.75	1.48	1.32	14.12	1.41	1.30
	2	11.79	1.18		13.37	1.34		12.19	1.22		12.83	1.28	
	3	13.06	1.31		13.01	1.30		11.40	1.14		13.56	1.36	
	4	13.87	1.39		13.51	1.35		11.45	1.14		13.04	1.30	
	5	12.97	1.30		12.05	1.21		13.48	1.35		13.05	1.31	
	6	12.32	1.23		12.59	1.26		13.88	1.39		13.29	1.33	
	7	13.41	1.34		12.66	1.27		13.64	1.36		12.19	1.22	
	8	12.95	1.29		13.52	1.35		14.48	1.45		11.63	1.16	
	9	12.90	1.29										
	10	13.63	1.36										
	11	13.06	1.31										
	12	12.75	1.28										
	13	13.15	1.32										
	14	12.95	1.29										
	15	13.30	1.33										
	16	13.27	1.33										

Praslin NE, Coral (regime shifted)	1	12.64	1.26	1.32	13.15	1.31	1.30	13.39	1.34	1.29	12.86	1.29	1.29
	2	13.98	1.40		13.24	1.32		12.98	1.30		12.78	1.28	
	3	13.16	1.32		12.91	1.29		12.91	1.29		12.73	1.27	
	4	13.72	1.37		12.76	1.28		12.86	1.29		12.93	1.29	
	5	13.23	1.32		12.97	1.30		12.95	1.29		12.90	1.29	
	6	13.66	1.37		12.84	1.28		12.92	1.29		12.60	1.26	
	7	12.98	1.30		12.92	1.29		12.89	1.29		13.05	1.30	
	8	13.20	1.32		13.19	1.32		12.37	1.24		13.12	1.31	
	9	13.30	1.33										
	10	13.50	1.35										
	11	13.14	1.31										
	12	12.82	1.28										
	13	14.09	1.41										
	14	12.52	1.25										
	15	12.76	1.28										
	16	12.79	1.28										

Praslin SW, Granite (recovering)	1	19.15	1.92	1.71	18.45	1.85	1.71	20.58	2.06	1.89	14.70	1.47	1.42
	2	18.98	1.90		15.05	1.51		19.73	1.97		15.02	1.50	
	3	18.54	1.85		17.27	1.73		18.46	1.85		13.61	1.36	
	4	17.68	1.77		18.15	1.81		18.31	1.83		13.49	1.35	
	5	18.22	1.82		18.27	1.83		21.11	2.11		13.83	1.38	
	6	17.07	1.71		17.09	1.71		17.92	1.79		15.18	1.52	
	7	17.37	1.74		16.20	1.62		17.64	1.76		13.27	1.33	
	8	15.74	1.57		16.61	1.66		17.30	1.73		14.63	1.46	
	9	15.93	1.59										
	10	17.35	1.73										
	11	15.62	1.56										
	12	15.62	1.56										
	13	18.04	1.80										
	14	15.23	1.52										
	15	14.94	1.49										
	16	17.48	1.75										

Praslin SW, Sand (regime shifted)	1	13.95	1.40	1.30	14.06	1.41	1.38	14.82	1.48	1.48	13.70	1.37	1.38
	2	13.77	1.38		14.12	1.41		12.67	1.27		13.58	1.36	
	3	13.00	1.30		14.16	1.42		14.89	1.49		14.08	1.41	
	4	14.27	1.43		13.71	1.37		16.14	1.61		13.38	1.34	
	5	13.24	1.32		14.31	1.43		14.39	1.44		13.62	1.36	
	6	12.20	1.22		13.06	1.31		14.51	1.45		13.01	1.30	
	7	12.46	1.25		13.69	1.37		14.42	1.44		15.02	1.50	
	8	12.58	1.26		13.61	1.36		16.59	1.66		14.07	1.41	
	9	13.60	1.36										
	10	12.60	1.26										
	11	12.76	1.28										
	12	12.80	1.28										
	13	12.70	1.27										
	14	12.39	1.24										
	15	12.99	1.30										
	16	12.36	1.24										
Praslin SW, Coral (regime shifted)	1	13.81	1.38	1.32	12.96	1.30	1.30	13.84	1.38	1.33	13.23	1.32	1.32
	2	12.69	1.27		12.91	1.29		13.31	1.33		13.07	1.31	
	3	13.27	1.33		12.90	1.29		13.19	1.32		12.95	1.30	
	4	12.93	1.29		12.70	1.27		12.80	1.28		12.95	1.30	
	5	13.04	1.30		12.94	1.29		12.96	1.30		13.07	1.31	
	6	13.00	1.30		13.12	1.31		14.14	1.41		13.16	1.32	
	7	12.87	1.29		13.29	1.33		13.22	1.32		13.52	1.35	
	8	14.48	1.45		13.07	1.31		13.29	1.33		13.65	1.37	
	9	13.84	1.38										
	10	13.16	1.32										
	11	13.46	1.35										
	12	12.93	1.29										
	13	13.03	1.30										
	14	13.25	1.33										
	15	12.96	1.30										
	16	13.11	1.31										
Ste. Anne, Granite (recoverin	1	13.77	1.38	1.38	14.54	1.45	1.62	14.96	1.50	1.52	14.18	1.42	1.41
	2				15.25	1.53		14.35	1.43		13.98	1.40	
	3				16.14	1.61		14.69	1.47		14.09	1.41	
	4				16.98	1.70		14.74	1.47		14.11	1.41	

	5				18.67	1.87		14.94	1.49		14.47	1.45	
	6				16.17	1.62		15.70	1.57		13.96	1.40	
	7				15.46	1.55		16.33	1.63		13.57	1.36	
	8				16.09	1.61		15.78	1.58		14.17	1.42	
Ste. Anne, Sand (recovering)	1	13.03	1.30	1.57	18.87	1.89	1.74	19.88	1.99	1.94	11.46	1.15	1.16
	2	15.01	1.50		12.37	1.24		25.41	2.54		11.88	1.19	
	3	16.95	1.70		13.27	1.33		22.00	2.20		12.15	1.21	
	4	13.64	1.36		13.72	1.37		19.30	1.93		10.99	1.10	
	5	13.93	1.39		20.96	2.10		15.39	1.54		11.91	1.19	
	6	13.20	1.32		17.01	1.70		15.68	1.57		11.54	1.15	
	7	17.24	1.72		17.67	1.77		22.13	2.21		10.90	1.09	
	8	17.53	1.75		19.53	1.95		15.31	1.53		11.90	1.19	
	9	16.63	1.66		17.84	1.78							
	10	17.20	1.72		17.83	1.78							
	11	14.41	1.44		15.94	1.59							
	12	14.41	1.44		19.42	1.94							
	13	21.67	2.17		16.84	1.68							
	14	18.97	1.90		19.28	1.93							
	15	14.36	1.44		22.86	2.29							
	16	13.05	1.30		14.86	1.49							
Ste. Anne, Coral (recovering)	1	12.89	1.29	1.39	12.84	1.28	1.47	14.48	1.45	1.42	13.21	1.32	1.30
	2	12.29	1.23		12.84	1.28		16.27	1.63		13.00	1.30	
	3	12.57	1.26		12.85	1.28		13.93	1.39		13.07	1.31	
	4	14.42	1.44		12.44	1.24		13.63	1.36		13.16	1.32	
	5	15.53	1.55		12.08	1.21		15.45	1.54		12.88	1.29	
	6	14.83	1.48		12.40	1.24		13.60	1.36		12.71	1.27	
	7	18.09	1.81		13.14	1.31		13.16	1.32		12.69	1.27	
	8	18.65	1.86		13.23	1.32		13.39	1.34		12.94	1.29	
	9	12.18	1.22		18.10	1.81							
	10	13.00	1.30		17.68	1.77							
	11	13.44	1.34		16.90	1.69							
	12	12.40	1.24		14.48	1.45							
	13	12.44	1.24		15.69	1.57							
	14	13.41	1.34		16.71	1.67							
	15	13.24	1.32		17.69	1.77							
	16	12.81	1.28		16.44	1.64							

Appendix E. Calculated rugosity percentage change as a mean for 21 reef sites in the Seychelles between 2008 and 2011, 2011 and 2014 and 2014 and 2017. Data is divided into 3 habitat types from 7 reef locations. Each site is identified as in a recovering or regime shifted phrase following the 1998 coral bleaching event.

			Rugosity percentage change (%)					
			2008-11		2011-14		2014-17	
Location	**Habitat**	**Phrase**	Mean site	Mean	Mean site	Mean	Mean site	Mean
Cousin	coral	regime shifted	0.31	0.32	0.97	5.20		
	granite	regime shifted	-1.42		-0.11			
	sand	regime shifted	2.06		14.73			
Mahe E	coral	regime shifted	-17.41	-7.72	5.42	2.62	-7.49	-6.92
	granite	regime shifted	-10.49		4.17		-6.64	
	sand	recovering	4.75		-1.73		-6.62	
Mahe NW	coral	recovering	12.83	9.33	20.69	12.39	-37.44	-23.50
	granite	recovering	8.72		9.74		-14.55	
	sand	recovering	6.44		6.75		-18.50	
Mahe W	coral	recovering	-0.78	11.37	32.45	11.43	-37.32	-27.69
	granite	recovering	10.20		10.96		-22.30	
	sand	recovering	24.70		-9.14		-23.46	
Praslin NE	coral	regime shifted	-1.68	-3.63	-0.66	0.42	-0.29	-5.49
	granite	recovering	-9.11		0.38		-14.72	
	sand	recovering	-0.11		1.54		-1.46	
Praslin SW	coral	regime shifted	-1.91	1.73	2.76	6.63	-1.09	-10.84
	granite	recovering	0.46		10.19		-24.71	
	sand	regime shifted	6.63		6.95		-6.73	
Ste. Anne	coral	regime shifted	5.98	11.36	-3.26	0.73	-9.01	-18.86
	granite	recovering	17.34		-6.05		-7.36	
	sand	recovering	10.75		11.48		-40.21	

Appendix F. Calculated contour lengths and rugosity of 22 transects virtually placed throughout three, 100 m^2 study sites (back reef, reef flat and reef crest) on UAV imagery of the Mahutigala reef. Data are shown for present reef conditions and for two predicted degradation stages 1-2 years (D.S.1) and 2-3 years (D.S.2) following a coral bleaching event.

Back reef						
	Contour Length (m)			Rugosity (planar / 10 m)		
T. no.	Present	D.S.1	D.S.2	Present	D.S.1	D.S.2
1	22.81	20.42	11.63	2.28	2.04	1.16
2	21.21	18.9	11.34	2.12	1.89	1.13
3	19.37	17.94	11.74	1.94	1.79	1.17
4	22.89	20.55	11.45	2.29	2.06	1.14
5	22.24	19.87	11.78	2.22	1.99	1.18
6	22.9	20.32	11.87	2.29	2.03	1.19
7	23.48	20.24	11.81	2.35	2.02	1.18
8	21.55	18.17	11.63	2.16	1.82	1.16
9	17.79	16.26	11.07	1.78	1.63	1.11
10	14.84	13.13	10.76	1.48	1.31	1.08
11	13.88	13.17	11.61	1.39	1.32	1.16
12	10.68	10.68	10.68	1.07	1.07	1.07
13	11.33	10.84	10.34	1.13	1.08	1.03
14	15.59	13.34	10.86	1.56	1.33	1.09
15	16.15	14.61	11.35	1.61	1.46	1.13
16	18.52	17.1	11.57	1.85	1.71	1.16
17	21.51	18.9	11.74	2.15	1.89	1.17
18	23.77	21.18	11.7	2.38	2.12	1.17
19	26.48	23.07	11.27	2.65	2.31	1.13
20	26.74	23.39	11.79	2.67	2.34	1.18
21	26.82	23.93	12.47	2.68	2.39	1.25
22	23.13	20.87	12.39	2.31	2.09	1.24

Reef flat						
	Contour Length (m)			Rugosity (planar / 10 m)		
T. no.	Present	D.S.1	D.S.2	Present	D.S.1	D.S.2
1	25.17	22.51	12.19	2.52	2.25	1.22
2	28.79	25.3	12.42	2.88	2.53	1.24
3	30.55	26.58	12.07	3.05	2.66	1.21
4	26.19	23.21	12.21	2.62	2.32	1.22
5	28.92	25.1	11.89	2.89	2.51	1.19
6	30.55	26.42	11.8	3.05	2.64	1.18
7	29.61	25.75	11.91	2.96	2.57	1.19
8	30.97	26.74	11.89	3.1	2.67	1.19
9	26.11	23.23	13.13	2.61	2.32	1.31
10	24.82	22.37	13.13	2.48	2.24	1.31
11	24.56	22.27	13.29	2.46	2.23	1.33
12	23.38	21.65	13.88	2.34	2.17	1.39
13	27.74	24.72	12.59	2.77	2.47	1.26
14	28.21	24.65	11.65	2.82	2.47	1.17
15	29.55	25.66	11.84	2.95	2.57	1.18
16	28.53	25.14	12.36	2.85	2.51	1.24
17	30.08	26.01	11.74	3.01	2.6	1.17
18	28.58	25.01	12.64	2.86	2.5	1.26
19	29.4	25.49	12.09	2.94	2.55	1.21
20	27.46	24.1	12.31	2.75	2.41	1.23
21	27.85	24.34	11.85	2.79	2.43	1.18
22	25.19	22.22	12.14	2.52	2.22	1.21

Reef crest						
	Contour Length (m)			Rugosity (planar / 10 m)		
T. no.	Present	D.S.1	D.S.2	Present	D.S.1	D.S.2
1	21.14	19.62	14.23	2.11	1.96	1.42
2	21.69	19.8	13.41	2.17	1.98	1.34
3	22.23	19.88	12.81	2.22	1.99	1.28
4	24.71	21.97	13.39	2.47	2.2	1.34
5	21.75	20.35	14.62	2.17	2.03	1.46
6	22.26	20.67	14.96	2.23	2.07	1.5
7	21.65	20.01	14.45	2.16	2	1.44
8	20.41	19.04	14.04	2.04	1.9	1.4
9	23.41	20.25	12.31	2.34	2.03	1.23
10	25.21	21.97	12.17	2.52	2.2	1.22
11	25.17	22.4	12.79	2.52	2.24	1.28
12	24.38	21.7	12.64	2.44	2.17	1.26
13	23.87	21.06	12.19	2.39	2.11	1.22
14	21.17	18.83	12.04	2.12	1.88	1.2
15	20.52	18.84	12.24	2.05	1.88	1.22
16	26.9	23.73	12.19	2.69	2.37	1.22
17	25.36	22.37	12.55	2.54	2.24	1.26
18	22.1	20.22	14.09	2.21	2.02	1.41
19	23.16	20.86	13.99	2.32	2.09	1.4
20	21.28	19.83	14.98	2.13	1.98	1.5
21	20.05	19.35	17	2.01	1.94	1.7
22	23.17	20.34	12.71	2.32	2.03	1.27

Appendix G. Coral community composition of three study sites (back reef, reef flat and reef crest) on the Mahutigala reef. Data shows the number of digitised polygons representing each coral taxa and abiotic reef substrate and total surface area they respectively cover in each site. Data are shown for present reef conditions and for two predicted degradation stages 1-2 years (D.S.1) and 2-3 years (D.S.2) following a coral bleaching event.

Back reef	**Present**		**D.S.1**		**D.S.2**	
Taxa	***n* =**	**Area (m^2)**	***n* =**	**Area (m^2)**	***n* =**	**Area (m^2)**
Competitive corals						
Acropora branching	22	30.47				
Acropora (plates and tables)	22	3.53				
Acropora corymbrose or digitate	201	8.46				
Other branching coral	32	2.92				
Large, open branching						
Other plates and tables	25	3.13				
Micro-atoll	1	4.02				
Stress tolerant corals						
Porites Lobata	42	1.22	42	1.22	42	1.22
Massive coral	16	0.65	16	0.65	16	0.65
Flabello-meandroid	1	0.12	1	0.12	1	0.12
Stress tolerant / weedy corals						
Submassive	3	0.23				
Abiotic substrate / algae covered coral						
Coral rubble	8	1.12	8	1.12	267	47.23
Boulder (massive morphology)	6	0.13	6	0.13	6	0.13
Algae covered coral	24	5.32	261	20.96	24	5.32
Branching algae covered coral			22	30.47		
Algae covered plate			47	6.67		
Limestone pavement					47	6.67
Sand 1:1 rubble	9	2.45	9	2.45	9	2.45
Sand (low ripple)	18	36.22	18	36.22	18	36.22
Total	430	100	430	100	430	100

Reef flat	Present		D.S.1		D.S.2	
Taxa	***n* =**	**Area (m^2)**	***n* =**	**Area (m^2)**	***n* =**	**Area (m^2)**
Competitive corals						
Acropora branching	84	64.12				
Acropora (plates and tables)	36	5.83				
Acropora corymbrose or digitate	459	14.25				
Other branching coral						
Large, open branching	6	0.50				
Other plates and tables	37	5.72				
Micro-atoll						
Stress tolerant corals						
Porites Lobata	118	4.96	118	4.96	118	4.96
Massive coral						
Flabello-meandroid						
Stress tolerant / weedy corals						
Submassive						
Abiotic substrate / algae covered coral						
Coral rubble	9	3.39	9	3.39	558	82.26
Boulder (massive morphology)	5	0.28	5	0.28	5	0.28
Algae covered coral			465	14.75		
Branching algae covered coral			84	64.12		
Algae covered plate			73	11.55		
Limestone pavement					73	11.55
Sand 1:1 rubble						
Sand (low ripple)	14	0.95	14	0.95	14	0.95
Total	768	100	768	100	768	100

Reef crest	Present		D.S.1		D.S.2	
Taxa	***n* =**	**Area (m^2)**	***n* =**	**Area (m^2)**	***n* =**	**Area (m^2)**
Competitive corals						
Acropora branching	18	14.95				
Acropora (plates and tables)						
Acropora corymbrose or digitate	827	37.27				
Other branching coral	44	10.92				
Large, open branching						
Other plates and tables	55	9.17				
Micro-atoll						
Stress tolerant corals						
Porites Lobata	103	20.03	103	20.03	103	20.03
Massive coral						
Flabello-meandroid	6	0.44	6	0.44	6	0.44
Stress tolerant / weedy corals						
Submassive						
Abiotic substrate / algae covered coral						
Coral rubble					898	63.79
Boulder (massive morphology)	23	6.57	23	6.57	23	6.57
Algae covered coral	9	0.65	880	48.84		
Branching algae covered coral			18	14.95		
Algae covered plate			55	9.17		
Limestone pavement					55	9.17
Sand 1:1 rubble						
Sand (low ripple)						
Total	1085	100	1085	100	1085	100

References

Ahmad, W., and Neil, D. T. (1994). An evaluation of Landsat Thematic Mapper (TM) digital data for discriminating coral reef zonation: Heron Reef (GBR). *International Journal of Remote Sensing*, *15*(13), 2583-2597.

AIMS. (2018). Long-term Reef Monitoring Program - Annual Summary Report on coral reef condition for 2017/18. Accessed 18th September, 2018, from https://www.aims.gov.au/reef-monitoring/gbr-condition-summary-2017-2018.

Alvarez-Filip, L. (2010). *Habitat complexity in coral reefs: patterns of degradation and consequences for biodiversity.* Doctoral thesis, University of East Anglia, UK.

Alvarez-Filip, L., Carricart-Ganivet, J. P., Horta-Puga, G., and Iglesias-Prieto, R. (2013). Shifts in coral-assemblage composition do not ensure persistence of reef functionality. *Scientific reports, 3,* 3486.

Alvarez-Filip, L., Dulvy, N. K., Côté, I. M., Watkinson, A. R., and Gill, J. A. (2011). Coral identity underpins architectural complexity on Caribbean reefs. *Ecological Applications*, *21*(6), 2223-2231.

Alvarez-Filip, L., Dulvy, N. K., Gill, J. A., Côté, I. M., and Watkinson, A. R. (2009). Flattening of Caribbean coral reefs: region-wide declines in architectural complexity. *Proceedings of the Royal Society of London B: Biological Sciences*, *276*(1669), 3019-3025.

Anderson, K., and Gaston, K. J. (2013). Lightweight unmanned aerial vehicles will revolutionize spatial ecology. *Frontiers in Ecology and the Environment, 11*(3), 138-146.

Aronson, R. B., and Precht, W. F. (1995). Landscape patterns of reef coral diversity: a test of the intermediate disturbance hypothesis. *Journal of Experimental Marine Biology and Ecology*, *192*(1), 1-14.

Bak, R. P., Nieuwland, G., and Meesters, E. H. (2005). Coral reef crisis in deep and shallow reefs: 30 years of constancy and change in reefs of Curacao and Bonaire. *Coral reefs*, *24*(3), 475-479.

Balmford, A., Crane, P., Dobson, A., Green, R. E., and Mace, G. M. (2005). The 2010 challenge: data availability, information needs and extra-terrestrial insights. *Philosophical Transactions of the Royal Society of London B: Biological Sciences*, *360*(1454), 221-228.

Beijbom, O., Edmunds, P. J., Kline, D. I., Mitchell, B. G., and Kriegman, D. (2012). Automated annotation of coral reef survey images. *Computer Vision and Pattern Recognition, IEEE Conference,* 1170-1177.

Beijbom, O., Edmunds, P. J., Roelfsema, C., Smith, J., Kline, D. I., Neal, B. P., ... and Chan, S. (2015). Towards automated annotation of benthic survey images: Variability of human experts and operational modes of automation. *PloS one*, *10*(7).

Bejarano, S., Mumby, P. J., and Sotheran, I. (2010). Predicting structural complexity of reefs and fish abundance using acoustic remote sensing (RoxAnn). *Marine biology, 158*(3), 489-504.

Bellwood, D. R., Hughes, T. P., Folke, C., and Nyström, M. (2004). Confronting the coral reef crisis. *Nature*, *429*(6994), 827-833.

Bertels, L., Vanderstraete, T., Van Coillie, S., Knaeps, E., Sterckx, S., Goossens, R., and Deronde, B. (2008). Mapping of coral reefs using hyperspectral CASI data; a case study: Fordata, Tanimbar, Indonesia. *International journal of remote sensing*, *29*(8), 2359-2391.

Bianchi, C. N., Morri, C., Pichon, M., Benzoni, F., Colantoni, P., Baldelli, G., and Sandrini, M. (2006). Dynamics and pattern of coral recolonization following the 1998 bleaching event in the reefs of the Maldives. *Proceedings of the 10th International Coral Reef Symposium 1,* 30-37.

Bozec, Y. M., Alvarez-Filip, L., and Mumby, P. J. (2015). The dynamics of architectural complexity on coral reefs under climate change. *Global change biology*, *21*(1), 223-235.

Brandou, V., Allais, A. G., Perrier, M., Malis, E., Rives, P., Sarrazin, J., and Sarradin, P. M. (2007). 3D reconstruction of natural underwater scenes using the stereovision system iris. *Oceans 2007,* (1-6).

Brock, J. C., Wright, C. W., Clayton, T. D., and Nayegandhi, A. (2004). LIDAR optical rugosity of coral reefs in Biscayne National Park, Florida. *Coral Reefs, 23*(1), 48-59.

Brock, J. C., Wright, C. W., Kuffner, I. B., Hernandez, R., and Thompson, P. (2006). Airborne LiDAR sensing of massive stony coral colonies on patch reefs in the northern Florida reef tract. *Remote Sensing of Environment*, *104*(1), 31-42.

Bruno, J. F., and Selig, E. R. (2007). Regional decline of coral cover in the Indo-Pacific: timing, extent, and subregional comparisons. *PLoS one*, *2*(8).

Bryson, M., Ferrari, R., Figueira, W., Pizarro, O., Madin, J., Williams, S., and Byrne, M. (2017). Characterization of measurement errors using structure-from-motion and photogrammetry to measure marine habitat structural complexity. *Ecology and Evolution*, *7*(15), 5669-5681.

Bryson, M., Johnson-Roberson, M., Pizarro, O., and Williams, S. (2013). Automated registration for multi-year robotic surveys of marine benthic habitats. *Intelligent Robots and Systems, IEEE/RSJ International Conference,* 3344-3349.

Burke, L., Reytar, K., Spalding, M., and Perry, A. (2011). Reefs at risk revisited. Accessed December 5th, 2017 from http://www.vliz.be/en/imis?refid=223234.

Burns, J. H. R., Delparte, D., Gates, R. D., and Takabayashi, M. (2015). Integrating structure-from-motion photogrammetry with geospatial software as a novel technique for quantifying 3D ecological characteristics of coral reefs. *PeerJ*, *3.*

Burns, J. H. R., Delparte, D., Kapono, L., Belt, M., Gates, R. D., and Takabayashi, M. (2016). Assessing the impact of acute disturbances on the structure and composition of a coral community using innovative 3D reconstruction techniques. *Methods in Oceanography*, *15*, 49-59.

Carbonneau, P. E., and Dietrich, J. T. (2017). Cost-effective non-metric photogrammetry from consumer-grade sUAS: implications for direct georeferencing of structure from motion photogrammetry. *Earth Surface Processes and Landforms*, *42*(3), 473-486.

Casella, E., Collin, A., Harris, D., Ferse, S., Bejarano, S., Parravicini, V., and Rovere, A. (2017). Mapping coral reefs using consumer-grade drones and structure from motion photogrammetry techniques. *Coral Reefs*, *36*(1), 269-275.

Chirayath, V. (2014). Fluid Lensing, Applications to High-Resolution 3D Subaqueous Imaging and Automated Remote Biosphere Assessment from Airborne and Space-borne Platforms. *AGU Fall Meeting Abstracts*, *1*, 1178.

Chirayath, V., and Earle, S. A. (2016). Drones that see through waves–preliminary results from airborne fluid lensing for centimetre-scale aquatic conservation. *Aquatic Conservation: Marine and Freshwater Ecosystems, 26*, 237-250.

Chivers, R. C. (1990). New acoustic processing for underway surveying. *Hydrogr. J.*, *56*, 9-17.

Collins, M. B., and Voulgaris, G. (1993). Empirical field and laboratory evaluation of a real-time acoustic sea bed surveying system. *Proceedings-institute of acoustics*, *15*, 343-343.

Commito, J. A., and Rusignuolo, B. R. (2000). Structural complexity in mussel beds: the fractal geometry of surface topography. *Journal of Experimental Marine Biology and Ecology*, *255*(2), 133-152.

Costa, B. M., Battista, T. A., and Pittman, S. J. (2009). Comparative evaluation of airborne LiDAR and ship-based multibeam SoNAR bathymetry and intensity for mapping coral reef ecosystems. *Remote Sensing of Environment*, *113*(5), 1082-1100.

Courtney, L. A., Fisher, W. S., Raimondo, S., Oliver, L. M., and Davis, W. P. (2007). Estimating 3-dimensional colony surface area of field corals. *Journal of Experimental Marine Biology and Ecology*, *351*(1), 234-242.

Cranfield, H. J., Rowden, A. A., Smith, D. J., Gordon, D. P., and Michael, K. P. (2004). Macrofaunal assemblages of benthic habitat of different complexity and the proposition of a model of biogenic reef habitat regeneration in Foveaux Strait, New Zealand. *Journal of Sea Research*, *52*(2), 109-125.

Dahl, A. L. (1973). Surface area in ecological analysis: quantification of benthic coral-reef algae. *Marine Biology*, *23*(4), 239-249.

Darling, E. S., Alvarez-Filip, L., Oliver, T. A., McClanahan, T. R., and Côté, I. M. (2012). Evaluating life-history strategies of reef corals from species traits. *Ecology Letters*, *15*(12), 1378-1386.

Darling, E. S., McClanahan, T. R., and Côté, I. M. (2013). Life histories predict coral community disassembly under multiple stressors. *Global Change Biology*, *19*(6), 1930-1940.

Davies, J., Foster-Smith, R., and Sotheran, I. S. (1997). Marine biological mapping for environment management using acoustic ground discrimination systems and geographic information systems. *Underwater Technology*, *22*(4), 167-172.

De'ath, G., Fabricius, K. E., Sweatman, H., and Puotinen, M. (2012). The 27–year decline of coral cover on the Great Barrier Reef and its

causes. *Proceedings of the National Academy of Sciences*, *109*(44), 17995-17999.

De'ath, G., Lough, J. M., and Fabricius, K. E. (2009). Declining coral calcification on the Great Barrier Reef. *Science*, *323*(5910), 116-119.

Dietrich, J. T. (2017). Bathymetric Structure-from-Motion: extracting shallow stream bathymetry from multi-view stereo photogrammetry. *Earth Surface Processes and Landforms*, *42*(2), 355-364.

Done, T. J. (1992). Phase shifts in coral reef communities and their ecological significance. *Hydrobiologia*, *247*(1-3), 121-132.

Downs, C. A., Woodley, C. M., Richmond, R. H., Lanning, L. L., and Owen, R. (2005). Shifting the paradigm of coral-reef 'health' assessment. *Marine Pollution Bulletin*, *51*(5), 486-494.

Dustan P, Doherty O, Pardede S. (2013). Digital Reef Rugosity Estimates Coral Reef Habitat Complexity. *PLoS ONE*, *8*(2).

Eakin, C. M., Lough, J. M., and Heron, S. F. (2009). Climate variability and change: monitoring data and evidence for increased coral bleaching stress. *Coral bleaching – Patterns, Processes, Causes and Consequences,* (41-67). Springer, Berlin, Heidelberg.

Edinger, E. N., Limmon, G. V., Jompa, J., Widjatmoko, W., Heikoop, J. M., and Risk, M. J. (2000). Normal coral growth rates on dying reefs: are coral growth rates good indicators of reef health? *Marine Pollution Bulletin*, *40*(5), 404-425.

Edwards, C. B., Eynaud, Y., Williams, G. J., Pedersen, N. E., Zgliczynski, B. J., Gleason, A. C., ... and Sandin, S. A. (2017). Large-area imaging reveals biologically driven non-random spatial patterns of corals at a remote reef. *Coral Reefs*, *36*(4), 1291-1305.

Ellison, A. M., Bank, M. S., Clinton, B. D., Colburn, E. A., Elliott, K., Ford, C. R., ... and Mohan, J. (2005). Loss of foundation species: consequences for the structure and dynamics of forested ecosystems. *Frontiers in Ecology and the Environment*, *3*(9), 479-486.

English, S., Wilkinson, C., and Baker, V. (1994). Survey manual for tropical marine resources, ASEAN-Australian Marine Science Project: Living Coastal Resources. *Australian Institute of Marine Science, Townsville*, 68-80.

Ferrari, R., McKinnon, D., He, H., Smith, R. N., Corke, P., González-Rivero, M., and Upcroft, B. (2016). Quantifying multiscale habitat structural complexity: A cost-effective framework for underwater 3D modelling. *Remote Sensing*, *8*(2), 113.

Figueira, W., Ferrari, R., Weatherby, E., Porter, A., Hawes, S., and Byrne, M. (2015). Accuracy and precision of habitat structural complexity metrics derived from underwater photogrammetry. *Remote Sensing, 7*(12), 16883-16900.

Fonstad, M. A., Dietrich, J. T., Courville, B. C., Jensen, J. L., and Carbonneau, P. E. (2013). Topographic structure from motion: a new development in photogrammetric measurement. *Earth Surface Processes and Landforms*, *38*(4), 421-430.

Friedman, A., Pizarro, O., and Williams, S. B. (2010). Rugosity, slope and aspect from bathymetric stereo image reconstructions. *Oceans, IEEE, 1-9.*

Friedman, A., Pizarro, O., Williams, S. B., and Johnson-Roberson, M. (2012). Multi-Scale Measures of Rugosity, Slope and Aspect from Benthic Stereo Image Reconstructions. *PloS one*, 7(12).

Frost, N. J., Burrows, M. T., Johnson, M. P., Hanley, M. E., and Hawkins, S. J. (2005). Measuring surface complexity in ecological studies. *Limnology and Oceanography: Methods, 3*(4), 203-210.

Fuad, M. A. Z. (2010). *Coral reef rugosity and coral biodiversity. Bunaken National Park-North Sulawesi, Indonesia.* Doctoral Thesis, International Institute for Geo-information Science and Earth Observation Enchede, The Netherlands.

Gardner, T. A., Côté, I. M., Gill, J. A., Grant, A., and Watkinson, A. R. (2003). Long-term region-wide declines in Caribbean corals. *Science*, *301*(5635), 958-960.

Garpe, K. C., Yahya, S. A., Lindahl, U., and Öhman, M. C. (2006). Long-term effects of the 1998 coral bleaching event on reef fish assemblages. *Marine Ecology Progress Series*, *315*, 237-247.

GBRMPA (2014). Great Barrier Reef outlook report 2014. Accessed June 18th, 2018 from http://elibrary.gbrmpa.gov.au/jspui/handle/11017/2855.

Gleason, A. C. R., Reid, R. P., and Voss, K. J. (2007). Automated classification of underwater multispectral imagery for coral reef monitoring. *Oceans, IEEE, 1-8.*

Goatley, C. H., and Bellwood, D. R. (2011). The roles of dimensionality, canopies and complexity in ecosystem monitoring. *PLoS One*, *6*(11).

González-Barrios, F. J., and Álvarez-Filip, L. (2018). A framework for measuring coral species-specific contribution to reef functioning in the Caribbean. *Ecological Indicators*, *95*, 877-886.

González-Rivero, M., Bongaerts, P., Beijbom, O., Pizarro, O., Friedman, A., Rodriguez-Ramirez, A., ... and Vevers, R. (2014). The Catlin Seaview Survey–kilometre-scale seascape assessment, and monitoring of coral reef ecosystems. *Aquatic Conservation: Marine and Freshwater Ecosystems*, *24*, 184-198.

Goodman, J. A., Samuel, J. P., and Stuart, R. P. (2013). *Coral reef remote sensing. A guide for mapping, monitoring and management.* Springer, Netherlands.

Gourley, M., Jell, J.S. (1993). Heron Island Spoil Dump. *A Report to the Great Barrier Reef Marine Park Authority,* Townsville. Accessed 22nd April 2018 from http://elibrary.gbrmpa.gov.au/jspui/handle/11017/479.

Graham, N. A. J., and Nash, K. L. (2013). The importance of structural complexity in coral reef ecosystems. *Coral Reefs*, *32*(2), 315-326.

Graham, N. A. J., Evans, R. D., and Russ, G. R. (2003). The effects of marine reserve protection on the trophic relationships of reef fishes on the Great Barrier Reef. *Environmental Conservation*, *30*(2), 200-208.

Graham, N. A., Jennings, S., MacNeil, M. A., Mouillot, D., and Wilson, S. K. (2015). Predicting climate-driven regime shifts versus rebound potential in coral reefs. *Nature, 518*(7537), 94.

Graham, N. A., Wilson, S. K., Jennings, S., Polunin, N. V., Robinson, J. A. N., Bijoux, J. P., and Daw, T. M. (2007). Lag effects in the impacts of mass coral bleaching on coral reef fish, fisheries, and ecosystems. *Conservation biology*, *21*(5), 1291-1300.

Gratwicke, B., and Speight, M. R. (2005). The relationship between fish species richness, abundance and habitat complexity in a range of shallow tropical marine habitats. *Journal of fish biology*, *66*(3), 650-667.

Gutierrez-Heredia, L., Benzoni, F., Murphy, E., and Reynaud, E. G. (2016). End to end digitisation and analysis of three-dimensional coral models, from communities to corallites. *PloS one*, *11*(2).

Harborne, A. R., Mumby, P. J., & Ferrari, R. (2012). The effectiveness of different meso-scale rugosity metrics for predicting intra-habitat variation in coral-reef fish assemblages. *Environmental Biology of Fishes, 94*(2), 431-442.

Harborne, A. R., Mumby, P. J., ZŻychaluk, K., Hedley, J. D., and Blackwell, P. G. (2006). Modelling the beta diversity of coral reefs. *Ecology*, *87*(11), 2871-2881.

Harris, D. L., Rovere, A., Casella, E., Power, H., Canavesio, R., Collin, A., ... and Parravicini, V. (2018). Coral reef structural complexity provides important coastal protection from waves under rising sea levels. *Science advances*, *4*(2).

Harris, P. M. M., Purkis, S. J., Ellis, J., Swart, P. K., and Reijmer, J. J. (2015). Mapping bathymetry and depositional facies on Great Bahama Bank. *Sedimentology*, *62*(2), 566-589.

Hattori, A. (2017). Aerial images can detect 3D small patch reefs that are potential habitats for anemonefish Amphiprion frenatus. *Ecological Research*, *32*(6), 943-949.

Hattori, A., and Shibuno, T. (2015). Total volume of 3D small patch reefs reflected in aerial photographs can predict total species richness of coral reef damselfish assemblages on a shallow back reef. *Ecological research*, *30*(4), 675-682.

He, H., Ferrari, R., McKinnon, D., Roff, G., Mumby, P., Smith, R., and Upcroft, B. (2012). Measuring reef complexity and rugosity from monocular video bathymetric reconstruction. *Proceedings of the 12th International Coral Reef Symposium*, 1-5. James Cook University, Townsville.

Hedley, J. D., Roelfsema, C. M., Chollett, I., Harborne, A. R., Heron, S. F., Weeks, S., ... and Ticzon, V. (2016). Remote sensing of coral reefs for monitoring and management: a review. *Remote Sensing*, *8*(2), 118.

Hill, J., and Wilkinson, C. (2004). Methods for ecological monitoring of coral reefs. *Australian Institute of Marine Science, Townsville*, *117*.

Hobson, E. S. (1972). Activity of Hawaiian reef fishes during the evening and morning transitions between daylight and darkness. *Fisheries Bulletin*, *70*(3), 715-740.

Hoegh-Guldberg, O. (1999). Climate change, coral bleaching and the future of the world's coral reefs. *Marine and freshwater research*, *50*(8), 839-866.

Hoegh-Guldberg, O., Mumby, P. J., Hooten, A. J., Steneck, R. S., Greenfield, P., Gomez, E., ... and Knowlton, N. (2007). Coral reefs under rapid climate change and ocean acidification. *Science*, *318*(5857), 1737-1742.

Hooper, D. U., Chapin, F. S., Ewel, J. J., Hector, A., Inchausti, P., Lavorel, S., ... and Schmid, B. (2005). Effects of biodiversity on ecosystem functioning: a consensus of current knowledge. *Ecological monographs*, *75*(1), 3-35.

House, J. E., Bidaut, L. M., Christie, A. P., Pizarro, O., and Dornelas, M. (2016). Moving to 3D: relationships between coral planar area, surface area and volume. *PeerJ Preprints, 4*.

Hughes, T. P., Graham, N. A., Jackson, J. B., Mumby, P. J., and Steneck, R. S. (2010). Rising to the challenge of sustaining coral reef resilience. *Trends in ecology and evolution*, *25*(11), 633-642.

Jackson, J. B., Alexander, K., and Sala, E. (2012). Shifting Baselines: The Past and the Future of Ocean Fisheries-by Trevor Kenchington. *International Journal of Maritime History*, *24*(1), 482.

Jackson, J., Cramer, K., Donovan, M., Friedlander, A., Hooten, A., & Lam, V. (2012). Tropical Americas Coral Reef Resilience Workshop. *IUCN Report.*

Januchowski-Hartley, F. A., Graham, N. A., Wilson, S. K., Jennings, S., and Perry, C. T. (2017). Drivers and predictions of coral reef carbonate budget trajectories. *Proceedings of the Royal Society B: Biological Sciences*, *284* (1847).

Jupp, D.L.B., Mayo, K.K., Kuchler, D.A., Claasen, D.V.R., Kenchington, R.A. and Guerin, P.R., (1985). Remote sensing for planning and managing the Great Barrier Reef of Australia. *Photogrammetria*, *40*, 21-42.

Kennedy, E. V., Perry, C. T., Halloran, P. R., Iglesias-Prieto, R., Schönberg, C. H., Wisshak, M., ... and Mumby, P. J. (2013). Avoiding coral reef functional collapse requires local and global action. *Current Biology*, *23*(10), 912-918.

Kleeman, K., (1996). Coral Communities at Lizard Island, Great Barrier Reef, Australia. *Beitr. Palaont,* 21, 57-67.

Knowlton, N., and Jackson, J. B. (2008). Shifting baselines, local impacts, and global change on coral reefs. *PLoS biology*, *6*(2).

Knudby, A. and LeDrew, E. (2007). Measuring structural complexity on coral reefs. *American Academy of Underwater Sciences*, 26th Symposium, 181-188.

Knudby, A., LeDrew, E., and Newman, C. (2007). Progress in the use of remote sensing for coral reef biodiversity studies. *Progress in Physical Geography*, *31*(4), 421-434.

Komyakova, V., Munday, P. L., and Jones, G. P. (2013). Relative importance of coral cover, habitat complexity and diversity in determining the structure of reef fish communities. *PLoS One*, *8*(12).

Kuffner, I. B., Brock, J. C., Grober-Dunsmore, R., Bonito, V. E., Hickey, T. D., and Wright, C. W. (2007). Relationships between reef fish communities and remotely sensed rugosity measurements in Biscayne National Park, Florida, USA. *Environmental biology of fishes*, *78*(1), 71-82.

Lasagna, R., Albertelli, G., Colantoni, P., Morri, C., and Bianchi, C. N. (2010). Ecological stages of Maldivian reefs after the coral mass mortality of 1998. *Facies, 56*(1), 1.

Lavy, A., Eyal, G., Neal, B., Keren, R., Loya, Y., and Ilan, M. (2015). A quick, easy and non-intrusive method for underwater volume and surface area evaluation of benthic organisms by 3D computer modelling. *Methods in Ecology and Evolution*, *6*(5), 521-531.

Lefsky, M. A., Cohen, W. B., Parker, G. G., and Harding, D. J. (2002). Lidar remote sensing for ecosystem studies: Lidar, an emerging remote sensing technology that directly measures the three-dimensional distribution of plant canopies, can accurately estimate vegetation structural attributes and should be of particular interest to forest, landscape, and global ecologists. *AIBS Bulletin*, *52*(1), 19-30.

Leiper, I. A., Siebeck, U. E., Marshall, N. J., and Phinn, S. R. (2009). Coral health monitoring: linking coral colour and remote sensing techniques. *Canadian Journal of Remote Sensing*, *35*(3), 276-286.

Lentz, J. A. (2012). *Developing a Geospatial Protocol for Coral Epizootiology.* Doctoral thesis, Louisiana State University and Agricultural and Mechanical College, Louisiana.

Leon, J. X., Roelfsema, C. M., Saunders, M. I., and Phinn, S. R. (2015). Measuring coral reef terrain roughness using 'Structure-from-Motion 'close-range photogrammetry. *Geomorphology*, *242*, 21-28.

Leujak, W., and Ormond, R. F. G. (2007). Comparative accuracy and efficiency of six coral community survey methods. *Journal of Experimental Marine Biology and Ecology*, *351*(1-2), 168-187.

Levin, P. S., Tolimieri, N., Nicklin, M., and Sale, P. F. (2000). Integrating individual behaviour and population ecology: the potential for habitat-dependent population regulation in a reef fish. *Behavioural Ecology*, *11*(5), 565-571.

Lirman, D., Gracias, N. R., Gintert, B. E., Gleason, A. C. R., Reid, R. P., Negahdaripour, S., and Kramer, P. (2007). Development and application of a video-mosaic survey technology to document the status of coral reef communities. *Environmental monitoring and assessment*, *125*(1-3), 59-73.

Long, B. G., Andrews, G., and Wang, Y. G. (2004). Sampling accuracy of reef resource inventory technique. *Coral Reefs*, *23*(3), 378-385.

Luckhurst, B. E., and Luckhurst, K. (1978). Analysis of the influence of substrate variables on coral reef fish communities. *Marine Biology*, *49*(4), 317-323.

Lundblad, E. R., Wright, D. J., Miller, J., Larkin, E. M., Rinehart, R., Naar, D. F., ... and Battista, T. (2006). A benthic terrain classification scheme for American Samoa. *Marine Geodesy*, *29*(2), 89-111.

Madin, J. S., Anderson, K. D., Andreasen, M. H., Bridge, T. C., Cairns, S. D., Connolly, S. R., ... and Gates, R. D. (2016). The Coral Trait Database, a curated database of trait information for coral species from the global oceans. *Scientific Data*, *3*, 160017.

Madin, J. S., Black, K. P., and Connolly, S. R. (2006). Scaling water motion on coral reefs: from regional to organismal scales. *Coral Reefs*, *25*(4), 635-644.

Magno, M., and Villanoy, C. (2006). Quantifying the complexity of Philippine coastlines for estimating entrainment potential. *Proceedings of the 10th International Coral Reef Symposium*, 1471-1476.

Maynard, J. A., Anthony, K. R., Marshall, P. A., and Masiri, I. (2008). Major bleaching events can lead to increased thermal tolerance in corals. *Marine Biology*, *155*(2), 173-182.

McCarroll, D. (2016). *Simple statistical tests for geography*. New York: Chapman and Hall/CRC.

McCarthy, J., and Benjamin, J. (2014). Multi-image photogrammetry for underwater archaeological site recording: an accessible, diver-based approach. *Journal of maritime archaeology*, *9*(1), 95-114.

McCook, L. J. (1999). Macroalgae, nutrients and phase shifts on coral reefs: scientific issues and management consequences for the Great Barrier Reef. *Coral reefs*, *18*(4), 357-367.

McCormick, M. I. (1994). Comparison of field methods for measuring surface topography and their associations with a tropical reef fish assemblage. *Marine ecology progress series, 112*(1), 87-96.

McGavin, K., Head, J., and Smith, D. (2017). Coral communities in the Seychelles, Annual Report for the Seychelles National Parks Authority. Accessed 18th September, 2018, from https://earthwatch.org.uk/images/Publications/Seychelles-Programme-Report-Online-Version.pdf.

McKinnon, D., He, H., Upcroft, B., and Smith, R. N. (2011). Towards automated and *in-situ*, near-real time 3-D reconstruction of coral reef environments. *Oceans, IEEE,* 1-10.

McManus, J. W., and Polsenberg, J. F. (2004). Coral–algal phase shifts on coral reefs: ecological and environmental aspects. *Progress in Oceanography*, *60*(2-4), 263-279.

Moberg, F., and Folke, C. (1999). Ecological goods and services of coral reef ecosystems. *Ecological economics*, *29*(2), 215-233.

Montefalcone, M., Parravicini, V., and Bianchi, C. N. (2011). Quantification of coastal ecosystem resilience. *Treatise on estuarine and coastal science, 10*(3), 49-70.

Mora, C. (2008). A clear human footprint in the coral reefs of the Caribbean. *Proceedings of the Royal Society B: Biological Sciences*, *275*(1636), 767-773.

Mumby, P. J. (2006). The impact of exploiting grazers (Scaridae) on the dynamics of Caribbean coral reefs. *Ecological Applications*, *16*(2), 747-769.

Mumby, P. J. (2016). Stratifying herbivore fisheries by habitat to avoid ecosystem overfishing of coral reefs. *Fish and Fisheries*, *17*(1), 266-278.

Mumby, P. J., and Steneck, R. S. (2008). Coral reef management and conservation in light of rapidly evolving ecological paradigms. *Trends in ecology and evolution*, *23*(10), 555-563.

Mumby, P. J., Green, E. P., Edwards, A. J., and Clark, C. D. (1997). Coral reef habitat mapping: how much detail can remote sensing provide? *Marine Biology*, *130*(2), 193-202.

Mumby, P. J., Skirving, W., Strong, A. E., Hardy, J. T., LeDrew, E. F., Hochberg, E. J., ... and David, L. T. (2004). Remote sensing of coral reefs and their physical environment. *Marine pollution bulletin*, *48*(3-4), 219-228.

NASA. (2018). Airborne Fluid Lensing and Machine Learning for Automated Coral Classification. Accessed September 18th, 2018 from https://www.nasa.gov/ames/las/coral-classification.

Nash, K. L., Graham, N. A., Wilson, S. K., and Bellwood, D. R. (2013). Cross-scale habitat structure drives fish body size distributions on coral reefs. *Ecosystems*, *16*(3), 478-490.

Nature Seychelles. (2006). The effects of coral bleaching in Seychelles. Accessed 18th June, 2018 from http://natureseychelles.org/natureseychelles_new/index.php?option=com_content&view=article&id=208:the-effects-of-coral-bleaching-in-seychelles&catid=47&Itemid=276

Naughton, P., Edwards, C., Petrovic, V., Kastner, R., Kuester, F., and Sandin, S. (2015). Scaling the Annotation of Subtidal Marine Habitats. *Proceedings of the 10th International Conference on Underwater Networks and Systems, 31.*

Newman, S. P., Meesters, E. H., Dryden, C. S., Williams, S. M., Sanchez, C., Mumby, P. J., and Polunin, N. V. (2015). Reef flattening effects on total richness and species responses in the Caribbean. *Journal of Animal Ecology*, *84*(6), 1678-1689.

Norse, E. A. (1993). *Global marine biological diversity: a strategy for building conservation into decision making*. Washington, D.C: Island Press.

Parsons, M., Bratanov, D., Gaston, K., and Gonzalez, F. (2018). UAVs, Hyperspectral Remote Sensing, and Machine Learning Revolutionizing Reef Monitoring. *Sensors*, *18*(7), 2026.

Perry, C. T., & Morgan, K. M. (2017a). Bleaching drives collapse in reef carbonate budgets and reef growth potential on southern Maldives reefs. *Scientific reports*, 7, 40581.

Perry, C. T., & Morgan, K. M. (2017b). Post-bleaching coral community change on southern Maldivian reefs: is there potential for rapid recovery? *Coral Reefs*, 36(4), 1189-1194.

Perry, C. T., Murphy, G. N., Kench, P. S., Smithers, S. G., Edinger, E. N., Steneck, R. S., and Mumby, P. J. (2013). Caribbean-wide decline in carbonate production threatens coral reef growth. *Nature communications, 4,* 1402.

Perry, C. T., Spencer, T., and Kench, P. S. (2008). Carbonate budgets and reef production states: a geomorphic perspective on the ecological phase-shift concept. *Coral Reefs*, *27*(4), 853-866.

Peterson, G., Allen, C. R., and Holling, C. S. (1998). Ecological resilience, biodiversity, and scale. *Ecosystems*, *1*(1), 6-18.

Phinn, S. R., Roelfsema, C. M., and Mumby, P. J. (2012). Multi-scale, object-based image analysis for mapping geomorphic and ecological zones on coral reefs. *International Journal of Remote Sensing*, *33*(12), 3768-3797.

Pichon, M., and Morrissey, J. (1981). Benthic zonation and community structure of south island reef, Lizard Island (Great Barrier Reef). *Bulletin of Marine Science*, *31*(3), 581-593.

Polunin, N. V. C., and Roberts, C. M. (1993). Greater biomass and value of target coral-reef fishes in two small Caribbean marine reserves. *Marine Ecology-Progress Series*, *100*, 167-167.

Purkis, S. J. (2017). Remote sensing tropical coral reefs: The view from above. *Annual review of marine science, 10*, 149-168.

Purkis, S. J., Graham, N. A. J., and Riegl, B. M. (2007). Predictability of reef fish diversity and abundance using remote sensing data in Diego Garcia (Chagos Archipelago). *Coral reefs*, *27*(1), 167-178.

Raoult, V., Reid-Anderson, S., Ferri, A., and Williamson, J. E. (2017). How Reliable Is Structure from Motion (SfM) over Time and between Observers? A Case Study Using Coral Reef Bommies. *Remote Sensing*, *9*(7), 740.

Reaka-Kudla, M. L. (1997). The global biodiversity of coral reefs: a comparison with rain forests. *Biodiversity II: Understanding and protecting our biological resources, 2,* 551.

Rees, S. A., Opdyke, B. N., Wilson, P. A., Fifield, L. K., & Levchenko, V. (2006). Holocene evolution of the granite based Lizard Island and MacGillivray reef systems, Northern Great Barrier Reef. *Coral Reefs, 25*(4), 555-565.

Richardson, L. E., Graham, N. A., and Hoey, A. S. (2017). Cross-scale habitat structure driven by coral species composition on tropical reefs. *Scientific reports*, *7*(1), 7557.

Riegl, B. M., and Purkis, S. J. (2005). Detection of shallow subtidal corals from IKONOS satellite and QTC View (50, 200 kHz) single-beam sonar data (Arabian Gulf; Dubai, UAE). *Remote Sensing of Environment*, *95*(1), 96-114.

Risk, M.J. (1972). Fish diversity on a coral reef in the Virgin Islands. *Atoll Research Bulletin 153,* 1-6.

Rogers, C. S., Suchanek, T. H., and Pecora, F. A. (1982). Effects of hurricanes David and Frederic (1979) on shallow Acropora palmata reef communities: St. Croix, US Virgin Islands. *Bulletin of Marine Science*, *32*(2), 532-548.

Santos, I. R., Glud, R. N., Maher, D., Erler, D., and Eyre, B. D. (2011). Diel coral reef acidification driven by porewater advection in permeable carbonate sands, Heron Island, Great Barrier Reef. *Geophysical Research Letters*, *38*(3).

Saunders, M. I., Bayraktarov, E., Roelfsema, C. M., Leon, J. X., Samper-Villarreal, J., Phinn, S. R., ... and Mumby, P. J. (2015). Spatial and temporal variability of seagrass at Lizard Island, Great Barrier Reef. *Botanica Marina*, *58*(1), 35-49.

Schiagintweit, G. E. O. (1993). Real-time acoustic bottom classification for hydrography a field evaluation of RoxAnn. *Engineering in Harmony with Ocean. Proceedings, IEEE,* III-214,

Schuhmacher, H., Loch, K., Loch, W., and See, W. R. (2005). The aftermath of coral bleaching on a Maldivian reef—a quantitative study. *Facies, 51*(1-4), 80-92.

Scopélitis, J., Andréfouët, S., Phinn, S., Arroyo, L., Dalleau, M., Cros, A., and Chabanet, P. (2010). The next step in shallow coral reef monitoring: Combining remote sensing and in situ approaches. *Marine Pollution Bulletin*, *60*(11), 1956-1968.

Sheppard, C. R., Spalding, M., Bradshaw, C., and Wilson, S. (2002). Erosion vs. recovery of coral reefs after 1998 El Niño: Chagos reefs, Indian Ocean. *AMBIO: A Journal of the Human Environment*, *31*(1), 40-48.

Sheppard, C., Davy, S., Pilling, G., and Graham, N. (2017). *The biology of coral reefs*. Oxford: Oxford University Press.

Sheppard, C., Dixon, D. J., Gourlay, M., Sheppard, A., and Payet, R. (2005). Coral mortality increases wave energy reaching shores protected by reef flats: examples from the Seychelles. *Estuarine, Coastal and Shelf Science*, *64*(2-3), 223-234.

Shihavuddin, A. S. M., Gracias, N., Garcia, R., Gleason, A. C., and Gintert, B. (2013). Image-based coral reef classification and thematic mapping. *Remote Sensing*, *5*(4), 1809-1841.

Shumway, C. A., Hofmann, H. A., and Dobberfuhl, A. P. (2007). Quantifying habitat complexity in aquatic ecosystems. *Freshwater Biology, 52*(6), 1065-1076.

Smith, V.E., Rogers, R.H., and Reed, L.E. (1975). Automated mapping and inventory of Great Barrier Reef zonation with Landsat data. *Oceans, IEEE,* 775-780.

Spalding, M. D., and Grenfell, A. M. (1997). New estimates of global and regional coral reef areas. *Coral Reefs, 16*(4), 225-230.

Spalding, M., Ravilious, C., and Green, E. P. (2001). *World Atlas of Coral Reefs*. California: University of California Press.

Stier, A. C., and Osenberg, C. W. (2010). Propagule redirection: Habitat availability reduces colonization and increases recruitment in reef fishes. *Ecology*, *91*(10), 2826-2832.

Storlazzi, C. D., Dartnell, P., Hatcher, G. A., and Gibbs, A. E. (2016). End of the chain? Rugosity and fine-scale bathymetry from existing underwater

digital imagery using structure-from-motion (SfM) technology. *Coral Reefs, 35*(3), 889-894.

Sweatman, H., Delean, S., and Syms, C. (2011). Assessing loss of coral cover on Australia's Great Barrier Reef over two decades, with implications for longer-term trends. *Coral reefs*, *30*(2), 521-531.

UNEP/AIMS, (1993), Monitoring Coral Reefs for Global Change. *Reference Methods for Marine Pollution Studies*, 61.

von Szalay, P. G., and McConnaughey, R. A. (2002). The effect of slope and vessel speed on the performance of a single beam acoustic seabed classification system. *Fisheries Research*, *56*(1), 99-112.

Walker, B. K., Jordan, L. K., and Spieler, R. E. (2009). Relationship of reef fish assemblages and topographic complexity on southeastern Florida coral reef habitats. *Journal of Coastal Research*, 39-48.

Wedding, L. M., Friedlander, A. M., McGranaghan, M., Yost, R. S., and Monaco, M. E. (2008). Using bathymetric LiDAR to define nearshore benthic habitat complexity: Implications for management of reef fish assemblages in Hawaii. *Remote Sensing of Environment*, *112*(11), 4159-4165.

Westoby, M. (1998). A leaf-height-seed (LHS) plant ecology strategy scheme. *Plant and soil*, *199*(2), 213-227.

Westoby, M. J., Brasington, J., Glasser, N. F., Hambrey, M. J., and Reynolds, J. M. (2012). 'Structure-from-Motion' photogrammetry: A low-cost, effective tool for geoscience applications. *Geomorphology*, *179*, 300-314.

White, W. H., Harborne, A. R., Sotheran, I. S., Walton, R., and Foster-Smith, R. L. (2003). Using an acoustic ground discrimination system to map coral reef benthic classes. *International Journal of Remote Sensing*, *24*(13), 2641-2660.

Wilson, S. K., Graham, N. A. J., and Polunin, N. V. C. (2007). Appraisal of visual assessments of habitat complexity and benthic composition on coral reefs. *Marine Biology*, *151*(3), 1069-1076

Wright, C. W., and Brock, J. C. (2002). EAARL: A LiDAR for mapping shallow coral reefs and other coastal environments. *Proceedings of the Seventh International Conference on Remote Sensing for Marine and Coastal Environments*, 20-22. Miami: Veridian International.

Yates, K. K., Zawada, D. G., Smiley, N. A., and Tiling-Range, G. (2017). Divergence of seafloor elevation and sea level rise in coral reef ecosystems. *Biogeosciences*, *14*(6), 1739.

Young, G. C., Dey, S., Rogers, A. D., and Exton, D. (2017). Cost and time-effective method for multi-scale measures of rugosity, fractal dimension, and vector dispersion from coral reef 3D models. *PloS one, 12*(4).

Zawada, D. G., Piniak, G. A., & Hearn, C. J. (2010). Topographic complexity and roughness of a tropical benthic seascape. *Geophysical research letters, 37*(14).

For Grandad Joe who has always been my number one supporter.

And for Grandad Harold who was there with me the entire time.